UV LASER ABLATION OF MOLECULAR CRYOGENIC FILMS

Ph. D. Dissertation

Antonis Koubenakis

UNIVERSITY OF CRETE
Department of Physics

Heraklion, Crete, Greece
March 2002

Examination Committee

Prof. C. Fotakis (Dept. of Physics) (Supervisor)

Assoc. Prof. S. Anastasiadis (Dept. of Physics)

Assoc. Prof. D. Charalambidis (Dept. of Physics)

Prof. E. Economou (Dept. of Physics)

Prof. S. Farantos (Dept. of Chemistry)

Assoc. Prof. T Kitsopoulos (Dept. of Chemistry)

Assoc. Prof. I. Perakis (Dept. of Physics)

Dedication

To my Parents

Athina Panagiotaki Koubenaki

Constantino Koubenaki

SUMMARY

In the irradiation of condensed phases at high laser irradiances, the ejection/removal of a high quantity of material is observed, and this is usually denoted by the term laser pulsed ablation (or explosive desorption). This phenomenon has found extensive and very important applications, but its mechanistic understanding is very poor. The present work addresses two questions: Can a physically significant criterion be established for defining the phenomenon? How physical and chemical processes in this regime differ from those at low light irradiances where conventional photophysics/chemistry holds?

To address these questions, model systems composed of simple organic compounds frozen at low tempeartures are studied. Time-of-flight mass spectrometry is employed to probe ejection efficiencies as a function of laser parameters and optical/imaging techniques are employed for probing morphological/structural changes induced in the film.

Through the comparative examination of nonabsorbing dopants of different binding energies to the matrix ($C_6H_5CH_3$), it is demonstrated that in the UV irradiation, two fluence ranges can be delineated where different material ejection mechanisms operate. At low fluences, ejection is consistent with surface vaporization/desorption, whereas at higher fluences, ejection is clearly different, entailing the unselective ejection of a volume of material. Therefore, the term “ablation” should be employed for denoting exclusively this higher fluence range. This differentiation has important implications for the applications of ablation. The ejection of dopants strongly-bound to the matrix is established as a direct experimental criterion for the identification of ablative regime.

By the use of optical techniques, film melting and gas bubble formation is demonstrated below the threshold. Consequently, ablation of molecular solids with nanosecond pulses is due to “explosive boiling”. Besides the implications for ablation, this demonstration may provide new ways for studying organic compounds in metastable states.

The translational distributions of the ejected desorbates in the UV irradiation are shown to exhibit distinctly different dependences above vs. below the threshold. In contrast to most models, in the ablation regime they are shown to be determined by the gas phase collisional dynamics and the ejection process, as well. A number of additional features are determined that can provide the basis for the development of more elaborate theoretical models on the flow dynamics of the ejected material.

The photochemical processes are studied for prototypical organic compound (C_6H_5Cl). It is shown that UV ablation does not modify qualitatively the reactivity patterns. However, quantitatively, significant deviations from conventional kinetics are noted, suggesting that the description of reactivity in UV ablation requires consideration of the parallel influence of the thermal and physical processes. In particular, product formation is shown to occur mainly in the film and as a result, photolysis yields and photoproduct formation efficiencies depend critically on the time scale of material ejection.

Finally, preliminary studies on the femtosecond irradiation of these systems show significant differentiations from the nanosecond case, suggesting that laser pulse width is crucial for the desorption and ablation ejection processes.

TABLE OF CONTENTS

THIS PAGE INTENTIONALLY LEFT BLANK

LIST OF FIGURES

THIS PAGE INTENTIONALLY LEFT BLANK

LIST OF TABLES

1. INTRODUCTION

1.1. IRRADIATION OF MOLECULAR SOLIDS

In the irradiation of molecular solids with highly intense laser pulses, there occurs the removal of a significant material amount resulting in the formation of a crater (depth from nm to ìm) in the irradiated material [1]. This phenomenon has been named (pulsed laser) Ablation. Despite this simple description, the physical/chemical processes involved in the phenomenon are very complicated and so far they are not well understood. As a result, the description of the phenomenon remains largely phenomenological.

UV laser ablation has found many important applications in a wide spectrum of fields [2], ranging from microelectronics (polymer processing and laser cleaning [4], matrix assisted pulse laser evaporation of organic microstructures etc. [3,6]) , chemical analysis (Matrix Assisted Laser Desorption of Biomolecules-MALDI- and Laser Ablation Mass Spectrometry [5]), biology and medicine (photorefractive keratectomy), etc. Thus, understanding of the phenomenon is important for the optimization of all these applications. Most importantly, the phenomenon raises important questions in a range of scientific fields such as thermodynamics, photophysics, photochemistry, etc. UV ablation may involve at the same time high temperatures, the formation of a high number of electronically excited states, the generation of high amplitude pressures etc. Molecular physical processes under these conditions will deviate much from those described by conventional photophysics/chemistry. As a result, the study of UV ablation can be expected to result finally in new information about molecular photophysics/chemistry and also result in the development of new concepts.

Clearly, the first question is how the incident photon energy results finally in the observed macroscopic morphological changes and in material removal. This problem is new to condensed phase photophysics/chemistry, since no major morphological changes are observed in the irradiation at low laser intensities. The process of material removal/crater formation is observed to become significant only at high fluences, with the etching depth per pulse increasing with the laser fluence (usually the etching depth d per pulse is scaled logarithmically to the fluence according to the formula $\propto \ln (F/F_{th})$ where F_{th} is the threshold-fluence, reaching a plateau at higher fluences or changing into an almost linear dependence $\propto (F-Fo)$). At low

fluences, little or no material is removed [1]. However it is not clear if there is a well-defined fluence (threshold) defining the phenomenon or if there is just a gradual evolution from the one fluence range to the other. In the Fig. 1 we present a typical curve of the dependence of etching depth on laser fluence.

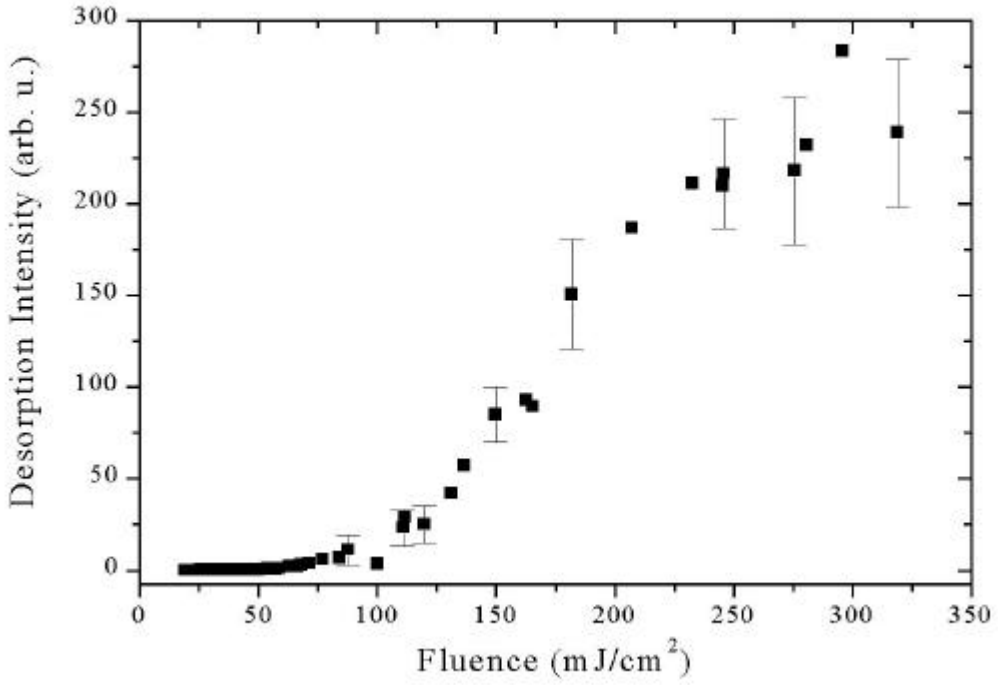

Figure 1-1 Desorption intensity as a function of the laser fluence in the irradiation of neat toluene solid at 248 nm, with 30 ns laser pulses.

Besides the issue of the material removal, there are several novel aspects in the phenomenon, which evidently are responsible for its wide success and applicability of the phenomenon. Several of these aspects are not expected on the basis of convetional photophysics/chemistry of condensed phases. Some of these aspects in the UV ablation of molecular solids are illustrated in the consideration of Matrix Assisted Laser Desorption.

1.2. MATRIX-ASSISTED LASER DESORPTION TECHNIQUE

A most important application of laser ablation of molecular substrates, directly relevant to this Thesis, is the Matrix Assisted Laser Desorption Ionization (MALDI). MALDI is based on the discovery of Tanaka [7] and of Karas and Hillenkamp [8] that dissolving a biomolecule (like enzyme, proteins, DNA, e.t.c.) within a great excess of a matrix (usually DHB-dihydroxybenzoic acid) specifically chosen to absorb at the irradiation wavelength can lead to its ejection into the gas phase. The most important advantage of the method is that the disolved bio-molecules can be ejected in the gas-phase with minimal or little degradation. In that way, there is the capability of the identification of biopolymer using mass spectrometry. MALDI has become the leading technique for performing mass analysis of non-volatile organic and biological molecules (biopolymers, proteins, polymers etc.) especially for the accurate determination of their molecular weight. Furthermore, the capability of the technique for charcterization of the structure (i.e., sub-group identification) of biopolymers has been demostrated. Until now a wide range of polymers, etc proteins have been analyzed, with molecular weights usualy around 300,000 amu, while recently a protein of 1,500,000 amu has been measured. Besides mass spectrometry, the intact ejection of biopolymers enables the application of the wide variety of spectroscopic techniques that have been developed for gaseous species to their examination.

Despite the very important applications of the technique, its mechanism is not yet well understood, so the technique is used mainly empirically. Thus, up to now, the studies have been concentrated on finding appropriate molecular matrices for the various types of biomolecules in a largely trial-and-error approach.

Empirically a successful matrix should exhibit the following criteria.

- Absorption of the irradiation. The absorption of the UV laser light by the matrix molecules has as a result the fast deposition of a large amount of energy in the system. This drives to disintegration a small volume of the system and to the ejection in the gas phase, of the analyte (also of the matrix molecules) with little internal energy excitation.
- Dilution of the analyte molecules. This results in the ejection of individual biopolymers instead of ill-defined clusters.
- Promoting the ionization of the analytes molecules. The ions that are produced in the MALDI process are generally “semi-molecular” ions, instead of radical cations, i.e. protonated (e.g. $M\text{-}H^+$) or alkalinated molecular ions (e.g. $M\text{-}Na^+$). At present, it is

assumed that the matrix plays an important role in the protonation process, but the various hypothesis that are proposed are fully contradictory[1].

Yet, the most fundamental question to be answered is how the highly thermally labile and photosensitive, nonvolatile biomolecules can be "vaporized" by a laser pulse without being destroyed (f.e several of the analyzed proteins are complexes that thermally decompose to monomers ³ 60-100 °C. On the other hand, desorption of even dipeptides thermally requires T>200 C° and results in extensive decomposition. Furthermore, several undergo extensive photodegradation upon excitation at ë<300 nm). A number of mechanisms have been proposed for the explanation of this characteristic. Since these mechanisms are related to UV ablation of molecular solids in general, they are presented subsequently in a more general form.

1.3. PROPOSED ABLATION MECHANISMS

Despite the wide range of techniques like mass spectrometry, ultrafast imaging, fluorescence, molecular dynamic simualtions e.t.c that have been used for examing the phenomenon, the mechanisms of the ablation process remain still ill understood.

One reason for this is the many experimental problems in Section 1.3.5. in probing processes during material ejection. The second relates to the fact that several processes take place in parallel. However, the relative importance/contribution of these processes cannot be assesed and as a result, there is a large number of models proposed for explaining the phenomenon

The proposed models range from photothermal models that invoke rapid heating of the system, to photomechanical mechanisms in which ejection occurs "via momentum transfer processes", to photochemical mechanisms in which ejection is induced by high number of photoproducts. These mechanisms will be presented in next sections. *The models are quite elaborate, but since eventually no agreement exists even on the fundamental aspects, only the very basic/physical idea of each model will be presented.*

[1] This is most indicated that in issue of Chem. Rev. dedicated to ablation of molecular/solids, the three out of the four articles on MALDI present the studies on the ionization process with completely different views: processes in the film, processes in the gas phase, processes in clusters.

1.3.1. Photothermal Models

1.3.1.1. Desorption via Surface Evaporation

In the photothermal mechanism, the electronic and/or vibrational excitation of the molecules is assumed to be rapidly converted (~psec) to thermal energy in the condensed phase. Many different mathematical treatments have been published differing in the imposed boundary conditions, extent thermal conductivity, inclusion of electronically excited species desorbing etc. The basic idea however is simply that surface temperature increases according to $\Delta T = \frac{a \cdot F_{LASER}}{r \cdot C_p}$ where á (cm^{-1}) is the absorption coefficient of the molecule F_{LASER} the laser fluence (J/cm^2), ñ (mol/cm^3) the density and C_p (J/mol K) the heat capacity of the compound. The numerator represents the absorbed energy per volume unit in the solid. An increase in the desorption signal is expected given by the Clausius-Clapeyron equation. Accordingly desorption rate is $-\frac{dN}{dt} = A \times e^{-E_{des} / R(To + BF_{LASER})}$ is a simple function of F_{LASER}, so there isn't any real threshold value. The thermal mechanism can explain some of the characteristics of the UV laser ablation:

(1) The nearly exponential increase of the desorbed number of molecules as a function of laser fluence and the general observation that substrates with small cohesive energy tend to have smaller ablation threshold (after correction for the difference in the absorption coefficient)[2]. These appear to be the most important indications in favour of a thermal mechanism. Nevertheless, it must be noted that E_{des} values that are determined from the analysis of the dependence of the desorption intensities are generally different from the standard thermodynamic values (e.g. vaporization energy ΔH_{vap}, sublimation energy ΔH_{subl} e.t.c).

(2) The observation of highly irregular, often with the appearance of a solidified melt, of the irradiated area. The observation of melted area is usual for substrates that absorb moderately at the irradiation wavelength, but not in the case of strongly-absorbing. Furthermore, in most cases, formation of gas bubbles and other defects are observed in the bulk, thereby affecting the "appearance" of the substrate. So the morphological observations give indications for a thermal mechanism, but are affected by optical and other properties of the material and cannot be regarded as a proof.

On the other hand, the thermal mechanism cannot explain some basic characteristic of the ablation f.e. how it is possible in MALDI to effect protein ejection when these large

[2] **Thermal Ablation being a usual term for denoting it. As shown in this Thesis, this is wrong. Similarly, the term Desorption in MALDI and MAPLE are misleading (wrong). (Chapter 4)**

molecules have almost zero vapor pressure. Additionally, how it is possible that the highly thermally sensitive proteins is ejected with little degradation.

1.3.1.2. The Bottleneck Model

In order to explain the minimal thermal degradation of the ejected biomolecules in the framework of thermal models, the "bottleneck" model have been introduced. This idea was first introduced in relationship with laser-induced thermal desorption of molecules adsorbed on metallic surfaces. Vertes and Levine [10-9] extended this idea to explain the desorption of molecules surrounded by a matrix that absorbs the desorption laser pulse. They suggest that because the vibrational frequencies of the "internal" modes of the biomolecule differ from those of the biomolecule-matrix bonds, a "bottleneck" to energy transfer is present, i.e., the rate of energy transfer through that bond is restricted (rate depending inversely on ÄE energy mismatch). If the heating rate is high enough, the bio-molecule may desorb with little additional internal energy other than that present at t=0. The idea was supported by a hydrodynamic modeling of the temperature and density of the system as a function of time and distance from the laser solid interaction region. The biomolecule was demostrated to desorb with internal energies much lower than the temperature of the matrix molecules, which accounts for its limited thermal degradation.

Yet, despite its apparent success, the model appears difficult to accept for its very principle, i.e. it is very difficult to assume major mismatches between the vibrational frequencies of the biopolymer and organic matrix molecules. (both having similar C-H, N-H, etc bonds). Furthermore, the model fails to explain a number of major observations (f.e., how is eventually the protein ejected in the gas phase, etc).

1.3.1.3. Explosive Boiling

According to Gibbs thermodynamic theory [11] there are two limits to the existence of the condensed phase; the binodal line, the equilibrium curve (P,T) for the liquid and vapor, and the spinodal line, the boundary of thermodynamic stability of the liquid phase. The spinodal line is defined by the condition $-(\frac{\partial P}{\partial V})_T = 0$, $(\frac{\partial T}{\partial S})_P = 0$ which is a physical impossibility.

Between these boundaries there is a region of metastable (superheated) liquid. In crossing the spinodal line loss of stability of the liquid phase occurs, with the spontaneous disintegration of the system in to a two phase, consisting of individual gas molecules and liquid droplets.

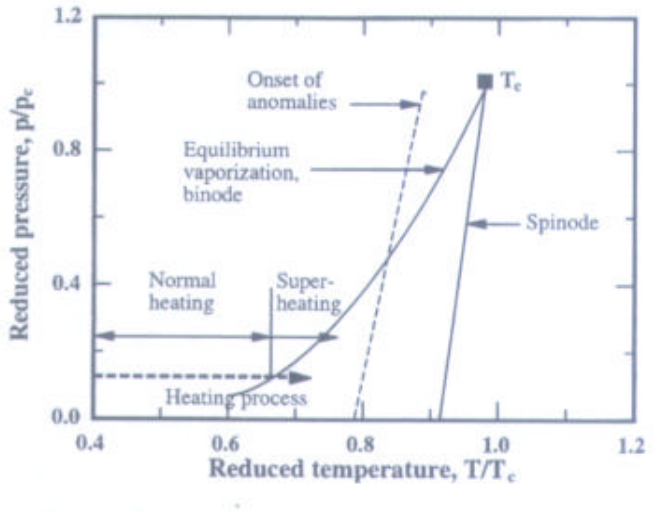

Figure 1-2 The figure illustrates the spinodal and binodal curve and the region of metastability.

Alternatively, the metastability can be understood in terms of the barrier to the formation of vapor bubbles (nucleus) as necessary for boiling. The creation of homogeneous vapor bubbles in a defect-free volume of the liquid is accompanied by an increase in the Gibbs free energy; $\Delta G_k = \frac{16ps^3}{3g^2}$ the parameter g characterizes the depth of penetration into the region of metastable states. A given metastable state at the point (p_o,T) can be reached by raising the temperature from T_o to T at constant p_o (T_o is the boiling point at the pressure p_o). In that case, $\Delta G_k = \frac{16ps^3}{3(r_V \Delta H_{vap} b)^2}$ where $\tilde{n}_V$ is the density of saturated vapor, $\ddot{A}H_{vap}$ is the specific heat of vaporization at the point (p_o,T_o) and â=(Ô-Ô$_i$)/Ô$_i$ is the relative superheat [12]. Under stationary conditions, the rate of nucleus formation of homogeneous nucleation at a temperature T is given by $J = J_o \exp(-\Delta G_k / k_B T)$ where J_o is a function which depends weakly on temperature and pressure in comparison with the exponential factor. The nucleation

rate J(t) under nonstationary conditions is related to J by $J(t) = J \times \exp(-\frac{t}{t})$ where t is the time and ô is the time for establishment of stationary nucleation after instantaneous superheating of the system.

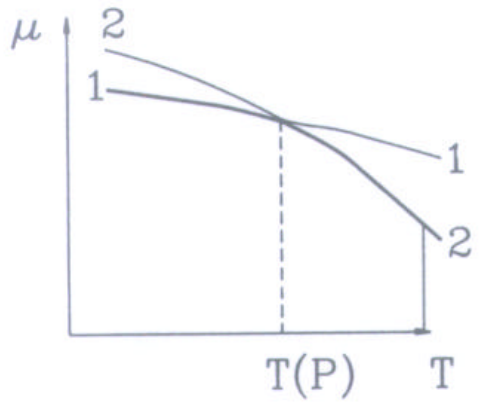

Figure 1-3 Chemical potentials of liquid (1) and gas phase (2) as function of temperature (at constant pressure) [13]. The diagram illustrates the metastability for system that remains in the liquid phase beyond the intersection point (equilibrium of the two phases).

According to the previous, at low rates of heat deposition no significant superheating of the liquid is achieved, since practically all the heat goes into the growth of heterogeneous vapor nuclei (ordinary boiling) which arise in the liquid at pre-existing centers (impurity). At very high heating rate (as those that may be attained by laser heating) the time for vaporization and thus the mass of material which is vaporized within heterogeneous nuclei (suggested to be ³ 1ìs) will be insignificant; therefore, the achievement of high superheating close to the spinodal line may be possible. This possibility, in relation with laser damage of metals was first advanced by Martynyuk but little attention was given to it [14]. Recently, the Martynuk suggestion have been reconsidered in the laser ablation of metal [15] and semiconductor [16,17] substrates. The last 2-3 years [18], through the parallel contribution of molecular dynamics simulations and thermodynamic considerations it has been suggested that the explosive boiling mechanism may be feasible in the laser irradiation of molecular solids.

In the , the particles are represented by a breathing sphere model: (i.e., spheres with varying radius, one internal degree of freedom). The interaction potential of the particles is

given by a Lennard-Jones potential. A more detailed description on the simulations is presented in Appendix I. The simulations have shown that above a certain laser fluence value, ejection of clusters is observed. It was proposed that this is the main characteristic of the ablation phenomenon. At lower fluences, no clusters are observed, with the molecules desorbing in the form of monomers. Furthermore, at these fluences, the desorbed signal as a function of the incident laser fluence is found to be exponential and will described by Clausius-Clayperon formula. Thus, the ejection process at these fluences was suggested to be essentially thermal in nature. Above the threshold, where ejection of clusters is observed, the irradiated material suffers pronounced structural changes during the laser pulse. However, the real "reason" for the material ejection is not evident from the simulations. Initially, Garrison and coworkers [18-20] determined the increase in the molecular kinetic energy and the atomic stresses and showed that both increased importantly in the irradiation regime. Therefore, they suggested that ablation is a combination of the photomechanical phenomenon and intense boiling.

Kelly and Miotello [21-23] report a thermodynamic analysis essentially similar to that of Martynuk and related it to the various experimental and theoretical findings [23]. In analyzing the MD simulations [23], they suggested that the simulations are consistent with explosive boiling. This explanation has in turn been adopted by the Garrison group. A more detail description for the explosive Boiling process and its consequencies will be given at chapter 4 in this Thesis[3].

1.3.2. Phonon Avalanche Model

Fain and Lin have tried to describe the ablation or explosive phenomenon by considering the electronic processes [24]. The main outcome of this work is the establishment of laser fluence and coverage dependent threshold conditions of the explosive regime. Because the rate of energy transfer from the electronically excited molecules in van der Waals

[3] As indicated in these chapters, Kelly and Miotello have presummed some parameters in their analysis. However, it is not clear if these parameters (f.e.,Jo, ô) are necessarily acceptable. The only cases where superheating has been realy demonstrated is : overheating of liquids in top of absorbing substrates (Grigoropoulos, Leiderer [75]) in which the superheating is very low ~ 20-50 K (because of heterogeneous vapor bubble formation), studies at very high fluences, very much higher than the ablation threshold [17], and studies with fs irradiation, where it is still debatable if explosive boiling can occur.

molecular crystal to the low frequency vibronic states and phonons increases with decreasing ΔE_{dif}, the rate will increase/accelerate as the energy is "dumped" into the higher and higher populated phonons. When energy flow into the vibrations and/or the phonons exceeds their respective decay, the phonon number begin to increase exponentially, i.e. an "avalanche" phenomenon. This would lead to explosive, nonselective desorption similar to high temperature thermal desorption. The threshold condition (i.e., the laser fluence) for this avalanche effect is determined by the equality of negative absorption (amplification) and the corresponding decay rate.

Recently, similar idea has been advanced by MD simulations of the vibrational energy distribution in the irradiation of molecular O_2 solids by intense laser pulses [25]. With increasing laser fluence the role of vibrational energy transfer was shown to increase rapidly resulting in explosive desorption.

1.3.3. The photomechanical Mechanism

In few cases, massive material ejection or laser damage has been reported to occur at energy irradiances much lower than those required for vaporization [26]. (liquids [26], polymers [27], biological tissues [28], IR-MALDI [29]).

As a possible explanation photomechanical mechanism was proposed caused by laser-induced stresses [30]. The magnitude of the laser induced stresses becomes significant when the laser pulse duration $\hat{o}_p$, is shorter than the time of mechanical equilibration of the absorbing volume $\hat{o}_s$ so that heating occurs under nearly constant volume. This condition usually referred as stress confinement, can be expressed as $\hat{o}_{pulse} \pounds \hat{o}_s \sim L_p/C_s$, where C_s is the speed of sound in the irradiated material and L_p the opical penetration depth. The initial compressive wave upon reflection from the free surface of the irradiated sample becomes tensile which can cause mechanical fracture/spallation. Since this results in the ejection of large and relatively cold "slices" of the material, the required energy density should be lower than that required for thermal mechanisms.

Larger and more numerous clusters with higher ejection velocities are indicated in the regime of stress confinement as compared to the regime of thermal confinement. According to this description, the fluence threshold should change with varying laser pulse length.

Therefore, using picosecond and femtosecond laser to desorb molecules may perform a critical test of the model. Such a case is examined in this thesis in the femtosecond laser ablation in chapter 7.

1.3.4. Photochemical Mechanism for Molecular Ejection

According to this mechanism, UV ablation of molecular solids is intricately related with the cleavage of chemical bonds and formation of new products. In its simplest version, the photochemical mechanism assumes that material ejection from molecular systems occurs when the number of broken bonds exceeds a critical value $N_D(z) = h \times \frac{s\, NF_{LASER}(z)}{hn} \geq N^{cr}_D$ where ç is the quantum yield and N the total number density of absorption centers (chromophores). If $N_D(z \pm \Delta z) \geq N^{cr}_D$, then from Beer's law, $\Delta z = \frac{1}{a} \times \ln(\frac{F}{F_{thr}})$ with $F_{thr} \propto \frac{hn}{ha} N_D^{cr}$. However, there is no criterion usually in specifying the critical number of bonds to be broken.

A different scenario is that the fragments that are formed in the photolysis produce gases (e.g. CO_2, CH_4 e.t.c.) by reactions with surrounding molecules. In that case, material ejection is due to the forces that are created by the expanding gases in the underlayers. In fact, very recently, on the basis of the study reported in chapter 6 (ablation of chlorobenzene solids), the Garrison group advanced a more elaborate scheme for the photochemical mechanism [31]. (see also Appendix II)

The photochemical mechanism has been advanced for explaining the observation that in a number of molecular systems (organic liquids [32-33] and polymers [34]), there is no evidence for melting or other morphological changes in the substrate and the ablation threshold does not correlate with the thermodynamic properties of these compounds. For instance, in a comparative study of the photoablation of *liquids* C_6H_6, $C_6H_5CH_3$, C_6H_5Cl, $C_6H_5CH_2Cl$, the Masuhara group using both imaging shadowgraphy [35] and photoacoustical techniques [33], estimated the values presented in Table 1.1 for the temperature that is attained in the irradiation with laser fluences close to the threshold regime.

Table 1-1 UV laser Ablation of liquids

Liquid	F_{thr} (mJ/cm^2)	Estimated T_{thr} (°K)	Boiling Point (°K)
Benzene	100	410	353
Chlorobenzene	60	370	405
Toluene	35	350	383

As shown, the temperatures are not correlated with the boiling points of the compounds. They proposed that the indicated decrease of the threshold is consistent with the photolysis yield of the compounds. Additionally, by laser induced flouresence (LIF) and imaging techniques [34], fragments in the ejected material were detected, which appears to be consistent with the photochemical mechanism.[4]

However, at least, with ns pulses, the fast deactivation processes suggest that at least part of the energy results in a high temperature rise. This increase must affect the photochemical processes.

1.3.5. Problems in the Study of Ablation Mechanism

Evidently, despite the large number of studies, it has been proved difficult to determine in detail the mechanisms of UV ablation of molecular solids. Experimentally, there are several complexities in the ablation phenomenon that are responsible for the difficulties in the mechanistic determination. (a) Because of the high laser irradiances, light absorption, can be highly non-linear, so it is very difficult to determine the exact energy absorbed by the substrate that drives to the ejection. (b) As discussed above, thermal, chemical and mechanical (stress wave) process occur in parallel, so it is very difficult to monitor the relative importance of these processes.

Spectroscopic examinations of the irradiated substrate suffer from the fact that the morphology of the surface is highly modified, which severaly affects the spectroscopic signals,

[4] But, the examination was performed at high laser fluences. Thus, it is possible that the observed fragments derive from multiple absorptions and dissociations of the molecules when already have been in the gas phase.

and their quantification. On the other hand, the examination of the ejected material is affected by two basic parameters: (a) A part of the desorbed material is ejected during the laser pulse and consequently absorption of additional photons in the gas phase take place, resulting in secondary (additional) fragmentation/dissociation and changes of their final energy differs. Furthermore, because of the plume ejection, it is very difficult to monitor processes in the film during irradiation experimentally (even, the amount of light actually absorbed cannot be established accurately). (b) Because of the great amount of the ejected material, the molecules suffer many collisions that change significantly their kinetic distributions from the initial one. In fact, there is thus far no fully established model for the description of the "flow" of the material ejected during ablation. For both reasons, the correlation of the kinetic distributions of the desorbed particles with processes take place on the solid in the irradiation is extremely doubtful.

In the case of polymers and MALDI substrates, there are additions difficulties: (a) The structure of the polymers and the molecules used as matrices in MALDI are quite complex from a chemical standpoint. Thus it is difficult to monitor in detail and quantify the processes that take place during ejection. (f.e., amount of the absorbed energy, or to monitor all chemical changes). (b) The photophysics/chemistry of these systems is not known in detail, which hinders the analysis/elucidation of the observed processes and changes (c) In general, the explosive decomposition of these systems requires (because of the high cohesive energies of the systems) irradiation at rather high laser fluences. As a result, there is high probability of multiphoton processes, or saturation phenomena etc, introducing additionally difficulties in understanding of the mechanisms.

1.4. CRYOGENIC FILMS

1.4.1. Advantages of study

It is well understood from the previous discussion that photodesorption/ablation is a complex phenomenon. The examination in polymer and MALDI substrates introduces additional parameters that further hinder the understanding of the mechanisms. It is obvious

that the detailed examination of the possible mechanisms to study molecular ejection demands the use of simpler molecular systems. The simplest systems would be solids of simple molecular/organic compounds. However, at normal temperatures simple molecules (e.g. NO H_2O, Benzene etc.) are either gaseous or in liquid. Thus, cryogenic or van der Waals solids/films of these compounds, i.e. solids formed by the condensation of vapors of those compounds on low temperature substrates are employed. The advantages of examining molecular photodesorption mechanims using van der Waals solids are presented.

First, the employed compounds have been studied extensively in the gas-phase, solution and in matrices (matrix isolation spectroscopy). The extensive information that is available about their photophysics/chemistry ensures that detailed interpretation and analysis of the experimental results can be attained.

Second, the interaction forces between these molecules are weak (van der Waals forces, dipole-dipole interaction). Mechanisms of energy transfer in these films are relatively simple (at least, in comparison with polymers and MALDI matrices) and thus easier to probe and characterize.

Third, and very importantly, mixed solids of different compounds can be prepared in various relative concentrations. This capability gives us the opportunity to change in a systematic way the physical and chemical properties of the film for examining the effect of these properties on the photodesorption and ablation processes. Indeed, as we present in this thesis, this approach enables “separation” of the stage of the energy absorption process from the ejection step and the systematic examination of each step “individually”. An example of this capability is given in chapters 3 and 4 of the Thesis.

Fourth, the structure of these solids can be varried in controlled way (either by deposition conditions or by thermal annealing) from highly amorphous to semicrystalline. This gives the capability on one hand, of preparing films of high optical quality (f.e. for monitoring processes via optical techniques-chapter 3) and on the other, of studying the influence of structure on material ejection process.

Finally, the study of cryogenic films is related directly with MALDI technique. Because of the similarity that present, as concern the physicochemical properties, with the matrices that are used in this technique, cryogenic films offer the ability of the examination of

the mechanims ejection of biomolecules. Indeed, studies have shown that the ablation of cryogenic films presents many similarities with MALDI effect. In conclusion van der Waals films/solids are ideal systems for the examination of the interaction mechanisms light-molecular solid state.

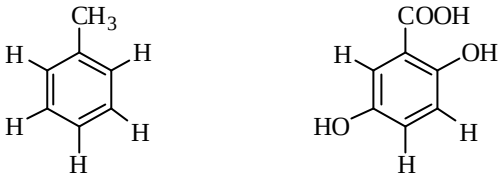

Figure 1-4 Toluene (left) and 2,5 dihydroxybenzoic acid (right)

1.4.2. Previous Studies on Cryogenic Films

At the middle of eighties '80 [36], there was intense interest in using techniques already developed for studying reactions and photofragmentation in the gas phase for the examination of the photophysics/chemistry of adsorbed molecules on cold surfaces (condensed molecules) [37]. The goal was to understand the photophysics of molecules in condensed phases and how this differentiates from that in the gas phase. In the framework of these studies [38-39], it was established that, *At very low fluences (£ 1mJ/cm^2 depending on adsorbate absorptivity) only fragments or excited molecules are observed to desorb, establishing the existence of molecular selectivity in the desorption process, i.e. only excited surface molecules may contribute to the desorption signal.* For example in a mixture of CH_2I_2 and NH_3[5], only CH_2I or I fragments are desorbed, while the desorption of NH_3 is negligible. At low laser fluences, the translational distribution (e.g. shape and $<E_{TRANS}>$) of the photodesorbed molecules/fragments is independent on laser fluence F_{LASER}, while the photodesorption yield increases linearly with F_{LASER}. The molecular ejection is generally a surface-mediated photodesorption, i.e., to the repulsion developed between a photoexcited state of a molecule and to neighborhood molecules. Additionally, in this case, because of the small number of desorbing particles, no collisions take place above the surface, and it was shown that the measured distributions correspond well to the initial translational energies of leaving particles.

[5] NH_3 does not absorb at 308 nm

At higher fluences and for thicker solids, the intense ejection of parent molecule has been generally observed and accordingly this phenomenon was named "explosive photodesorption". Furthermore, no molecular selectivity has been indicated in this fluence range. The translational energies are generally found to be very high, while the distributions are not well described by Maxwellian. Domen and Chuang [38] first suggested that "explosive photodesorption" is very similar to the photoablation of polymers. Furthermore, they suggest that it must be thermal in nature. Interestringly, in one systematic study of laser induced ejection from NO cryogenic solids [40], at high fluences the translational distributions were found to change, becoming faster and sharper. This change was attributed to the formation/development of supersonic beam due to the large amount of the desorbing material. No other mechanistic explanation was given for this change in the translational characteristics. However, as shown in chapter 5, this change in fact may be characteristic of UV ablation.

In a series of studies, Leone's group, examined the characteristics of the translational distributions and internal energy distributions of ablated molecules from cryogenic films [41-44]. In the explosive desorption of a number of solids [42], the vaporized molecules are found to be translationally fast (T_{trans} ³ 1000 °K) but vibrationally and rotationally cold (£ 200 °K). These results support the idea, that in ablation, molecular ejection has the characteristics of a supersonic beam, where because of the high number of collisions between the desorbed molecules in the plume, the internal energy (vibrations-rotations) of the molecules is transferred into translational degrees. Yet, collision-induced cooling could not explain all observables and the authors conclude that further parameters affect the translational distributions in the explosive desorption process.

In another series of studies [45-48], Leone and co-workers, have studied photoproduct formation in the UV ablation of photosensitive compounds. Most interestingly, for photosensitive compounds such as Cl_2, ICl, XeF_2, etc, they observed that the photolysis yield is very small, even the photolysis quantum yield of these compounds in the gas phase is almost 1. They observed efficient formation of recombination products (f.e., I_2, Cl_2 from ICl), suggesting extensive radical recombination. However, they were not able to establish the mechanisms for reactivity. Most interestingly, despite the observed reactivity, they do not support a photochemical mechanism of ablation and instead a photothermal mechanism is advanced.

Most important work has been reported by Braun and Hess on the ablation of C_6H_6 films induced by pulsed IR irradiation [49]. They found that the desorbate most probable translational energy (E_{TRANS}) does not increase monotonically with laser fluence (F_{LASER}), but, instead it shows a "phase-transition"-like dependence. The F_{LASER} range over which the characteristic "plateau" of the diagram appears corresponds to film temperatures that are suggestive of the solid-liquid transformation of the compound. In view of this result, ablation, at least in the IR spectral region, seems to be essentially photothermal in nature. Furthermore they suggested their observations may also hold for the UV-induced ablation of cryogenic films. However, we can argue first, that the correspondence between a E_{TRANS} vs F_{LASER} diagram with a (P,T) thermodynamic diagram is certainly not necessarily valid. Second, in fact the authors did not really specify the ablation threshold of the system, so it is not clear the relationship between the plateau and the ablation threshold. In fact, as discussed on pg. 27 Masuhara et al. [33] failed to find any correspondence between the ablative thresholds and the thermodynamic properties of the compounds. Sputtering efficiencies were suggested to correlate, instead, with the photochemical activity of the studied compounds.

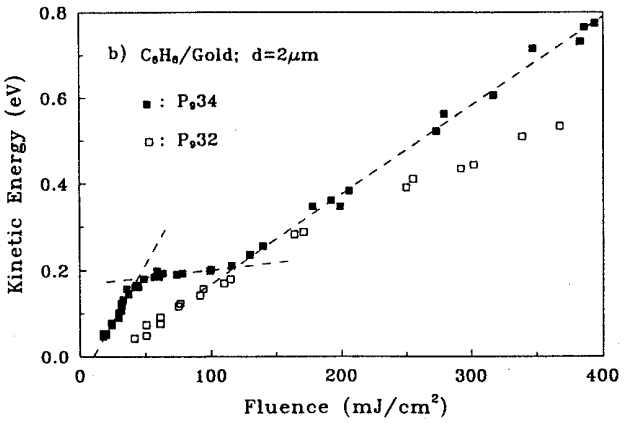

Figure 1-5 Kinetic energy as a function of incident laser fluence for benzene films. (Graph is from ref. [49])

Niino and coworkers have investigated the chemical reactivity of the intermediates produced in the ablation of solid films of photoreactive organic molecules [50,51]. To this end they have analyzed the ejected plume by optical techniques and have examined the reactivity of the ejected species with various surfaces/substrates (f.e. graphite). New compounds were shown to be formed on the graphite surface, indicating that the chemically activated species

that are produced by ablation may prove very useful for fabricating novel materials. Their studies generally strongly indicate the potential of the use of the cryogenic solids. However, aside from the potential for material processing, their mechanistic suggestions are generally indirect and thus we do not present in detail.

Finally, ejection fron frozen solutions doped with polymers have provided the basis of a novel deposition technique, Matrix Assisted Pulsed Laser Evaporation. Mechanistic studies from this group have been initiated only recently [52].

1.4.3. Scope and Outline of the Thesis

- The main objective of this thesis has been to examine if a physically significant criterion for defining/describing ablation can be established. Generally, the observation of intense material ejection is considered to be the main characteristic of the explosive desorption or Ablation. However, this observation doesn't give any information about the mechanisms of molecular ejection. To demostrate the problem, a typical curve of etching/ejection signal vs. F_{LASER} is illustrated for the case of the 248 nm irradiation of condensed films toluene in Fig. 1. The desorption signal is observed to increase sharply at » 100 mJ/cm^2, which may be considered to represent the ablation threshold. However, a closer examination indicates that the signal starts increasing already at a fluence of 45 mJ/cm^2. **This serves to illustrate that the specific value and even the existence of a well-defined threshold cannot be unambiguously ascertained.**

To address this question, the ejection efficiency of non-absorbing dopants dissolved within an absorbing matrix (toluene) is examined as a function of laser fluence. Since the dopants do not absorb at the irradiation wavelength, the desorption of dopants is characteristic of the nature of energy dissipation in the solid and of the subsequent dynamics of material ejection. (ejection process is clearly separated from the photoexcitation process) By employing dopants of different (inter-molecular) binding energies to the matrix, an assessment of the contribution of "thermal" vs. "non-thermal" processes is attained.

It is demonstrated that: *In the regime of explosive desorption, in fact, two fluence regimes with different material ejection mechanisms can be delineated. At the intermediate*

fluences, desorption is consistent with surface vaporization while at high fluences, molecular ejection is clearly different entailing the unselective ejection of a volume of material. Therfore the term "ablation" should be employed for denoting exclusively this regime. Criteria for the experimental identification of ablative regime is demonstrated.

The study is paralleled by optical monitoring of the morphological changes in the irradiation of the solids. By a combination of optical and imaging techniques, (homogeneous) bubble formation is shown. This is the first demonstration of melting and subsequent superheating of molecular systems in UV laser irradiation. In combination with the previous study shows that in the nanosecond case ablation is due to "explosive boiling" due to overheating of the film. Besides its importance for ablation/desorption mechanisms, the demonstration opens new ways for studying organic compounds in "unusual" metastable conditions. (f.e., electronic processes, photochemical processes, etc.)

- The second question concerns the nature and extent of the photochemical processes that take place in the ablation of molecular solids. This question is important in relationship with applications like laser cleaning and laser tissue interaction where evidently the nature of the induced photochemical modifications is crucial for the success of the techniques. But more importantly given the "unusual" conditions (f.e. high temperatures, formation of metastable liquids, high pressure, etc) it is important to examine how, photochemical processes in UV ablation differ from those taking place at the very low fluences where conventional photochemistry applies (surface-mediated processes). Thus, in contrast to the implicit assumption in all previous studies/models, (i.e. which assume a separation between thermal/photomechanical/photochemical mechanisms) , this is examines how electronic (photophysical) and chemical processes in the UV ablation are affected by these parallel contributions. In other words, how do you describe photochemical processes in the ablative regime.

To address this question the UV ablation of solids of the photosensitive compound has been used, namely Chlorobenzene. Upon excitation at 248 nm, C_6H_5Cl dissociates exclusively by scission of the C-Cl bond to yield C_6H_5 and Cl, which react with the precursor molecule to form a number of different products. Thus, the study of C_6H_5Cl films provides the possibility for examing reaction pathways/patterns in the UV ablation of molecular films.

A number of products is observed above vs. below the threshold, but it is demonstrated that this difference relates exclusively to the material ejection mechanisms. The observed photoproducts are fully consistent with the gas phase and solution chemistry of the compound. Thus, qualitatively, ablation does not modify molecular reactivity. It is shown that desorbate photoproducts are formed in the film before ejection and is limited by the time of the plume ejection. However, the formation of these products on the time scale of a single ablation event is inconsistent with the available rate cross sections. The discrepancy suggests "hot" reactivity of the fragments of the C_6H_5Cl photolysis. Preliminary study on the examination of deuterium effects on ablation and subsequent reactivity is also presented.

- Finally, a preliminary study of the UV desorption dynamics upon irradiation with 500 fs pulses is presented. The results clearly show that the laser pulse width has a pronounced effect on desorption dynamics (both above & below threshold), and will place a trigent test on theoretical models.

- Although, the study of the desorbate translational distributions was not an immediate objective of this study, nevertheless, the collected data provide novel information. In all examined neat solids an abrupt increase in the desorbate most probable velocities values is observed at the ablation threshold with distinctly different dependences of velocities on E_{LASER} observed in the fluence ranges above and below this point. *The change in the translational features is furthermore shown to be due to the transition from the subablation to the explosive desorption /ablation regime.*

Additionally, through the comparison of the systems with different desorption efficiencies of the dopants, it has been possible to separate at least qualitatively the influence of the gas-phase from that of processes in the solid. It is shown that in fact gas-phase effects is not as crucial/determining as that suggested by various models and in fact, a substantial contribution derives from the ejection process itself (in the solid).

- Finally, a preliminary study of the UV desorption dynamics upon irradiation with 500 fs pulses is presented. The results clearly show that the laser pulse width has a pronounced effect on desorption dynamics (both above & below threshold), and will place a trigent test on theoretical models.

2. EXPERIMENTAL

2.1. VACUUM APPARATUS

All experiments are performed in a home-built stainless steel ultra-high-vacuum (UHV) system consisting of three units. (a) The inlet system for the handling and introduction of the gases into the cell (b) The deposition cell for the growth of the solid. (c) The Mass spectrometer chamber where the ejected particles are detected. A schematic of the apparatus is depicted in Fig. 1. the deposition and spectrometer chambers are differentially pumped.

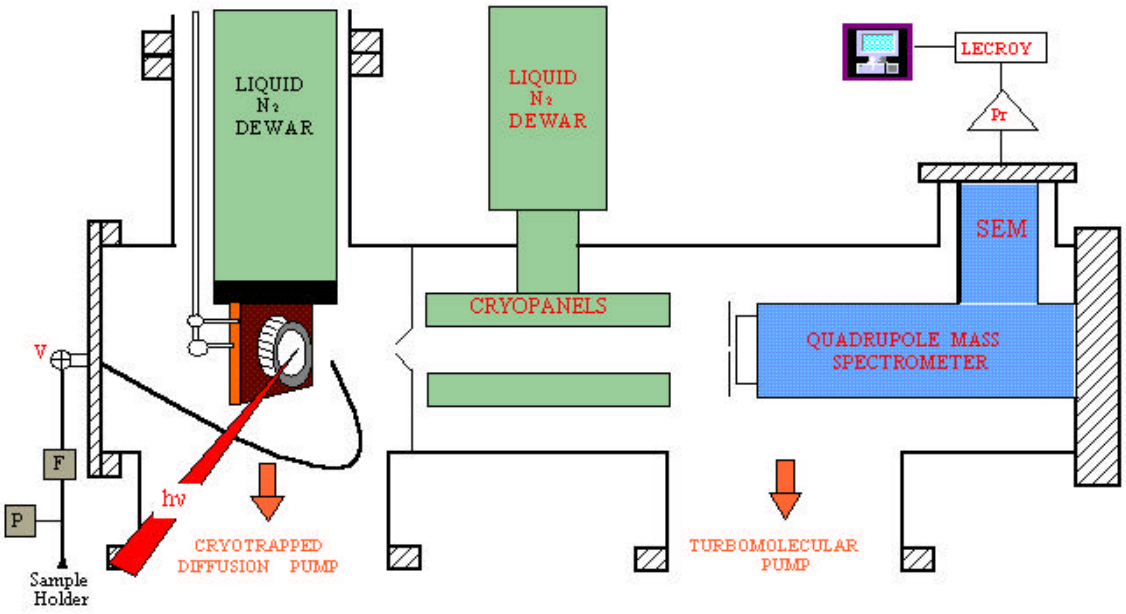

Figure 2-1 The vacuum experimental apparatus V (shutoff valve) F (finemetering valve) P (pressure gauge).

2.1.1. The Inlet System

The inlet system is fixed to the deposition cell. The system is equipped with three sample holders, a stainless steel tank for the gas mixing and a baratron pressure gauge. It is pumped to a background pressure of 10^{-5} Pa, by a turbomolecular pump (Alcatel). Pumping is necessary for removing humidity of atmosphere or remainings impurities that may react with the examined gases. For the same reason, the inlet system is subjected to baking (»300 °C) before every deposition procedure. Mixtures of gases are prepared by mixing vapors of the

compounds in the tank. Gas ratios in the tank are determined on the basis of the baratron pressure reading and the ideal gas law.

For deposition, the gases are introduced into the first chamber by a 1 mm ID stainless steel capilary tube positioned approximately 2 cm away from the center of the uv transparent glass substrate. The flow rate of gas is controlled with a needle valve. The use of the capilary tube is necessary for introducing the vapour with a flow highly directed to the one surface of substrate, thus most of the introduced gas condenses on this surface and the system remains at a low total pressure ($< 10^{-3}$ Pa). However in the case of the involatile (solid) compounds (adamantine and decapentane), their very low vapour pressure precludes the use of this approach. For this reason, in their case, introduction is achieved through the use of a solid-probe unit attached directly to the vacuum chamber. The pressure of the compound in the vacuum cell is adjusted to a pressure equal to that achieved for the volatile species in the case of the other mixtures.

All employed compounds are from Aldrich and Merck and are of high purity (99.5 % or better). In a typical experimental procedure, all samples are first subjected to further purification and for removing dissolved air via careful trap-to-trap distillation and repeated freeze-pump-thaw cycles.

2.1.2. The Deposition Cell

The deposition cell is pumped by a liquid nitrogen (LN_2) baffled 500 l/s diffusion pump (Edwards) and is separated from the mass spectrometer chamber by a 2 mm aperture located on axis. The presence of the aperture is necessary for the differential pumping of the two chambers and for protection of the detection system from the pressure increase during deposition process. The diffusion pump has been chosen because of its large pumping speed and its resistence to corrosion (since in our studies most of the examined samples are halo-derivatives which are extremely corrosive). However, the use of an oil-diffusion pump introduces the possibility that amounts of oil vapour will escape and contaminate the deposition cell. To avoid such problems, the operation of the pumping system is determined by an interlock electronic circuit as follows: a) Diffusion pump cannot be (warmed up) if first rotating pump is not turned on. b) The valve of diffusion pump cannot be opened unless

diffusion hasn't warmed up. Additionally the liquid nitrogen trap located above diffusion pump, traps any oil vapours escaping toward deposition cell. Finally the cell is equipped with a cold cathode pressure gauge (Edwards). The background pressure of the system is »5x10^{-6} Pa.

A copper frame (35 cm^2) holder attached to a LN_2 cryostat supports an UV-transparent substrate (supracil, 30 mm Æ) for the condensation of gases. Indium is fixed carefully between copper and supracil for attaining good thermal conductivity between them. In this way, the substrate is cooled down to 100-120 °K. The uncertainty in the temperature referrs to the temperature difference that may exist between the edge, (i.e, close to copper gasket) and at the center of the substrate. The temperature at the center (where irradiation is effected) has been measured by the thermocouple to be ≈120 °K. The supracil lies 10.5 cm from the apperture, which separates the deposition cell and the mass spectrometer chamber. The suprasil is positioned at an angle of è=75° to the axis of laser beam and è=15° according to the detection axis. This position has been chosen after many experimental tests for maximizing detected signal plume in ablation (ejected perpendicularly to the irradiated area) without obstructing the influence of the UV beam.

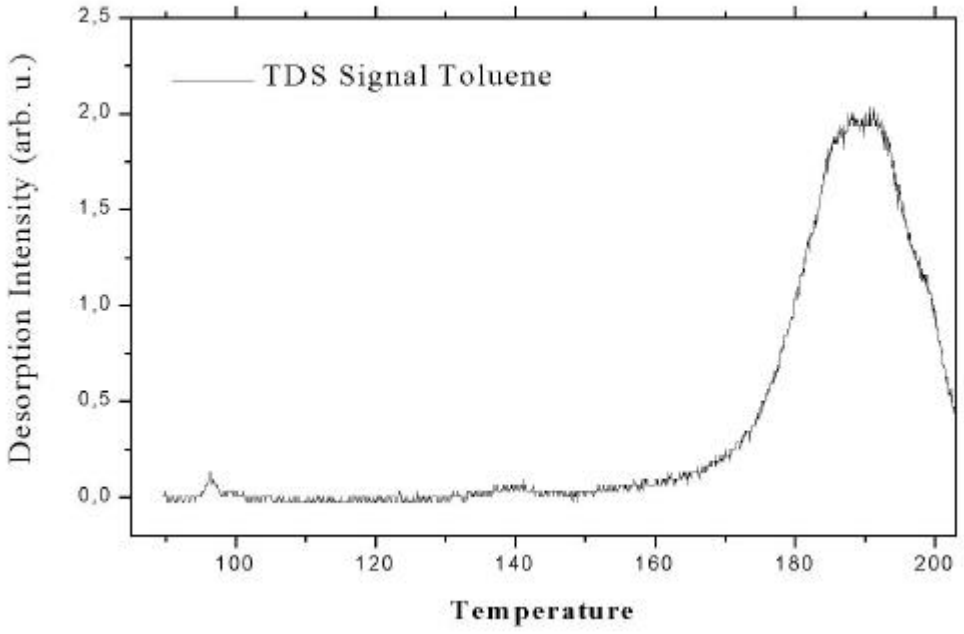

Figure 2-2 TDS spectrum of neat toluene.

For the Thermal Desorption Spectroscopy the copper holder is also equipped with a heater, and a thermocouple for the temperature measurement (Thermal desorption spectroscopy measurement). The heater is under computer control, so that a linear heating ramp from ~120 °K to 250 °K can be attained (i.e. T(t)=To+at). Probing of the desorption signal by the quadrupole mass spectrometer (described in the next sections) results in a TDS spectrum as a function of time, which can be then related to temperature (Fig. 2). The rising edge of the spectrum follows 0-order dependence : $-\frac{dN}{dt} = A\exp(-\mathrm{E}_{TDS} / RT)$ as expected for desorption from monolayers. The technique has been employed for establishing experimentally the binding energies of the analytes disolved within the toluene matrix (chapter 3).

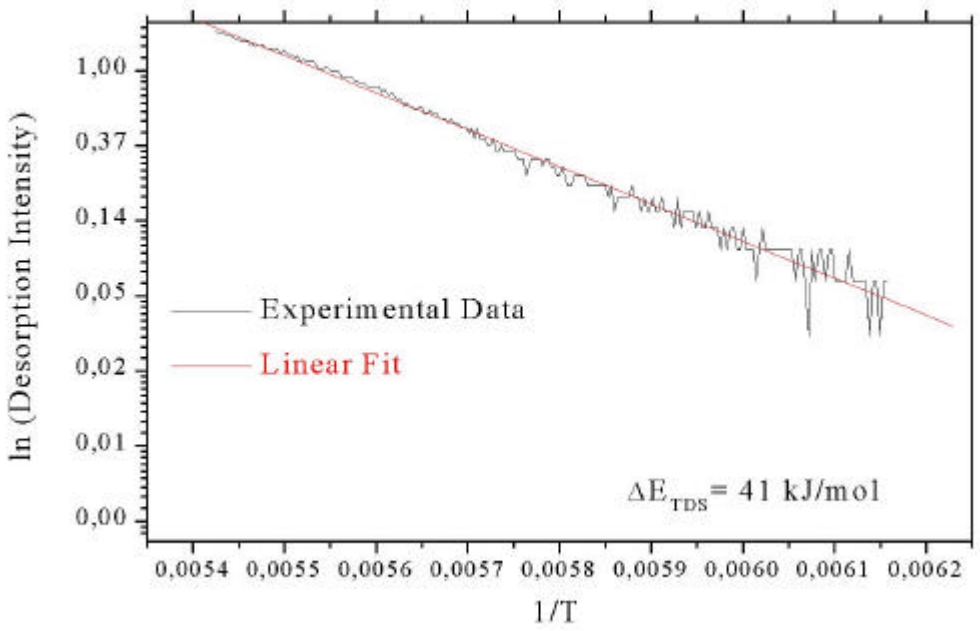

Figure 2-3 The Arrhenius (neat toluene) fit to the experimental data (Fig. 2-2)

2.1.3. The Deposition process

In a typical vapor condensation process, the substrate is cooled down to 100-120 °K. During gaseous exposure, the pressure in the vacuum chamber (≈4×10^{-3} Pa) is very carefully controlled throughout the deposition, since initial experiments indicated that the morphology

and crystalinity[6] of the solid is very sensitive to the pressure. Subsequently the system is pumped down to its base pressure ($5x10^{-6}$ Pa) before irradiation commences.

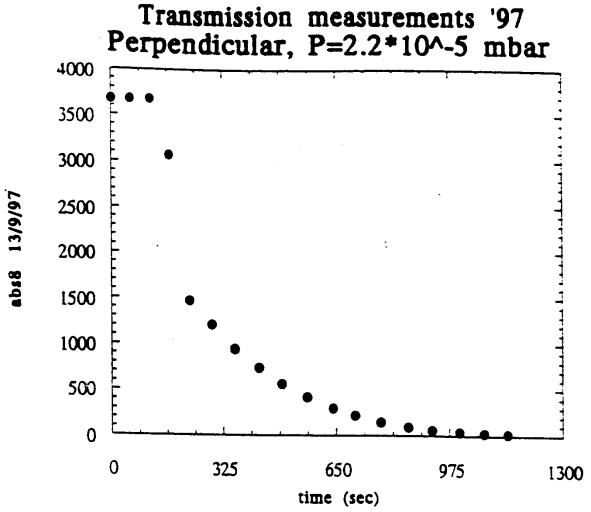

Figure 2-4 The graph depicts the change in the transmittance of the solid C_6H_5Cl, as a function of deposition time (the presence graph is for deposition at a pressure of $P_{dep}=2´10^{-5}$ mbar).

Because of using the capilary tube, the actual pressure between the tube and the deposition substrate differs from the pressure reading in the cold cathode gauge which is not located close to the substrate. Thus it is not accurate to estimate the solid thickness from kinetic theory of gas. Furthermore, this thickness can not be determined accurately from a measurement of the introduced gas quantity because not all introduced gas condenses on the substrate. For establishing the thickness of the solid, two different techniques have been used. The first is based on monitoring the absortpion of the solid at 248 nm. Fig. 4 illustrates the transmission of the solid during deposition at a P~$4x10^{-3}$ Pa as a function of time. According to Beer's law, the transmited light intensity is given by $I = Io\exp(-a\,x) = Io\exp(-a\,At)$ where Io is the incident intensity of the beam, and á is the absorption coefficient of the compound in the

[6] **We have found that indeed the structure of the solids can affect significantly both the desorption efficiencies of ablation and the translational distributions of the desorbates. We do not study these effects in this thesis, but because of this sensitivity, it is important to control very carefully the condensation process of the solid for having reproducible results. In fact we have found out that several difficulties noted in previous studies about explaining their results are not due to the phenomenon itself, but the fact that film deposition conditions were not carefully controlled. On the other hand, this sensitivity suggests that UV ablation may be eventually turn out to be a very sensitive "structural" diagnostic tool.**

irradiation wavelength and x the solid thickness[7]. The initial constant trasmision represents the actual cooling time for the substrate after filling the LN_2 Dewar plus the time for formation of a first well defined layer of the gas on the substrate (nucleation time).

The second examination technique is based on the phenomenon of the optical interference. A Uniphase He-Ne laser beam (ë=632,8 nm, an output power of 8 mW) is incident on the supracil surface at an angle of 4° off the surface normal. The laser beam is reflected from both the condensed solid/vacuum interface and the solid/supracil interface and the two beams interfere. As the molecular vapor condenses on the suprasil surface, because of the difference to the optical path, the interference signal (monitored by a photodiode) sinusoidally oscillated: $\frac{dx}{dt} = \frac{l}{2n\cos q \times \Delta t}$ where x is the solid thickness, n_f the index of refraction of the solid and è the incident angle and Ät is the oscillation period of the fringes (Fig. 5). For example for $4x10^{-3}$ Pa deposition pressure of toluene we find Ät to be 3.3 sec and for $5x10^{-4}$ Pa the Ät is 25 sec. The corresponding[8] rates are ca. 65 nm/sec for $4x10^{-3}$ Pa and 8.5 nm/sec for $5x10^{-4}$ Pa. In the Fig. 5 the difference in the width of the two first fringes corresponds to the initial time before the cooling/nucleation time noted before in the transmission experiments.

[7] For establishing the absorption coefficient of the solids of C_6H_6 and $C_6H_5CH_3$, similar experiments are performed in which deposition is effected via background gas dosing (i.e. a certain gas pressure is introduced in the cell without the using of the capilary tube) In that way the amount of the condensed material on the substrate can be calculated exactly. Assuming unit sticking probability, the time required for monolayer formation (1ML= 3.03×10^{14} molecules/cm^2) is $t = \frac{4}{n\bar{u}S}$ where n is the gas phase number density, $\bar{u}$ the average velocity and S the surface area per molecule. In all examined pressures we found good agreenment of the slope with the estimated from the kinetic gas theory rate, except in the case where the deposition take place in a low pressure ($<10^{-7}$ mbar), probably due to the competing condensation of the backround gases present in the vacuum system.

[8] The values for toluene are: n=1.496, è=4.8, ë=632.8 nm and Ät=3.3 sec

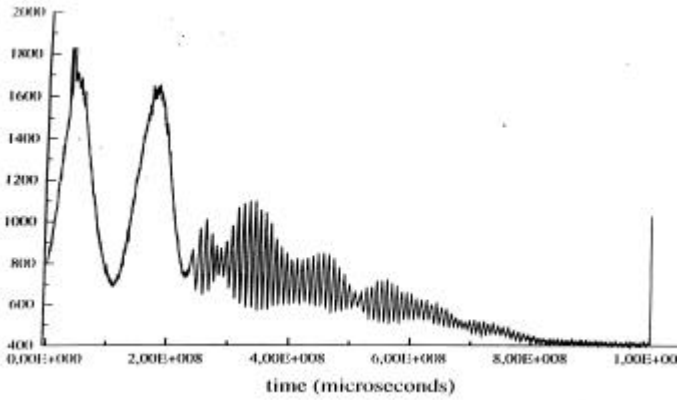

Figure 2-5 Reflected HeNe laser signal as a function of deposition time.

Using both techniques, we estimate that under deposition conditions that we use in our experiments (capilary tube and pressure of $2x10^{-3}$ Pa) the solid thickness (for 15 min deposition) is ~ 50-70 ìm. The optical penetration depth of the toluene is ~ 2.7 ìm, that is much less of the solid thickness. This means that the deposition substrate doesn't affect in any way the absorption process.

2.1.4. Mass spectrometer chamber

The desorbed/ejected particles are characterized by a quadrupole mass spectrometer QMS (Balzers QMG 311) housed in the second chamber [53]. The 2mm aperture that separates the QMS chamber from the desorption process limits the field of view from the irradiated area to the detector in the plane defined by the irradiation axis and the normal to the substrate under a solid angle of $7x10^{-5}$ðsr. The mass spectrometer chamber is pumped using a turbomolecular pump (Leybold lt./s), to a base pressure < 10^{-6} Pa. A set of LN_2 cryopanels are used to improve the vacuum in the detection chamber in order to decrease the noise and to avoid that off-axis particle will hit the walls and eventually will get into the mass specrometer (thus, resulting in time of flight spectra with wrong intensities, times and distributions). The pressure in the chamber is monitored by a hot cathode ion gauge.

2.1.4.1. *The Quadrupole Mass Spectrometer*

The Quadrupole mass spectrometer (QMS) consists of three parts, the ion source, the mass filter and the ion detector. The detection of a neutral particle in a quadrupole mass spectrometer may be divided into three processes. (a) The ionization of the incident particles by electron impact, a "cross-beam" ion source is used (i.e., emission of ionizing electrons perpendicularly to the axis of extraction of the ions) and its extraction and focusing from the ionization volume into the mass filter. (c) The transmission and mass-selection of the ions in the mass filter. (d) The detection of the ion.

2.1.4.2. *Optimization of Quadrupole Mass Spectrometer*

The QMS is a standard, commercial instrument. The commercial QMS instruments are optimized for high sensitivity in partial pressure measurements. Unfortunately, this mode of operation is claimed to be inappropriate for time-of-flight investigations. Serious distortions of the measured TOF can be avoided only by an optimized re-configuration and setting of the potentials of the instrument. The most systematic examination has been reported by Braun and Hess [54] and this was followed herein.

Considering first the ionization process in the ionization chamber (IC), the ionization probability P_{ion}, may be influenced by the electron current I_e and the electron energy eV_5. The integrated QMA signal in the laser induced desorption experiments, were found to be proportional to the electron emission current I_e in the IC, (as expected $I^+ = I_e n V P_{ion}$ where n is the number density, V the ionization volume. At high emission currents (depending on particle density in the IC), a tendency towards saturation in signal strength was observed and a broadening of the measured TOF distributions occured. The effect is due to space charge effects, which become important at excessive ion densities in the QMS. In our case I_e was set to 1 mA.

The electron (ionizing) energy eV_5 of 70eV has been used for most experiments in order to increase detection efficiency of the neutral particles. However, at this ionization/impact energy, the secondary fragmentation of the ions is rather extensive for the molecules we have studied (i.e. resulting in a distribution of ions with different masses). This complicates the detection and characterization of fragments and products emitted from the

laser-irradiated surface. Thus, in the study of the photosensitive C_6H_5Cl and CH_3I, the unambiguos identification of the fragments ejected from the surface calls for a highly reduced electron energy. To this end, the energy was reduced to 25 eV, a compromise between minimal e-impact fragmentation and sufficient ionization efficiency for detecting the ejected species.

Turning next to the ion extraction and focusing inside the mass filter, their efficiency depends on the ion extraction voltage V_1 the ion lens voltage V_2 and the ionization chamber voltage V_3. When the QMS is used in a molecular beam experiment as in our case, with the incident beam parallel to the z axis essentially, the extraction probability strongly depends on the location of ionization and the kinetic energy of the incident particles: the closer to the axis the neutrals are ionized, the higher is their probability of extraction. The extraction probability can formally be written as $P_{ext}(E_{kin}) \propto \int_0^{r_o} \int_{z_1}^{z_0} P_{ext}(E_{kin}, r, z) 2\pi r dr dz$ where r_o = 2.5 mm is the radius of IC inlet and z the distance parallel to the z-extraction axis. The voltages values of V_1, V_2 and V_3 were adjusted to the maximum signal level (i.e. maximum detection sensitivity) by systematic examination of the TOFs recorded in the laser desorption from C_6H_6 solids. Their values are given in Table 2.1 together with the other parameters/settings of the QMA.

Table 2-1 The Quadrupole Mass Spectrometer voltages values

V_1 (Volts)	V_2 (Volts)	V_3 (Volts)	V_4 (Volts)	V_5(Volts)	Deflector(Volts)
-168	47	55	46	70	-180

The transmission characteristics of the mass filter depend on various quantities such as the parameters of ion incidence at the inlet of the filter (IC parameters) and the mass resolution. The F.Axis voltage (V_4) multiplied by the elementary charge, is the nominal kinetic energy of the ions in the rod system. For the optimization of F.Axis voltage two aspects have to be considered. First, the ions have to remain in the filter for a minimum number of frequency ù periods to allow a mass separation. In that way, a lower limit value of V_4 can be determined. Second, focusing the ions in the outlet of the mass filter also depends on V_4. So, the value of V_4 should be chosen to obtain a maximum signal keeping in mind the first aspect. Concerning

the mass resolution, in all experiments reported in this work resolution was set to 300 for working at high mass scale 0-300 amu and a value over180 for the scale 0-100 amu.

2.1.4.3. Ion Deflection and Detection

After their selection in the mass filter the ions are detected by a channeltron. The channeltron is positioned perpendicularly to the mass filter axis in order to avoid noise from the laser irradiation or other electron or photon sources (ionization gauge, ion source). To this end, a cylindrical capacitor collector is used in deflect the ions to 90° degrees[9].

The channeltron (Galileo type CEM 4821G) operates in analoge mode with negative voltage for detection of the positive ions. Analogue CEMs produce a linear output up to about 10-20 % of the bias current. This is limited because the bias current supplies the electrons necessary to sustain the secondary emission process. Since CEM 4821G model has a 20 ìAmp bias current, the maximum linear output is of the order of 2-4 ìAmp. The dark current of CEM is measured to be 10^{-2}-10^{-3} pAmp. In the analogue mode, the gain of the CEM is calculated simply as $G = I_o/I_I$, where I_i is the input current (measured with Faraday collector)[10] and Io the output current as measured by CEM. As shown in Table 2.2 the gain is found to be log ($4.8\times10^{-7}/1.8\times10^{-12}$) =5.4 i.e., $G=10^{5.4}$ electrons/ion (at an applied -3 kV potential).

Table 2-2 The sensitivity of the Mass spectrometer

Preamplifier + CEM	9.6×10^{6} Volt/mbar
Electrometer + CEM	1 Amps/mbar
Electrometer + Faraday	4×10^{-6} Amps/mbar
Sensitivity of the QMS	2×10^{-5} Amps/mbar

[9] The ions, can be detected either with a Faraday collector and a Channeltron electron multiplier (CEM). In the simplest case, the ions strike a collector (metal plate) located on axis to the mass filter. The current that results is measured with a sensitive electrometer (617 Keithley). The limit of the measured current is bellow 10^{-12}Amp. For a typical pressure of 5×10^{-5} Pa is giving 1.8×10^{-12} Amp current. In this work Faraday collector was used only for measuring the gain of the CEM.

[10] The ion deflection voltage is adjusted for maximum signal at the CEM output. In our case a -180 V voltage is set. It is important to note that if the ion source potentials (Table 2.1) are changed the deflection voltage must be re-adjusted.

The resulting current is amplified on a fast current preamplifier (Keithley 427). Generally, values of gain 10^6 to 10^7 with 15 ìsec rise time were employed for recording TOF signal. The signal from the detector is recorded on a Lecroy LC9400 (250MHz) digital oscilloscope and sent to a computer for storing and further processing. A typical TOF curve is shown in Fig. 6.

The y-axis represents the output signal (in Volt) and the xaxis the time in sec (where t=0 corresponds to the time of the of the UV laser pulse determined by a photodiode.

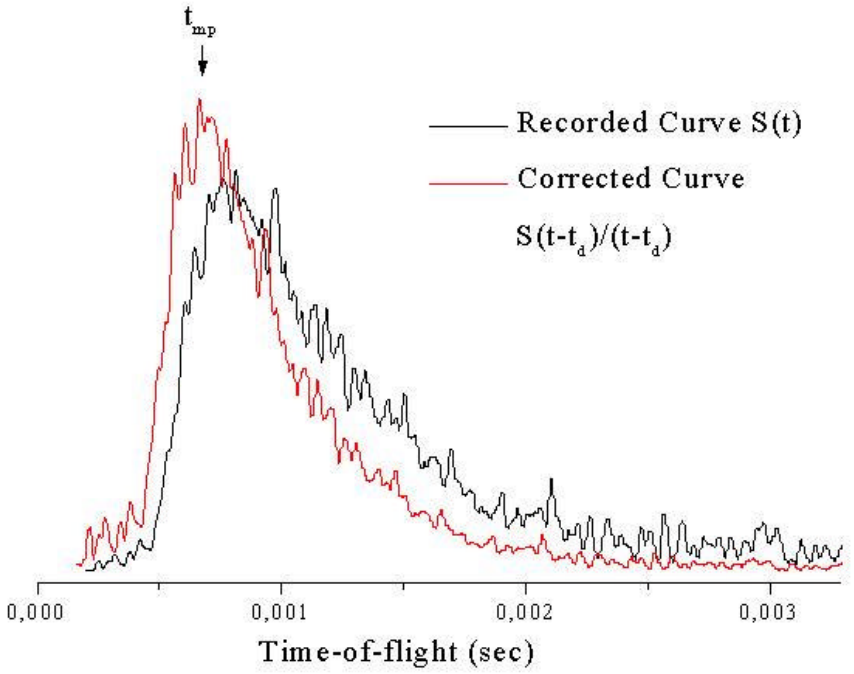

Figure 2-6 A typical time-of-flight spectrum. With the red line is the corrected for the drift time and ionization probability spectrum. The arrow indicates the most probable time.

2.1.5. Determination of the drift time

The measured time in the recording of a time-of-flight spectrum is a result of two terms, the free flight term, from condensed solid to the ion source of the mass spectrometer and the so-called drift time t_d i.e., the time spend the ions inside the mass filter. Because of the presence of fields, motion of the ion inside the quadrupole is not a free flight. So, the actual

time of flight distribution is obtained from the experimental TOF spectrum after substracting the drift time. The accurate determination of the drift time (t_d) is of great importance since a wrong drift-time correction may lead to an erroneous classification of the TOF distribution (e.g. Maxwellian or non-Maxwellian). Because of its complex mathematical description, drift time is better to be determined experimentally.

For the above reason, the multiphoton ionization signal of various molecules was temporally monitored by focusing the laser beam in the ion source of the mass spectrometer. The drift time is the delay between the detection of the ions and the laser pulse. The recorded signal is a symmetric curve, and its maximum gives the time of flight of the ions inside the mass spectrometer (drift time). The measurements have been done for a set of different molecules, in order to determine the dependence of drift time on molecular mass, in the two different mass scales, 0-100 and 0-300 amu. For two different values of electron energy has been used in the two cases (25 and 70 eV), the determined times are given in the Table 2.3

Table 2-3 The experimentaly detrmined drift time values

Mass Range / Electron Energy	25 eV	70 eV
0-100 amu	t_d=9.88+2.735$\sqrt{m}$	td=8+3.209$\sqrt{m}$
0-300 amu	t_t=12.433+2.746$\sqrt{m}$	td=7.612+3.284$\sqrt{m}$

Braun and Hess [54] using computer simulations (SIMION), suggest that the residence time of ions in the quadrupole filter can be approximated by $t_d = 7.5(ms) + \sqrt{mL^2/2e} \times \frac{1}{\sqrt{V_3^{ion} + \frac{E_{kin}}{e} - V_4}}$ where m and L denote the ion mass and the length of the filter and 7.5 ìs represents the time within the ionization chamber. Indeed for V_4=46 V, the formula gives $t_d = 7.5 + 2.586\sqrt{m}ms$ close to our experimental values.

2.1.6. Time and Energy Resolution

The velocity and thus translational energy resolution of the experiment depends on the distance from solid to mass spectrometer (L). The resolution increases with increasing length but on the other hand, since the solid angle of detection is inversely proportional to $1/L^2$ detection sensitivity decreases. Thus, an compromising value of distance from film to mass spec of L=28 cm was finally adopted.

The detection space is equal to the ion source length. The mass spectrometer cannot distinguish between the molecules that are inside the ion source and are ionized. Thus, the smaller increment of t that can be distinguished is Ät= Äx/u with Äx the ionization chamber length. Thus, translational velocity resolution is $\frac{\Delta u}{u} = \frac{\Delta x}{l} \Rightarrow \frac{\Delta E}{E} \propto (\frac{\Delta x}{l})^2$ which for typical TOF measured for the studied systems is ~ 1.6-6 ìsec. The time t is also affected by the time response of Channeltron, preamplifier and osciloscope. Since the time response of the channeltron is 8 nsec and the sampling rate of the oscilloscope > 0.5 msec/2500, whereas the time response of the preamplifier ~ 10-15 ìsec (for $G=10^7$) which thus is the limiting factor.

2.2. TOF ANALYSIS

This measured TOF spectrum (after correction for the drift time) does not represent yet the velocity distribution of the ejected particles, because the mass spectrometer is a "density" detector. As a result, faster molecules spend less time in the ionizer than slow molecules and are therefore less likely to be detected. We therefore refer to the signal S(t) as the TOF spectrum, not the TOF distribution. The TOF distribution is given by the flux I(t)=un(t) (density n weighted by velocity u), i.e., the number of molecules that pass through a certain area per unit time. The TOF distribution (flux versus time) $I(t)=un(t) \propto t^{-1}$ S(t) (Fig. 2.6) is converted to a velocity (or speed) distribution $P_u(u)$ by setting $I(t)dt=P_u(u)du$, and using $du/dt=x/t^2$ where x is the flight distance:$P_u(u)= t^2/x$ $I(t) \propto 1/u$ S(t) with t=x/u. Similarly, one obtains for the translational energy distribution $P_E(E_t)= t^3/m\ I(t)\} \propto 1/E_t$ S(t) with $t=x(m/2E_t)^{1/2}$.

The flux Maxwell-Boltzmann (MB) distribution differs from the density Maxwell Distribution by a prefactor u:

$$Pu(u)du = 1/2(\frac{m}{kT})^2 u^3 \exp(-\frac{mu^2}{2kT})du, \quad (1) \qquad P_E(E_t)dE_t = \frac{E_t}{(kT)^2}\exp(-\frac{E_t}{kT})dE_t$$

This distribution is called a "flux weighted" M-B distribution or (u^3) Maxwell distribution. For a density detector, it corresponds to the TOF spectrum $S(t) \propto \frac{1}{t^4}\exp(-\frac{b}{t^2})$ and for a flux detector, the TOF distribution is $I(t) \propto \frac{1}{t^5}\exp(-\frac{b}{t^2})$. The density ($u^2$) M-B distribution is characterized by $<E_t>=1.5$ kT and w = $(4/3)^{1/2} \approx 1.155$, while the flux weighted (u^3) M-B distribution has $<E>=2$ kT and w=1. Thermal desorption from a surface with unit sticking probability results in a flux weighted M-B distribution. Mean translational energies of desorbed species are therefore conventionally expressed as $<E_t>/2k_B$ which for a flux weighted M-B reduces to the translational temperature T_t.

An empirical formula that is frequently used to fit experimental velocity distributions is the so-called "modified" Maxwell-Boltzmann distribution $P_u(u)du \propto u^3 \exp(-\frac{m(u-uo)^2}{2kT})du$ which can be interpreted as a thermal distribution at temperature T, superimposed on a stream velocity u_o and reduces to Eq.(1) for $u_o=0$.

However, especially in the case of noisy experimental results, the fitting can be quite subjective. Second, in practice, usually it is found that just one "modified" Maxwell-Boltzmann distribution can not describe accurately distributions recorded in ablation. Thus, it is usualy to fit the experimental distributions to the sum of two-or-more Maxwell Boltzmann i.e., $J_u = \sum A_i u_i^3 \exp(\frac{-m(u-u_o)^2}{2kT})du$ but it is not at all clear what the physical meaning of the different components are. Finally, in many cases, good fitting is obtained only by making u_o negative. Of course, a negative u_o is difficult to be justified or it is just physically unreasonable. The fitting parameter u_o takes on negative values for distributions that are wider than a thermal distribution, obscuring the interpretention of u_o as a stream velocity.

2.2.1. The Detection Efficiency

The performance of the mass spectrometer in the usual residual gas detection mode is usually specified by the sensitivity factor K, defined from $I^+(t) = Kp = Kn(t)k_BT$ (where K Amp/Torr, k_B is the Boltzmann constant, and T is the chamber temperature, and P, n the pressure/density in the ion source). However, in the present case, the gas is sent through the ion source as a narrow, collimated gas beam and the performance of the instrument (Detection efficiency, D i.e., the number of the ionized particles which are detected per second per number of incident particles per second) must be specified in terms of flux $D = \frac{I^+}{eF}$ where I+ is the measured current, e the fundamental charge and F the flux. Because the flux is given by $F(t) = n(t) \times u \times A$ where õ is the velocity of the particle in the beam, n(t) the density and A the area of the beam, the D is given by $D = \frac{I^+}{en(t)uA}$ and in finale by $D = \frac{K}{ek_BTuA}$ where K is the sensitivity of the instrument.

In order to find K for the various compounds, their mass spectrometer signal (for gas "diffusely" introduced in the chamber) is monitored as function of pressure. Ion gauges are calibrated to the air. Because of that, the pressure reading is corrected for the sensitivity to compound (for toluene is 6.8). i.e. $P_{real} = \frac{P_{iongauge}}{6.8}$). The sensitivity factor (K) for the toluene has been found to be $(1.5 \pm 0.05) \times 10^7$ Volt/mbar.

$$n = \frac{P_{real}}{k_BT} \Rightarrow n(t)[\#/m^3] = \frac{Signal(t)[Volt]/K[Volt/Pa]}{k_B[J/K] \times T[K]}$$

$Signal(t)[Volt] = C[Volt/\#m^{-3}] \times n(t)[\#/m^3]$, for T_{vacuum} = 300 °K and where C is the calibration factor and correlated with the detection efficiency of the compound (f.e. for the case of toluene, the most widely used molecule in this thesis, the mean value of C is measured to be $(6.1 \pm 0.2) \times 10^{-16}$ Volt/#m^{-3}).

In the case of mixtures, the signals for the different molecules are corrected for the ionization/detection efficiency in the mass spectrometer vs. that of the matrix molecule (toluene). Given the importance of the measurements of the relative intensities of dopants vs. toluene for the arguments and conclusions of the work of chapters 4 and 5, considerable effort

was expended in establishing accurately the relative detection efficiencies (*at the parent peak, for each case*) of the mass spectrometer system for the various species (Table 2.4). To this end, two approaches have been employed, namely the examination of the pressure-dependence of the parent ion mass spectroscopic signals for various dopants, as well as comparison of the time-integrated mass signals for the introduction into the detection chamber of a given total pressure (as measured with the calibrated Baratron gauge), subsequently corrected for any pumping differences of the species in the mass spectrometer chamber. The two approaches gave results in good agreement, except for the difficult-to-pump D_2O.

Table 2-4 The relative to toluene efficiencies of the dopants

System	c-C_3H_6	C_6H_{12}	$(CH_3)_2O$	$C_{10}H_{22}$
Rel. Efficiency	2	1.3	1.9	10

2.2.1.1. Estimation of the Absolute Desorbing Amount

The total number of species leaving the surface from photodesorption process could be calculated given knowledge of the specie's angular distribution and the characteristics of the detection system. According to the previous, the mass spectroscopic signal S(t) relates to the flux of molecules F(t) through the ionizer as $S(t) = C \times \frac{F(t)}{u}$ where ũ is the molecular velocity in m/s. The differential yield of molecules N into the detector is the time integral over the flux distribution,

$$\frac{dN}{d\Omega} = \int n(t-t_d)\frac{l}{t-t_d}d(t-t_d) = \int \frac{S(t-t_d)(Volt)}{C(Volt/\#m^{-3})} \times \frac{l(m)}{(t-t_d)(s)}d(t-t_d) = \frac{l}{C} \times \int \frac{S(t-t_d)}{t-t_d}d(t-t_d)$$

where dÙ$_{det}$ is the solid angle of the detector as seen from the target surface and the transit time t_d of the ions through the mass filter, and l (=0.28 m) is the distance from target solid to the ionisation chamber and C the efficiency factor for the molecule. From the geometrical factors of the apparatus, the distance for target to separator and the diameter of the hole the solid angle of detection is found to be dÙ$_{det}$=7.5x10^{-5}ð srad. For the toluene the number of molecules in the solid angle of detection is given by $Int \times 4.7 \times 10^{14} \#/m^2$. The angular flux distributions for species leaving the surface follows typically a cos^{n}è form. The angular

distribution $P(J) = [(n+1)/2p\,]N_{tot}\cos^n J$ is normalizing for the hemisphere above the surface to yield the total number of species leaving, $N_{tot} = \int P(J)d\Omega$. The differential Yield is $N(J) = \frac{dN}{d\Omega} = Int \times \frac{l}{C} = P(J)d\Omega_{\det}$. The total number of molecules leaving the surface can be calculated from $N_{tot}(\#/m^2) = \frac{Int \times 4.7 \times 10^{14}}{(n+1)\cos^n J d\Omega / 2p}$. If we assume a thermal desorption process, the n=1 and N_{tot}=Int(Volt)´6.5´10^{18} #/m^2Volt. For ablation conditions, the angular distribution has been found to be more peaked to the normal to the surface and n=4 to n=8. (Assuming that the molecules are ejected into a 45 degrees cone, consistent with observations of Cho et al. [55], which suggest that the distributions are peaked toward normal.)

2.3. THE LASER SYSTEMS

In the nanosecond experiments, desorption is effected with the output of a KrF excimer laser (Lambda Physik Compex 110, 248 nm). The FWHM of the beam is 30 nsec, with peak at 18 nsec. The laser beam shaped by an iris and is focused weakly with a quartz lens (f.l. = 50 cm) onto the sample. Laser fluence is varied by adjusting the discharge voltage of the laser (21-30 kVolt) or by using filters and attenuators. A joulemeter (Molektron JPL 4050 10.1 V/J) was used for measuring the energy of the incident laser beam. On average, pulse-to-pulse fluctuation in the laser output is 5 %. The experiments reported herein are performed at fixed laser incident and detection angles (approximately 75° and 15° with respect to the normal to the surface). Reported fluence values are uncorrected for the light scattering at the solid surface. The analysis of the transmission experiments indicate scattering losses for most compounds to be 15-20 % of the incident light.

Femtosecond laser pulses were obtained from a hybrid excimer-dye laser system based on the concept of the distributed feedback dye laser (DFDL). Specifically, the 308 nm (XeCl) output of a double-cavity excimer laser (Lambda Physik EMG 150MSC) pumps a cascade of dye laser modules to produce pulses 0.5 ps long at 497 nm with an approximate energy of 100 ìJ. This seeding pulse is frequency doubled in a BBO crystal and amplified in a double pass through a KrF filling in the second cavity of the excimer unit. The resulting UV laser beam at

248 nm, has a bandwidth of 20 meV or 160 cm^{-1}. The FWHM pulse duration is typically 500 fs, and the output energy was 9 mJ/pulse.

2.4. OPTICAL IMAGING EXPERIMENT

Optical/imaging techniques have been employed for monitoring the morphological/structural changes of the solid during irradiation. To this end, a cw He-Ne laser beam (ë=632.8 nm, Uniphase, ~3-5 mW) is used to probe the spatial and temporal evolution of the film reflectivity and/or transmission upon UV irradiation.

The HeNe beam is shaped by via a pinhole and then is carefully aligned within the UV-irradiated area of the film (in those experiments, the UV beam was weakly focused to an area of 0.63 cm^2) at an angle of 8 degrees with respect to the normal of the solid surface. The reflected and transmitted beams are detected by either a fast photodiode ($ô_{res}$»1nsec, for establishing the temporal evolution together with a fast 400 MHz osciloscope) or CCD (578x365 pixels) / ICCD (1024x256, Andor) (for probing spatial changes) (chapter 3).

The ICCD camera is a combination of an Image Intensifier together with a CCD camera. Amplification can be up to 10^4. The gating can be achieved by switching on/off the voltage of the photocathode. Gating periods as short as 5 to 10 ns can be achieved.

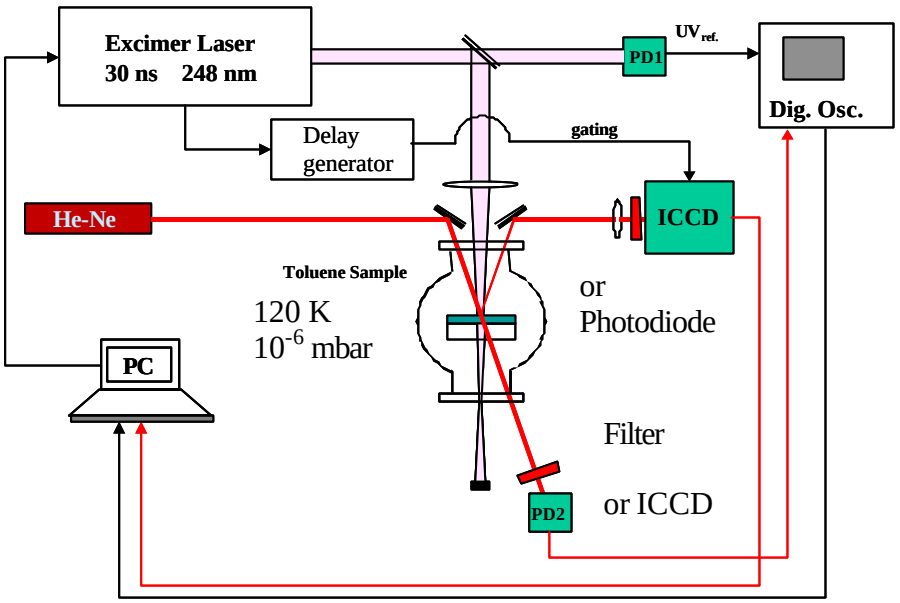

Figure 2-7 The optical/imaging experimental setup.

The synchronization of the ICCD gate trigger with respect to the UV pump pulse was achieved by SRS (Stanford Research Systems) delay generator. The SRS triggers the Excimer laser and after a variable delay the ICCD. The interval of gating (e.g. the ICCD collects photons) is set by a third pulse. In the experiments 30 to 100 ns have been used as gating periods ($Ät_{gate}$). Both transients photodiode signal and detected images was sent to a computer for recording and analysis. A standard commercial software (AndorMCD) is employed for the processing and analysis of the recorded images.

3. THE THERMAL NATURE OF EJECTION AT LOW LASER FLUENCES

3.1. INTRODUCTION

In order to elucidate the ejection mechanisms taking place upon uv laser irradiation, we have undertaken the comparative examination of the desorption efficiencies of *non-absorbing* dopants of varying binding energies[11] to the matrix as a function of laser irradiation parameters. Essentially, in the comparison, the particularities of the excitation step(s) remain the same (factored out), so that the relative ejection efficiencies of the dopants provide information on the nature of the energy dissipation in the film and of the mechanisms by which it results in material ejection (f.e. for surface vaporization process the desorption efficiencies should correlate with the binding energies of the dopants to the matrix). To this end, the employed dopants are chemically similar, differing only in their molecular size and strength of interaction with the matrix. The dopants include: alkanes (c-C_3H_6, c-C_6H_{12}, $C_{10}H_{22}$), and indicatively ethers/alcohols $(CH_3)_2(CH2)_nO$, D_2O. As a matrix we employ $C_6H_5CH_3$. It is selected because of the extensive thermodynamic and spectroscopic information available for the compound and second because of its minimal fragmentation, thereby avoiding complications due to any photoreactivity. Furthermore, it presents close analogies to the compounds employed as matrices in MALDI.

The study is paralleled by optical monitoring of the morphological/structural changes induced in the irradiation of the solids. By a combination of transient/static optical and imaging techniques, it is shown that melting of the solids occurs and at higher fluences, the (homogeneous) bubble formation is demonstrated.

3.2. RESULTS

The experimental results are organized into two sections. In section 3.2.1, the mass spectroscopic and optical/imaging examination in the irradiation of neat $C_6H_5CH_3$ solids are presented. In 3.2.2, the ejection dynamics of dopants of varying binding energies incorporated within $C_6H_5CH_3$ matrices are presented.

[11] For convenience, sometimes the terms “volatile” and “nonvolatile” are used; however, it is understood that it is really the relative binding energy to the toluene matrix.

3.2.1. Neat Toluene Solid

3.2.1.1. Fluence dependence of the desorption Signal

Toluene is a moderately strong absorber[12] at 248 nm. Fig. 1 depicts the desorption intensity of $C_6H_5CH_3$ recorded in the irradiation of neat solid of the compound as a function of laser fluence. In the figure, the values indicated for fluences > 80 mJ/cm^2 represent the signal recorded in the very first pulse from freshly deposited solid. At lower fluences, the signal is an average of less than 10 pulses because of the low S/N ratio[13]. Assuming that the etching depth follows the laser energy deposition and this is given by Beer's law, the total number of the ejected species has been suggested to be described by

$$N = N_o \times \ln(\frac{F_{LASER}}{F_{thr}}) \quad (3.1)$$

where No is the number of molecules in the irradiation volume and F_{thr} the laser fluence threshold. According to this, the ablation threshold for neat $C_6H_5CH_3$ films is at ~100 mJ/cm^2. However, as discussed in section 1.4, it is very difficult to consider this value in any certainty and easily » 45 mJ/cm^2 could be adopted instead.

---

[12] Although toluene is a spectroscopically well-characterized molecule, there was no accurate absorption coefficient value for the compound in the solid in the literature. Therefore, in situ measurements were performed, as described in chapter 2. The absorption coefficient of the compound was found to be » 3800 cm^{-1}. This value is somewhat larger than that reported in the liquid phase (2400 cm^{-1}) of the compound. Such a deviation was expected, as a similar difference has been reported in the case of benzene where the absorption coefficient increases upon the solidification of the compound. The increase has been related to the perturbation of the excited state, in the solid as compared with that in liquid.

[13] In the inset the graph illustrates the desorption yield as function of laser fluence at very low (F_{LASER} < 45 mJ/cm^2) and intermediated low (45 mJ/cm^2 < F_{LASER} < 100 mJ/cm^2) regimes.

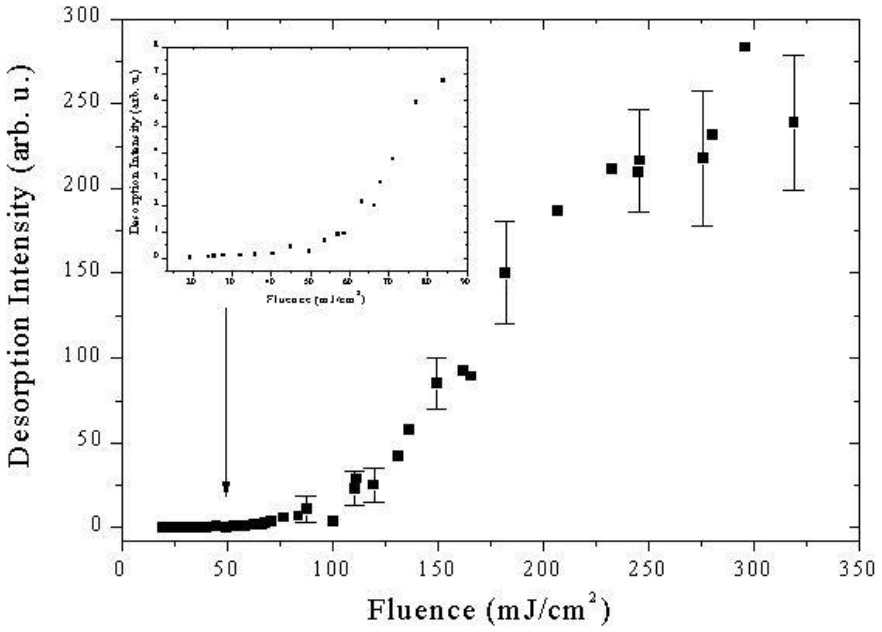

Figure 3-1 The Desorption Intensity of $C_6H_5CH_3$ recorded from freshly deposited solids as a function of the incident laser fluence. The error bars represent 2σ, as determined from at least 6-7 different measurements of each datum point. The inset depicts in higher detail the dependence observed at low laser fluences.

In fact, plotting the data of Fig. 1 in a semi logarithmic format (Fig. 2) as a function of $1/F_{LASER}$ illustrates that below the indicated threshold, the desorption intensity exhibits two regimes. In the 20-45 mJ/cm^2 range, the intensity has a very weak dependence on fluence, which increases abruptly at 45-100 mJ/cm^2. Based on this apparent change of the desorption intensity, the ablation threshold could be argued to be at 45 mJ/cm^2.[14]

[14] The change in the F_{LASER}-dependence of the desorption yield at 45 mJ/cm^2 is accompanied by different dependences of the desorption signals of $C_6H_5CH_3$ on number of successive laser pulses irradiating the film. Below 45 mJ/cm^2, the signal generally remains relatively constant with successive laser pulses, although because of low S/N, signal had to be averaged over at least 20-30 pulses. In contrast, at fluences 45-100 mJ/cm^2, generally the signal drops subsequently after the few first pulses to obtain a constant value. At much higher fluences (i.e. above 100 mJ/cm^2) the previous dependence becomes more pronounced. This effect is observed not only in the mass spectrometer signal, but also in the total desorption intensity measured by an open ionization gauge placed across the irradiated area. As it is indicated by the optical examination, this dependence may be due to the effect of laser irradiation on the morphology of the film.

However, as demonstrated in the subsequent sections, the comparative examination of the ejection efficiencies of dopants does establish that the threshold is at 100 mJ/cm^2. The observed increase in the signal at 45 mJ/cm^2 is instead related to the phase transformation namely melting, that the solid undergoes in the irradiation at the low fluence regime (20-45 mJ/cm^2).

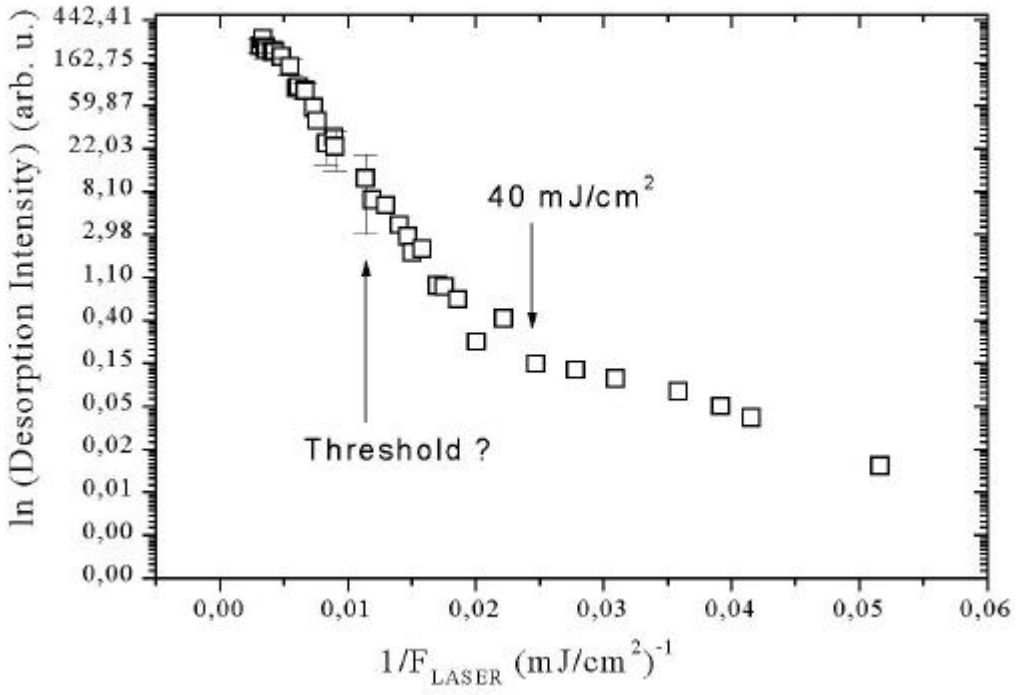

Figure 3-2 Semi logarithmic plot of the desorption intensity depicted in the Fig. 3.1 as a function of $1/F_{LASER}$.

3.2.1.2. Optical/Imaging Examination

As shown in the Discussion, the F_{LASER} (40 mJ/cm^2) at which the change in the desorption intensity dependence is observed corresponds to a temperature close to the melting point of toluene. Thus, at higher fluences the solid may melt, suggesting that it should be subject to morphological changes. To probe these changes, we take advantage of the fact that under carefully-controlled deposition conditions (condensation temperature 100-120 °K), $C_6H_5CH_3$ forms a highly transparent solid in the visible. Thus, any changes in the morphology

of the solid effected by the uv irradiation can be probed via optical and imaging of the reflected and/or transmitted portion of a He-Ne laser beam incident on the solid.

Fig. 3 shows the image of the transmitted probing beam (633 nm) through the toluene solid, recorded well after the UV laser pulse (> 1sec). At very low fluences < 35 mJ/cm^2, no noticeable changes in the images are observed, even after extensive irradiation of the film (>2000 pulses Fig. 3(left)). In contrast, at ≈45 mJ/cm^2 and above, changes and increasing opacity are observed in the irradiated area (Fig. 3(right) recorded following irradiation with 50 UV pulses at F_{LASER}» 60 mJ/cm^2)[15].

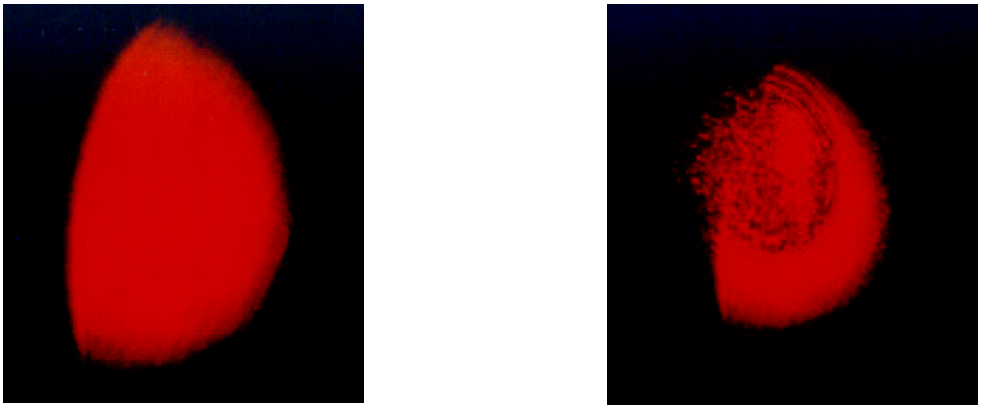

Figure 3-3 Transmission images of HeNe beam on $C_6H_5CH_3$ films that have been irradiated with (left) 2000 pulses at F_{LASER} < 45 mJ/cm^2, (right) 50 pulses at F_{LASER} » 60 mJ/cm^2. For recording the images, the left portion of the HeNe beam is blocked in order to more clearly illustrate the scattering effect

[15] These structural changes evidently do not relate to the formation of "etching pit" expected in ablation. Formation of an etching pit is evident only at fluences well over 100 mJ/cm^2 and although some isolated dark spots can be detected within this pit, most of it remains transparent. The appearance of the spot does not change much even after several number of pulses, thus contrasting the case of irradiation at low laser fluences where the accumulative effect of irradiation results in a highly "opaque" appearance.

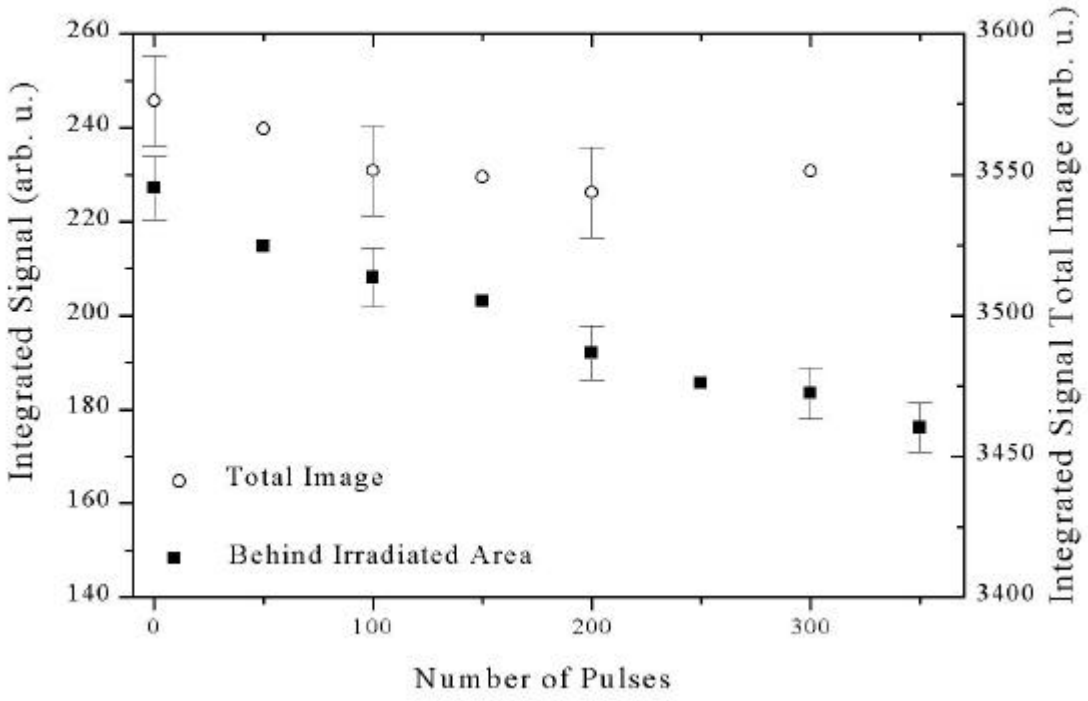

Figure 3-4 Integrated light transmitted intensity behind the irradiated area in the images as a function of successive laser pulses.

For the quantitative analysis, the total photon intensity (luminescence) in the images is plotted as a function of number of successive laser pulses (Fig. 4), along with the light intensity transmitted exactly behind the center of the irradiated spot. The total photon intenisty is established by direct integration of the total light (i.e., over the whole detected area) in the CCD images. With continuing irradiation, the transmitted signal through the irradiated area decreases down to its 70 percent of its initial value (depending on the UV laser fluence), whereas the total luminescence decreases much less. Thus, the decrease in the directly transmitted light intensity correlates with an increase in the totally, diffusely scattered intensity, around the UV-irradiated area. This conclusively demonstrates that the changes in the HeNe probing are due to scattering effects and not to the formation of absorbing photoproducts. This is further supported by the failure to detect any photoproducts by the mass spectroscopy (chapter 4 page 100)

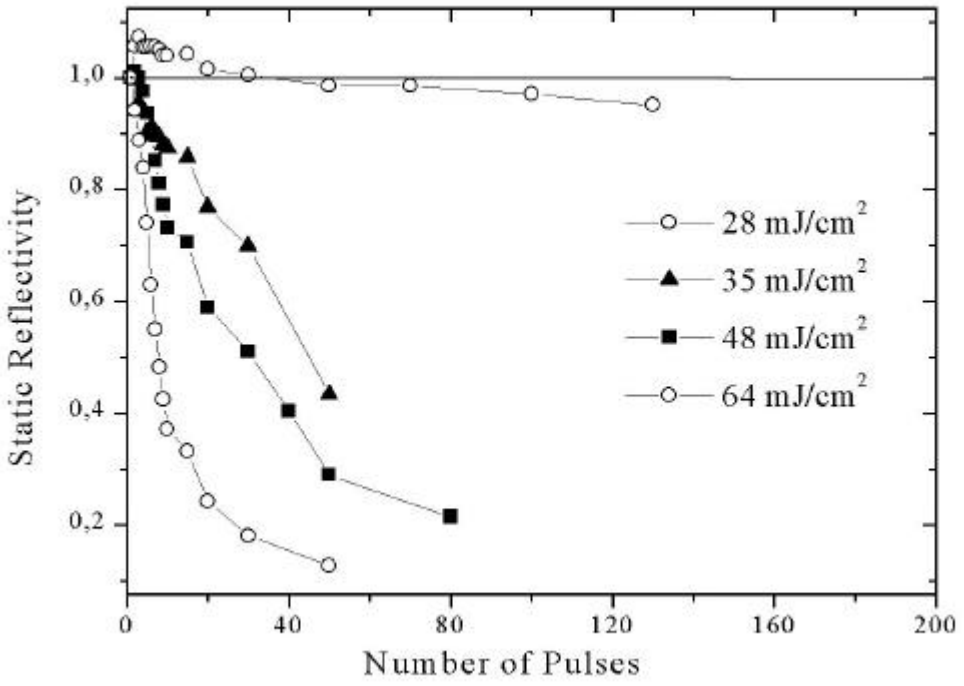

Figure 3-5 The graph depicts the permanent changes in reflectivity as a function of number of succesive laser pulses.

Similar changes are also noted in probing the specularly reflected HeNe beam (monitored by a photodiode), though the dependence on number of pulses is somewhat more pronounced (Fig. 5). This enhancement is due, evidently to the higher sensitivity of the reflected beam to surface modification. In particular, for irradiation at very low fluences ($\lesssim$30-40 mJ/cm^2), the surface sensitivity of the reflection probing reveals a change not observable in the transmission examination, namely a small signal increase in the very first few UV laser pulses. This clearly indicates that different processes operate below and above ~ 30-40 mJ/cm^2. This increase is probably indicative of partial annealing of the solid upon irradiation at low UV laser fluences and will be very interesting to be studied in the future[16].

[16] Laser annealing is very important both scientifically and for applications in the case of semiconductors. In the case of organic/molecular systems, as far as we know, these has been only one relevant study.

Temporal evolution

Fig. 3.6 and Fig. 3.7 illustrate the temporally-resolved HeNe laser transmitted and reflected signals (recorded by a fast photodiode) upon irradiation of the solid with the UV laser pulse. At fluences > 50 mJ/cm^2, a sharp minimum in the transmitted through the film beam peaking at t=60 ns to ~ 120 ns (respectively at 60 to 100 mJ/cm^2)is detected. Fig. 3.8 portrays the corresponding image recorded after 100 nsec (integrating time:100-180 ns) after the UV laser pulse (F_{LASER}=80 mJ/cm^2). The transient image is substracted from the initial background (static) image of the transmitted HeNe laser beam which illustrates enhansed scattering at the periphery of the UV irradiated area. In fact, the transmission loss is compensated, in the largest percentage, by an increase in the reflected signal (Fig. 3.7). It is noted that the increase does not reflect an increase in the specular reflection, but in the backscattered stray light collected by the mirror/lens (Fig. 2.7) (as established by the examination by images recorded in reflection mode). The nearly quantitative compensation clearly establishes that the changes are due to light scattering effects.

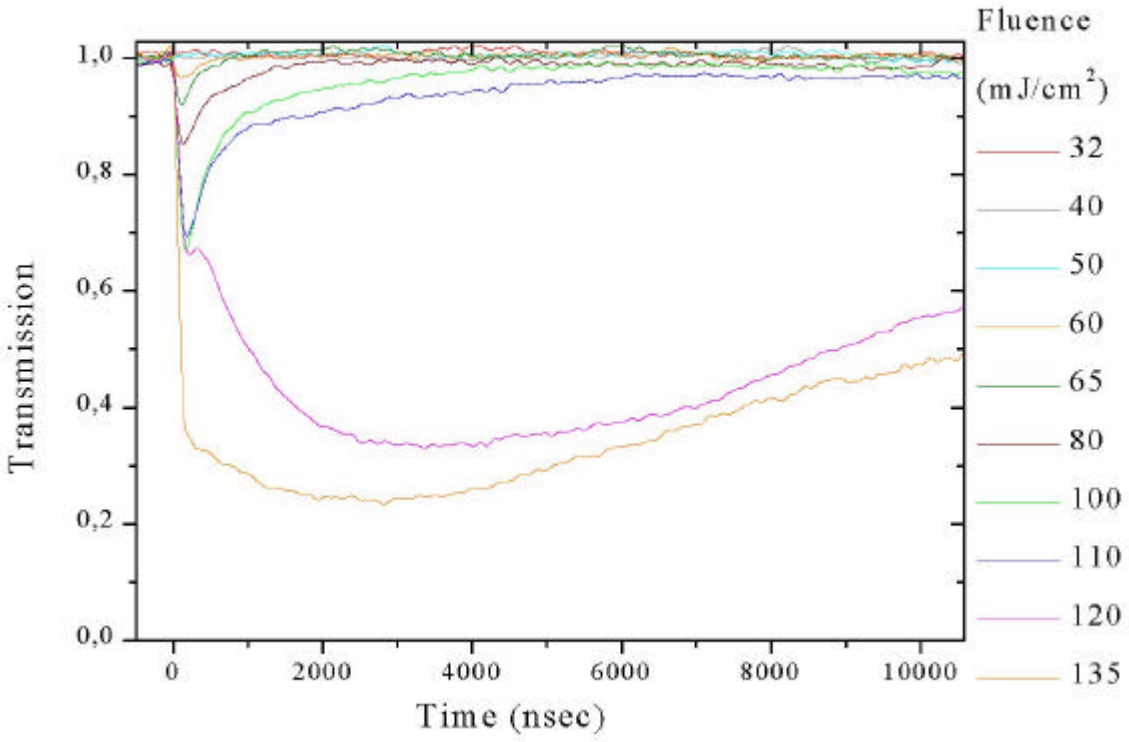

Figure 3-6 Time resolved transmission at ë=633 nm upon irradiation of the films with 1 UV pulse at the indicated fluences. The signal has been normalized to the transmitted intensity before the UV pulses.

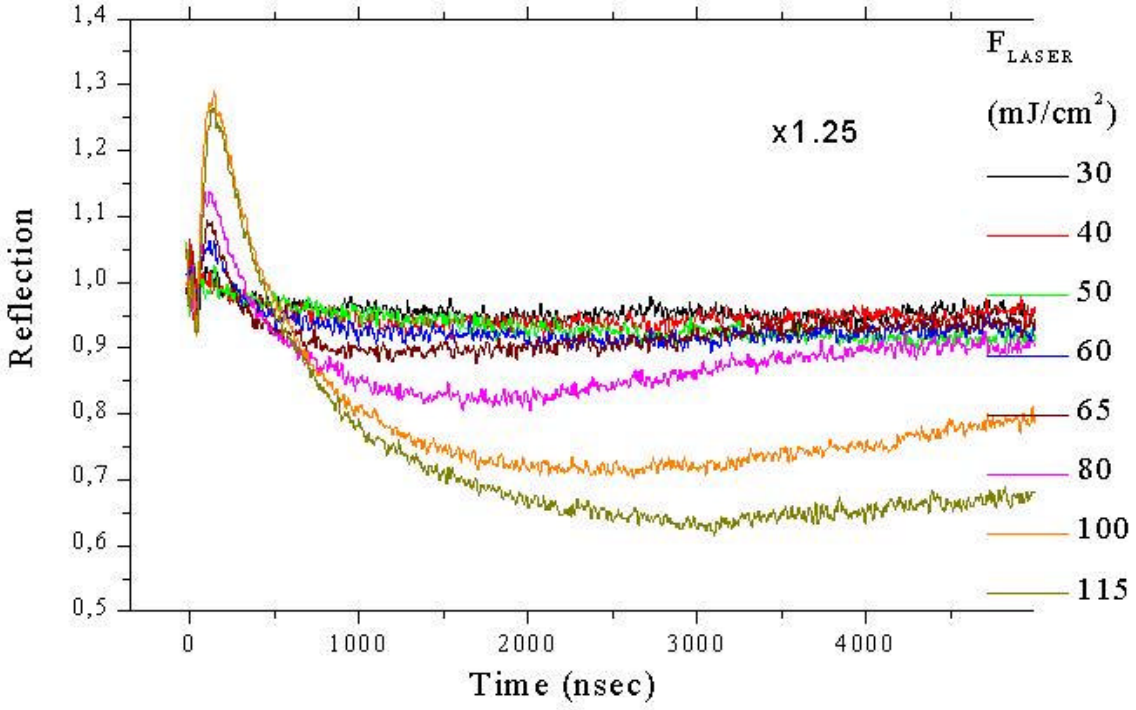

Figure 3-7 Time resolved reflectivity at ë=633 nm upon irradiation of the films with 1 UV pulse at the indicated fluences. The signal has been normalized to the reflected intensity before the UV pulses.

With increasing UV laser fluence, the curves broaden, the maximum is attained at higher times and the intensity changes are more pronounced. At longer times (t >1 ìsec), the transmission signal recovers to nearly its initial value. In contrast, the surface sensitivity of reflectivity provides further information on the subsequent evolution: thus upon recovering it overshoots its initial value and continues to drop (i.e., scattering loss) which evidently correlates with the reflectivity loss observed in the pulse examination (Fig. 5).

At fluences above 110 mJ/cm^2, the features of the transients evidently change. As shown below, this is the ablative regime, thus, the features in this case are due to scattering of the HeNe probing light by the plume (ejected material)[17]. The most interesting however feature

[17] **The very abrupt change in the shape of the curves on going from 100 mJ/cm^2 to 110**

is the curve recorded at just the threshold. In this curve, the evolution from low fluences to the ablative regime is uniquely demonstrated.

.

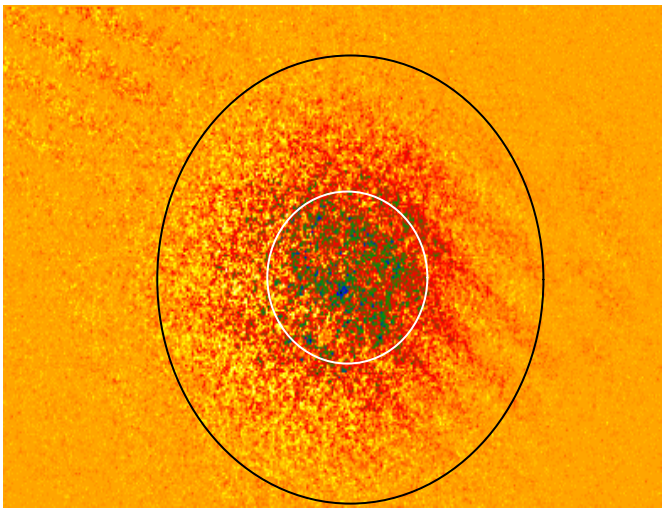

Figure 3-8 Transient Image of the of the transmitted HeNe beam.

The previous results conclusively demo nstrate the formation and decay of "scatterers", which as discussed below can be identified with homogeneously formed gaseous bubbles within the irradiated film[18].

3.2.2. Mass Spectroscopic Examination of Mixture Solids

In this section, we present the ejection dynamics of dopants from the toluene matrix in the UV irradiation. Fig. 9(a) depicts the desorption yields of dimethylether ($(CH_3)_2O$) and toluene in the irradiation of the $C_6H_5CH_3/(CH_3)_2O$ (5:1 molar). For a more clear depiction of

mJ/cm2 clearly demonstrates the presence of a well-defined threshold for massive material ejection to occur. This aspect is addressed in chapter 4.

[18] Quantitative information about the size and number of the bubbles from the scattering experiments is not directly plausible very unreliable (since no callibration system can be defined). As a first step, an interferometric measurement has been attempted. (Michelson type) Although, the vacuum systems were not designed for this high mechanical stability required for interferometric measurements, interference pattern changes could be monitored; thus, this approach will enable quantification of the effective bubble size.

the dependencies, the data in Fig. 9 are replotted in Fig. 10, as the percent concentration of the dopant measured in the plume (i.e. gas phase) *(in all cases signals have been corrected for the different ionization/detection efficiencies by procedures 2.2.1).* As shown in Figures (9), (10), a $(CH_3)_2O$ high signal is detected even at the lowest fluences and its signal increases further with increasing laser fluence. In fact, for fluences up to ~ 120 mJ/cm^2 its desorption yield is higher than that of $C_6H_5CH_3$, although its concentration in the film is only 1/5 of the matrix. Only at fluences above 120 mJ/cm^2, $C_6H_5CH_3$ desorption is enhanced over that of the dopant, until finally its relative ratio to that of the dopant becomes, within the experimental error, representative of the stoichiometry in the initial mixture. Exactly similar dependence is observed for cyclopropane (c-C_3H_6) and CH_3OH inside Toluene matrices.

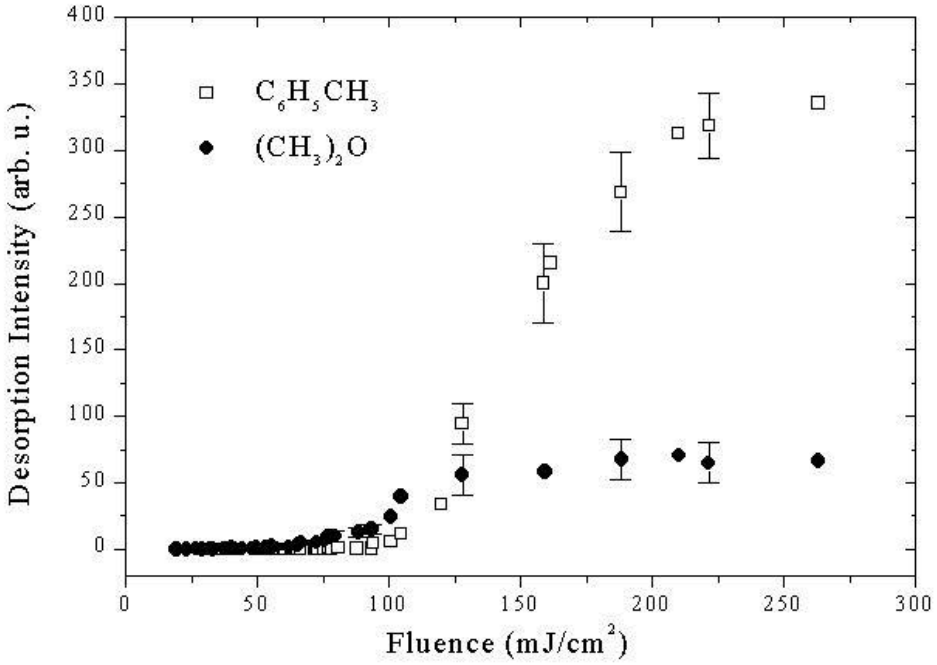

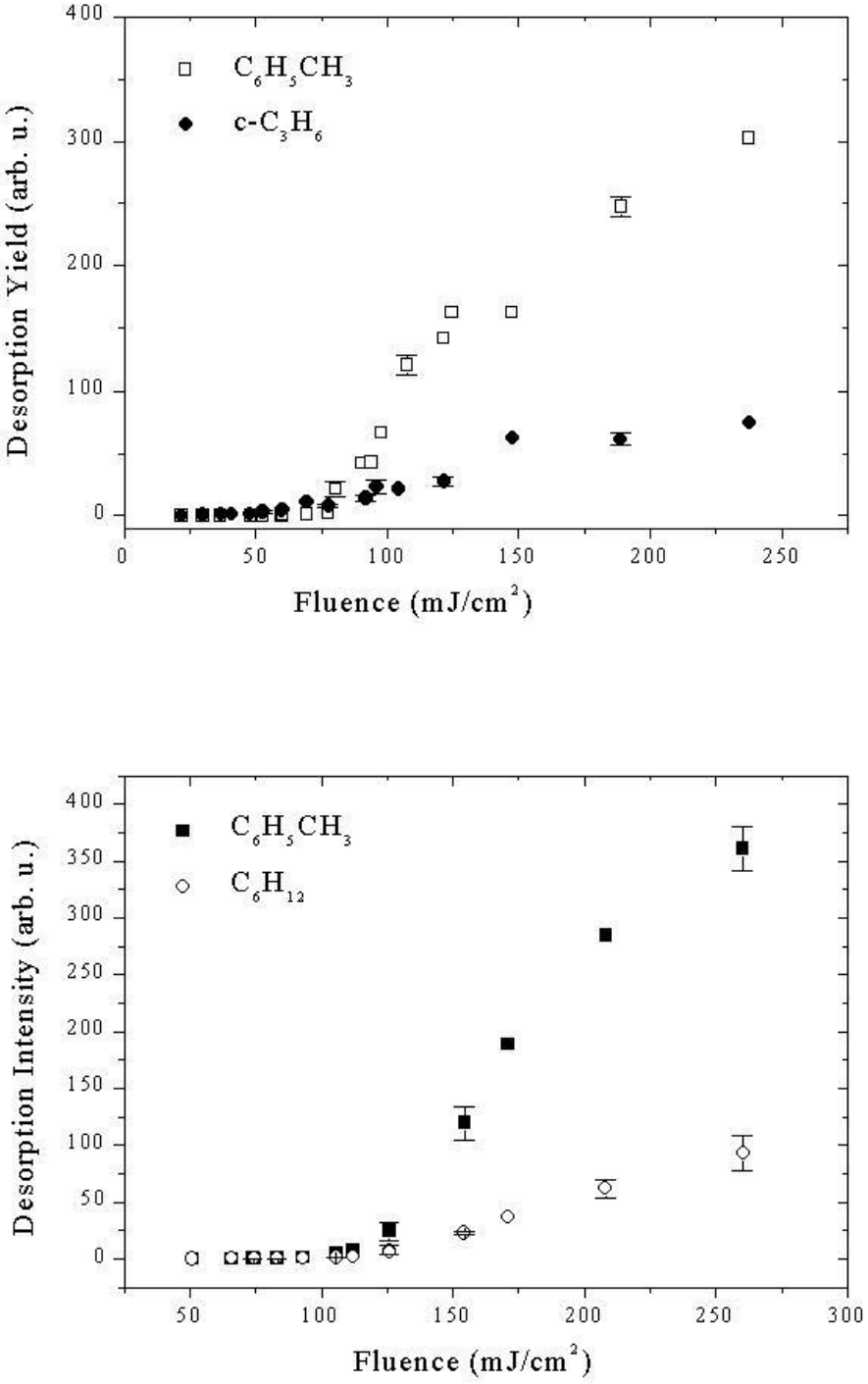

Figure 3-9 F_{LASER}-dependence of the desorbate intensities of the alkane analyte and of $C_6H_5CH_3$ from a 1:5 (molar) mixture of the two compounds as a function of the laser fluence.

(a) $(CH_3)_2O/C_6H_5CH_3$ (b) $c\text{-}C_3H_6/C_6H_5CH_3$ (c) $c\text{-}C_6H_{12}/C_6H_5CH_3$ The intensities are corrected for the different relative ionization efficiencies of the two compounds in the mass spectrometer.

In general, for a given class of dopants (i.e., ethers, alkanes, etc), the desorption intensities in the 20-100 mJ/cm^2 range decrease with increasing molecular "size". Thus, for the just higher homologues $(CH_3CH_2)_2O$, and CH_3CH_2OH of the dopants presented in Fig. 10, desorption yields are found to decrease by a factor of 2. For even higher homologues, the reduction is even higher. Thus, for C_6H_{12}, weak signal is observed while for $C_{10}H_{22}$ no signal at all is detected at these fluences (<100 mJ/cm^2). This decrease cannot be ascribed simply to molecular size considerations, as the previous comparison may seem to suggest. This is clearly illustrated by the fact that, at these fluences, minimal, if any, signal is detected for D_2O as a solute (Fig. 11). Signal for D_2O is detected only at fluences well above 100 mJ/cm^2. Thus, the desorption efficiencies of the dopants does not relate to molecular size (which could be an important factor if, for example, diffusion was a rate-limiting process).

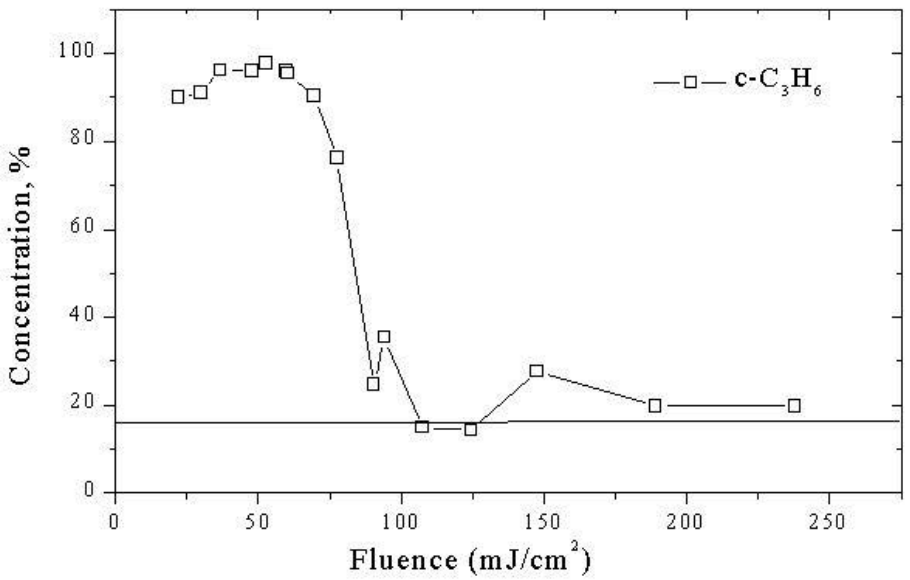

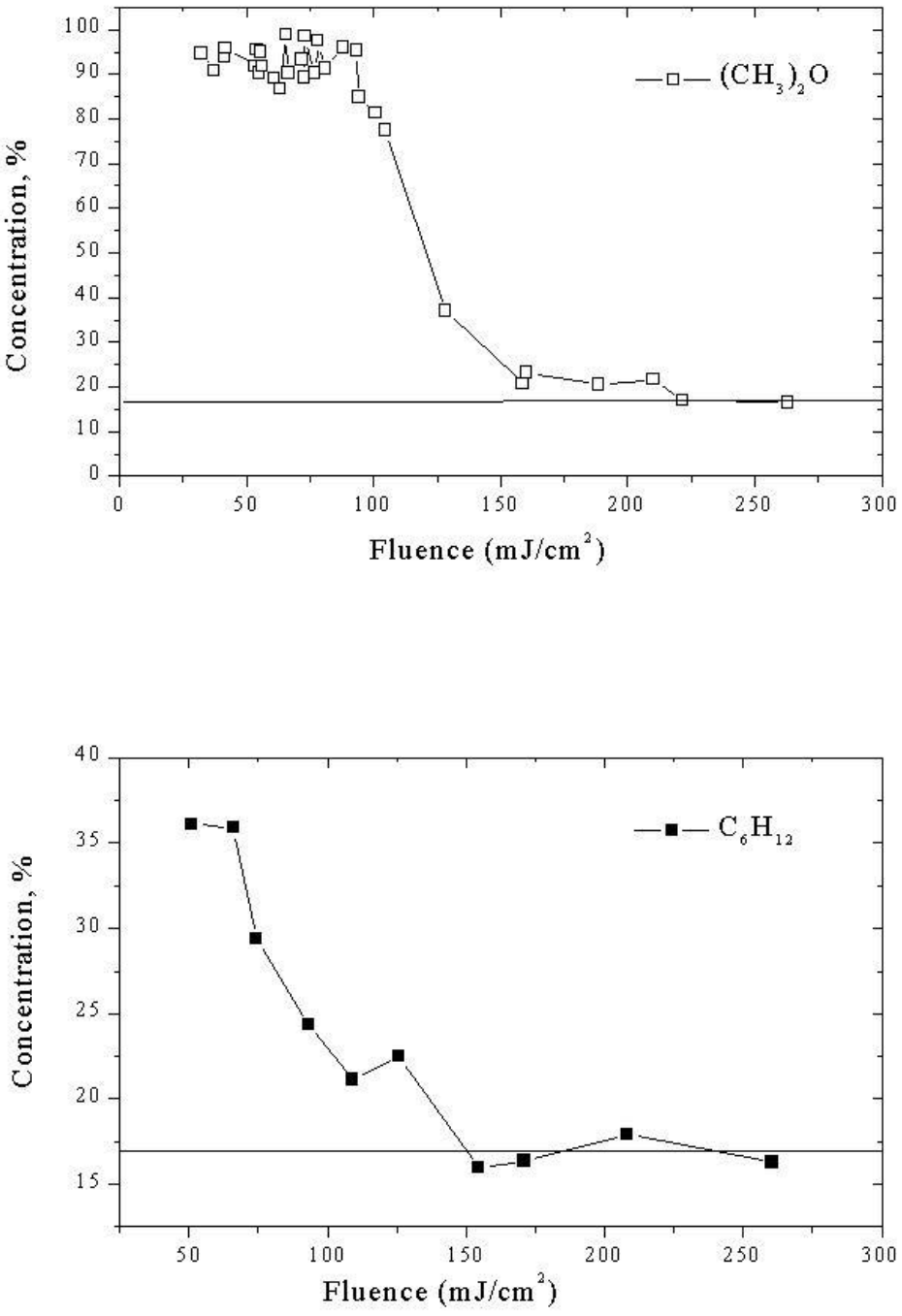

Figure 3-10 Concentration (i.e. I(dopant)/I(dopant)+I(toluene) for (up) c-C_3H_6, (middle) $(CH_3)_2O$, (bottom) C_6H_{12} in the plume as a function of laser fluence in the irradiation of the

indicating mixtures of the compounds with $C_6H_5CH_3$. The horizontal lines indicate the initial molar concentration of solutes in the sample.

A most interesting feature becomes evident when the dependences described above are plotted in semi-logarithmic form as a function of $1/F_{LASER}$ (Fig. 11). Clearly, two fluence ranges can be identified with significantly different slopes. At low fluences, the slope is very small, although usually not zero. However, above some specific fluence, the slope abruptly increases. In the case of doping with dopants that do desorb, the change is observed in the desorption signal of toluene, as well as of the dopant. This two-range delineation is observed for toluene even in the case of its doping with non-desorbing dopants. On the other hand, the

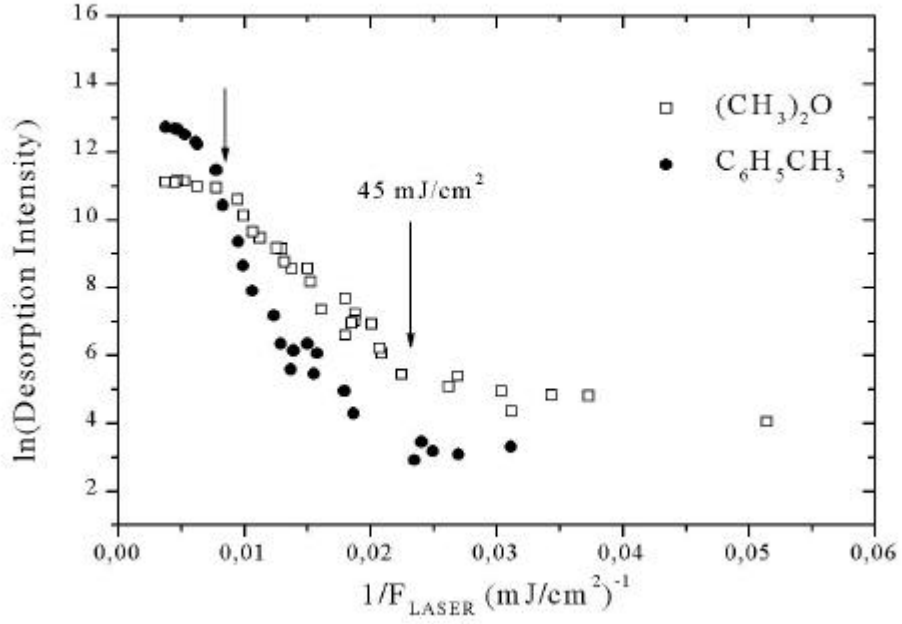

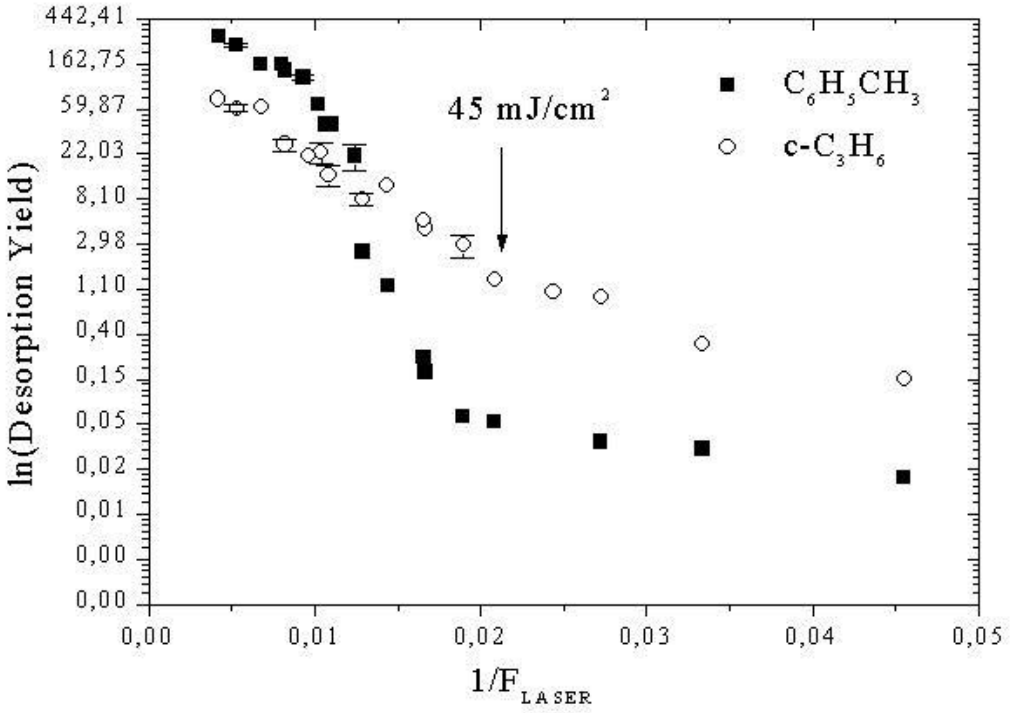

Figure 3-11 Semi-logarithmic plot of the desorption yield depicted in the Fig. 9 for toluene and c-C_3H_6, $(CH_3)_2O$ as a function of $1/F_{LASER}$.

fluence at which this change occurs differs for the different systems: (Table 3.1), increasing as the solid is enriched with dopants such as C_3H_6, $(CH_3)_2O$ and highest for dopants such as $C_{10}H_{22}$.

Insight into the physical significance of the delineation derives form the examination of the pulse dependences of the desorption efficiencies of the dopants that do desorb at low fluences (<100 mJ/cm^2). At the lowest fluences, their signal generally drops with successive laser pulses (Fig. 3.12), while in parallel, $C_6H_5CH_3$ desorption is enhanced. The drop in the dopant signal is weak, but systematic. In sharp contrast, in the 50-100 mJ/cm^2 range, the dopant signal is observed to increase sharply with successive laser pulses (whereas the toluene signal decreases), despite the fact that the amount of dopant desorbing per pulse is much higher than that below 50 mJ/cm^2.

Table 3-1 The results from the arrhenius-type ln(Signal) vs. $1/F_{LASER}$ fit

System	Molecule	Slope (20–45 mJ/cm^2) (mJ/cm^2)$^{-1}$	Slope (45-100 mJ/cm^2) (mJ/cm^2)$^{-1}$
Neat Toluene	$C_6H_5CH_3$	88	405
Cyclopropane/Toluene	$C_6H_5CH_3$	50	300
	c-C_3H_6	133	133
Cyclohexane/Toluene	$C_6H_5CH_3$	-	415
	C_6H_{12}	-	367
Dimethylether/Toluene	$C_6H_5CH_3$	88	350
	$(CH_3)_2O$	82	290
Decane/Toluene	$C_6H_5CH_3$	170	1300

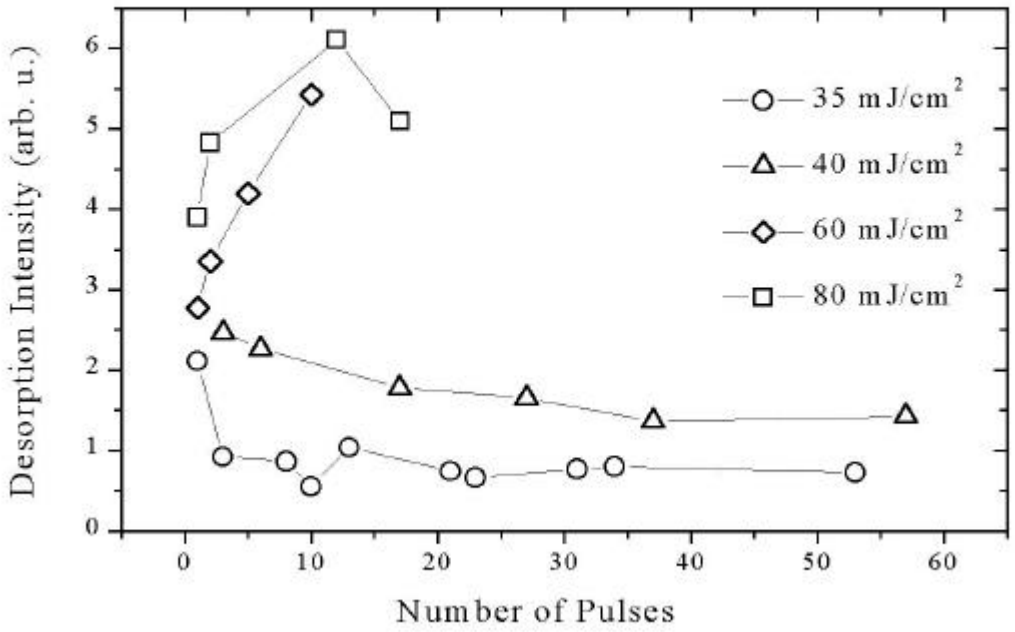

Figure 3-12 Desorption intensities of $(CH_3)_2O$ as a function of number of successive laser pulses in the irradiation of its mixture with toluene at the indicated fluences.

The increase is higher with increasing laser fluence. Thus, its "supply" does not appear to be limited as in the case of irradiation at lower laser fluences.

3.3. DISCUSSION

The present work has examined in detail desorption dynamics in the 20 mJ/cm^2 - 100 mJ/cm^2 fluence range from condensed solids of $C_6H_5CH_3$ enriched with dopants (molecules) of varying binding energies. It is important that all employed dopants absorb negligibly at the 248 nm irradiation wavelength [56]. Furthermore, the interaction between the dopants (especially the cyclic alkanes) and $C_6H_5CH_3$ is such that the incorporation of these dopants should not affect the absorption coefficient of the matrix (except for the concentration factor). Even in the case of the more polarizing D_2O and $(CH_3)_2O$, in-situ measurements do not show any significant change of the absorption coefficient. Thus, for all systems the deposited energy per unit solid volume should be the same. Consequently, the difference in desorption efficiencies observed for the different dopants must relate exclusively to the nature of the energy dissipation in the solid and subsequent material ejection mechanisms The major observations in this respect can be summarized as follows:

A. Considering the desorption efficiencies of the various dopants, it was shown that some of them desorb efficiently even at low laser fluences, whereas others are only observed at much higher fluences ($\geq$ 100 mJ/cm^2).

B. In all cases, the semilogarithmic dependence of signal vs $1/F_{LASER}$ indicates two fluence ranges with different dependences. In addition, different pulse dependences of the desorption efficiencies are observed in these two ranges.

In the following, we show that these effects unambiguously demonstrate that desorption dynamics at fluences below 100 mJ/cm^2 can be characterized as a thermal surface evaporation process. In particular, we show that the two ranges in the $1/F_{LASER}$ dependence of the desorption signals corresponding to desorption from partially melt and from overheated liquid,

respectively. The importance of the present study derives from the fact that as shown in the subsequent chapter, the considered fluence range represents the sub-ablative regime.

We consider briefly various plausible mechanisms that have been advanced in a number of photodesorption studies from multilayer condensed solids and show that they are not applicable in the present case. First, the electronically mediated photodesorption of the dopants can be safely discounted, on the basis of the fact that none of the dopants has low-lying electronic states [56] that could act as electronic energy acceptors. All dopants (water, dimethylether and n-alkanes) absorb at wavelengths lower than 200 nm [57]. Electronic to Vibrational or Translational E→V,T energy transfer mechanisms can be discounted by the observation that the intensity of the dopants does not correlate with the number of their degrees of freedom (f.e., for the comparable, in terms of degrees of freedom $(CH_3)_2O$ and CH_3CH_2OH, $I(CH_3)_2O >> I (CH_3CH_2OH)$ at all fluences, whereas $I(CH_3)_2O \approx I\ CH_3OH$), whereas in contrast the efficiency E→V,T mechanisms depends sensitively on the number of accepting modes. A mechanism based on simple mechanical, collisional ejection mechanisms (i.e. desorption of the dopants via collisions with the $C_6H_5CH_3$) can be discounted by the observation that for c-C_3H_6 and $(CH_3)_2O$, the desorption yield exceeds considerably the corresponding $C_6H_5CH_3$ signal. Finally, desorption due to the absorption by the suprasil substrate can be discounted by the fact that this is transparent at 248 nm and the solid thickness (»50 ìm) is much larger than its optical penetration depth (L_p=2.6 ìm). Failing these mechanisms, we consider next a thermal surface vaporization mechanism and we demonstrate that all results are fully consistent with this suggestion.

3.3.1. Demonstration of solid-liquid phase transformation at low fluences

On the assumption that all absorbed energy is converted into thermal, the surface temperature is estimated from the following formulae, (in the absence of heat conduction losses) where ÄÇ represents the enthalpy at temperature T:

$$\Delta H(T,z)(Jmol^{-1}) = \frac{a(cm^{-1}) \times F_o(Jcm^{-2})}{r(molcm^{-3})} \times e^{-az} \quad (3.2)$$

$$\Delta H(T) = Cp_{s\$ystem} \times (Tm - To) + \Delta H_f + Cp_{l\$ystem} \times (T - Tm) \quad (3.3)$$

where s/l refer to solid/liquid[19]. The formula assumes a single-photon absorption, which was established experimentally to be the case (Chapter 4).

Table 3-2 The TDS results

Compound/System	T_{des} (°K)	E_{TDS} (kJ/mol)	$AÇ_{vap}$(kJ/mol) neat
$C_6H_5CH_3$/neat	170	41±3	44.01
$(CH_3)_2O$/mix.	145	16±3	21.51
c-C_3H_6/mix.	135	15±3	20.05
C_6H_{12}/mix	176	33±4	38.33
$C_{10}H_{22}$/mix	-	77	51.38

From equations (3.2) and (3.3)[20] the *surface* temperature of neat $C_6H_5CH_3$ at F_{LASER} = 32.4 mJ/cm^2 is estimated to be ≈ 178 °K (total energy 11.22 kJ/mol, with fusion energy included) and comparable temperatures are calculated for the mixtures at somewhat higher fluences. This temperature correspond well to the temperatures established by Thermal Desorption Spectroscopy (TDS) for the thermal desorption of $(CH_3)_2O$ and c-C_3H_6 from $C_6H_5CH_3$ matrix under vacuum (respectively at ≈ 140 °K and ≈ 130 °K), consistent with the detection of these species in the < 50 mJ/cm^2 fluence range. Thermal Desorption of physisorbed $C_6H_5CH_3$ is observed at a little higher temperatures (≈150 °K) and peaks at 170

[19] In the formula α is the extinction coefficient. For the neat $C_6H_5CH_3$ solid, has been measured in situ to be ≈ 3700 cm^{-1} . T_o=120 °K and T_m=178.15 °K are the initial temperature of the solid and the melting point of the toluene, ΔH_f =6.64 kJ/mol is the molar fusion energy and $r = 0.01 mol/cm^3$ (178.15 °K) the density of the compound at 178.15 °K. Cp is the heat capacity (Cp_s=80 J/mol K, Cp_l=142 J/mol K) [57,59-60]. Approximately the same T values are obtained if instead the experimental values for glass toluene are employed.

[20] For the mixtures $a_{mix} = 5/6 \times a$ =3150 cm^{-1}, since the dopants do not absorb at 248 nm. The molar average values of dopants and $C_6H_5CH_3$ have been assumed in these calculations. For example for $(CH_3)_2O$ and $C_6H_5CH_3$ are assumed for the heat capacity Cp_{mix} (72 J mol^{-1} K^{-1} for the solid (120-178 °K) and 135 J mol^{-1} K^{-1} for liquid (178-380 °K), s/l refer to solid/liquid state) and the density r_{mix} (0.9 x 10^{-2} mol/cm^3). For the melting point (T_m) and the latent heat of fusion (ΔH_f), the values of neat toluene are assumed (178 °K and 6.64 kJ/mol respectively) [62].

°K. On the other hand, the estimated temperatures are quite lower than the temperature indicated by the TDS study as necessary for the evaporation of the heavy non-volatile dopants ($C_{10}H_{22}$ presented in Ch. 4), thereby accounting for the failure of observing them at these fluences.

As shown before in all cases, in the plot of the signal vs $1/F_{LASER}$ two ranges can be clearly delineated with the change at 40 mJ/cm^2. On the other hand, it is estimated that ~32.4 mJ/cm^2 to melt the *surface* solid[21,22]. The melting temperature of neat toluene is T_m=178.15 K (at P=1 atm, but the phase transition is weakly affected by the pressure). Therefore, the solid should melt during irradiation at these and higher fluences (melting of organic solids is indicated to be fast within the ns pulse [J. Phys. Chem. vol 100 (1996)]). Thus, it is suggested that the range that corresponds to the negligible slope reflects desorption from partially melt, whereas the slope at higher fluences reflects desorption from a liquid heated well above the threshold.

Strong support for the suggested delineation comes from the different pulse dependences of the dopants and of the toluene desorption signals observed at fluences above vs. below 45 mJ/cm^2. At fluences well below 45 mJ/cm^2, the signal for the volatile dopants drops with successive laser pulses, thereby indicating a limited "supply" of dopant. On the basis of accurate calibration of the mass spectroscopic signal, at these fluences, less than 10^{14} molecules/cm^2 of the dopant desorb per pulse and thus the total desorption signal detected within the probed pulses corresponds to desorption from only the upper $\leq$10 nm of the film. This value is typical of the "desorption depth" estimated in surface-mediated desorption studies at very low fluences (<1 mJ/cm^2).

In sharp contrast, in the 50-100 mJ/cm^2 range, there is no evident limitation on the amount of the desorbing dopant, even though the amount of dopant desorbing per pulse is much higher. Based on the calibration of the mass spectroscopic signals, about 2.4×10^{14} molecules/cm^2 to 6.8×10^{15} molecules/cm^2 of $(CH_3)_2O$ desorb per pulse in the 50 - 100 mJ/cm^2

[21] If scattering losses are taken to account the experimental value (40 mJ/cm^2) is in very good agreement with this estimation.

[22] From matrix-isolated studies it is known that the structure of vapor-deposited films is not well defined [65]. This does not affect the estimation of the temperature (since values appropriate for vapor-deposited toluene have also been employed [59]).

range (the numbers correspond the two limiting fluences). Consequently, the total desorbed signal in the probed pulses corresponds to 7.2×10^{15} up to 2.04×10^{17} molecules/cm^2. Estimating that mixture $=1 \times 10^{21}$ molecules/cm^3 (or 1ML of the mixture $\approx 3.85 \times 10^{14}$ molecules/cm^2 of ether). The previous numbers suggest, respectively, desorption from $\frac{7.2\times10^{15}}{10^{21}} \sim 7.2\times10^{-6}\,cm = 72nm$ and $\frac{2.04\times10^{17}}{10^{21}} \sim 2\times10^{-4}\,cm = 2mm$ in excellent agreement with the estimation that at ~ 100 mJ/cm^2 the film within optical penetration depth should have melted.

Evidently, there is sample replenishment of the dopant from underlying layers. The efficient replenishment from the indicated depth over the indicated number of pulses requires diffusion constants[23] of at least $D \geq x^2/2t = (2.5\times10^{-14}\,cm^2)/2\times10^{-6}\,\text{sec} \sim 1.25\times10^{-8}\,cm^2/\text{sec}$ if diffusion is possible on microseconds (from the optical reflectivity monitoring, the resolidification of the film is indicated to be completed within ~ 1-5 ìsec). Evidently, these values are too high and are much more indicative of a liquid phase. Typical diffusivity values for molecules as small as NO within frozen liquids reported to be well smaller than 10^{-12} cm^2/s [58].

Direct demonstration for phase transformation comes from the optical/imaging examination of the solid upon irradiation. It is clear that the film undergoes pronounced structural modifications upon irradition at F_{LASER} > 50 mJ/cm^2. In the transient examination, enhanced scattering of the probing HeNe beam is observed between 60~100 ns, with a subsequent recovery of the reflectivity/transmission[24]. Therefore, "scatterers" must be formed which are suggested to be gaseous bubbles. Indeed, similar scattering effects have been observed for bubble nucleation and growth in the overheating of transparent liquids on

[23] For comparison purposes, the diffusion constant of dimethylether inside the toluene matrix in the temperature range of 200 to 350 °K has been estimated by the Stokes-Einstein equation $D_{dopant} = \frac{k_B T}{6\pi h_{Tol} r_{dopant}}$. However the Wilke-Chang and Scheibel formula have been used giving similar results [61]. In the formula T is the temperature η_{TOL} the viscocity of the toluene, V the molar volume, r the radius of the dopant. We estimate the mean value of diffusivity constant for the range 200-380 K to be $D \simeq 2.5\times10^{-5}\,cm^2/\text{sec}$.

[24] The change of the refractive index is too weak (» 5.68×10^{-4} K^{-1}) to account for this efficient scattering of the HeNe light. Even, upon melting, the change in n of toluene cannot explain the observed high scattering.

irradiated, absorbing metallic surfaces [75,78]. It was, indeed, first shown that our experimental setup yields for liquid (CH_3OH) spread over an absorbing substrate (Si wafer) identical optical transients with literature. In the case of liquids, the experimental investigation of the angular distribution of the scattering is possible and it has been shown that scattering is highly forward concentrated within a collection angle of ~ 10° around the specular [129]. This angular distribution was ascribed to the effect of multiple scattering (due to a high number of vapor bubbles formed and the very irragular bubble shape surface), rather than the size of the bubbles. In any case, the very good correspondence of the present observations to the liquid studies etsablishes that bubble formation is the origin of the observed scattering.

The formation of bubbles can be understood by the temporal evolution of the film temperature, estimated by considering the energy density changes in the solid:

$$\frac{d(re)}{dt} = \frac{d(re)_{heat}}{dt} - \frac{d(re)_{cool}}{dt} \quad (3.4)$$

The first rerm represents the energy input due to the UV light absorption, whereas the second term represents the energy loss (cooling process). The energy density increase due to laser heating is given by:

$$\frac{d(re)_{heat}}{dt} = a \times \Phi_o \left\{0 < t < 30\times10^{-9}\ \text{sec}\right\} \quad (3.5)$$

$$\frac{d(re)_{heat}}{dt} = 0 \left\{t > 30\times10^{-9}\ \text{sec}\right\}$$

Here, Öi stands for the laser irradiance (W/cm^2), and á (cm^{-1}) the absorption coefficient. On the other hand there are two main cooling mechanisms: heat conduction and surface thermal evaporation (evaporation cooling). The time necessary to smear the temperature by heat conduction[25] on a scale comparable to the light penetration depth: $t_{hc} \approx (4ak)^{-1} \approx 1.7\times10^{-6}$ sec. Thus, for times £ ìsec, the only important cooling mechanism is due to evaporation. In that case the cooling rate, expressed by the evaporation enthalpy, ΔH_{phtr} and temperature, T_{phtr}, is written as

[25] ê=0.01 cm^2/sec as a typical value for the heat diffusivity of solids

$$\frac{d(re)_{cooling}}{dt} = (z_{eff})^{-1} \times p_o \Delta H_{phtr} \times \frac{\exp(\Delta H_{phtr}(T - T_{phtr}) / RTT_{phtr})}{\sqrt{2p\,MRT}} \quad (3.6)$$

where po is the ambient pressure and z_{eff} should be the "heat conduction depth", given by $z = \sqrt{2Dt}$ where D is the diffusivity[26] constant (cm^2/sec) given by $D = \frac{K}{r \times C_P}$ (for the calculation zeff for an effective time t~100 ns)[27]. The denominator realates the pressure to the desorption rate. The temperature is then expressed by $T = \frac{V_M \times re}{Cp}$. V_M and C_p are the molar volume and the specific heat of the toluene (T(t=0)=178.15 °K e.g. the melting point of the compound).

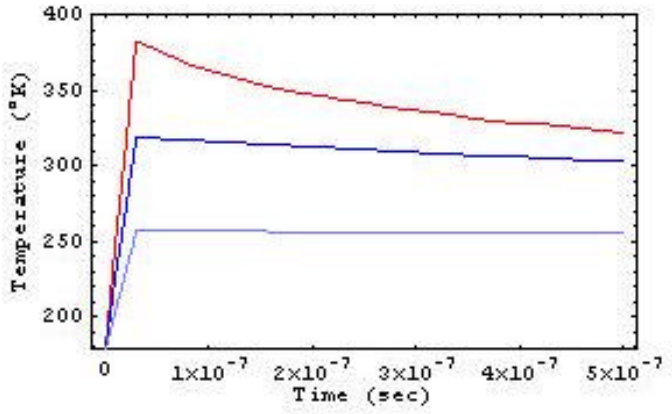

Figure 3-13 The figure illustrates the temperature calculated from the theoretical model as a function of time (red 110 mJ/cm^2, blue 85 mJ/cm^2, purple 60 mJ/cm^2).

The maximum temperature (Fig. 3.13 f.e., for 110 mJ/cm^2 T_{max}=385 °K) is attained close to the end of the laser pulse, after which it falls as a result of the evaporation. As compared with this, the initial bubble growth (under inertia control) is assumed to be given by [67]:

$$R(t) = \sqrt{\frac{p}{7} \times \frac{P_V - P_\infty}{r_l}} \times t \sim \sqrt{\frac{p}{7} \times \frac{r_v \Delta H_{lv}(Tv - Tsat(P_L))}{r_l Tsat(P_L)}} \times t \quad (3.7)$$

[26] K=1.6´ 10^{-3} W/cmK

[27] It is noted that the assumption of z_{eff}=á$^{-1}$ where á is the absorption coefficient as used in similar calculations [10] does not seem to give resonable result.

where $\tilde{n}_v$ and $\tilde{n}_l$ are the vapor and liquid densities at T, the temperature of the film, $T_{sat}(P_L)$ is the saturation temperature for the P_L (P_L the effective external pressure) $\ddot{A}H_{lv}$ the vaporization enthalpy (in kJ/kgr). The bubble growth velocity is estimated to be 6-15 m/sec, so that in the limiting 100 nsec, bubble can grow even up to 0.6-1 ìm (this is an upper bound, since the actual size will be limited by the depth overheated and not by the rate of increase in Equation (3.7). This clearly indicates the feasibility of bubble growth in the considered time interval, and also accounts for the comparable temporal evolution to those reported before for the overheating of liquids on absorbing surfaces. The subsequent dynamics, as revealed by the reflectivity examination, reveals the much more complex dynamics in the cooling of the liquid and its solidification. The processes are indicated to proceed for ~10 ìsec (consistent with an estimation on the basis of heat conduction), resulting in the "freezing" of the wavelike as well as of the splashing effects noted in the imaging examination (Fig. 3.3) of the irradiated films.

3.3.2. Quantitative Analysis

The thermal nature of desorption is further secured by the quantitative analysis of the observed desorption intensities. For a thermal process, the dependence of the integrated Yield Y on fluence F_{LASER} is given by an Clausius-Clayperon type expression:

$$Y = Yo \times \exp\left\{ -\frac{E_{des}}{k_B \times (T_o + \frac{a}{rC_P} \times F_{LASER})} \right\} \quad (3.8)$$

where To is the initial temperature of the substrate, k_B is Boltzmann's constant. Strictly speaking, the above equation is equal to the rate of desorption and thus, the total desorption yield should be equal to the integration of this rate over the temporal profile of the solid temperature. However, the error from this approximation is usually small and thus the formula is employed as such for the analysis of the data.

In Table 3.3 , we summarize the results from the thermal and laser induced desorption measurements. The TDS values derive from fits of the rising edge to zeroth-order peaks (i.e., $-\frac{dN}{dt} = Ae^{-E_{TDS}/RT}$) as commonly accepted for desorption from multilayers. For neat toluene

film, the determined desorption energy of 41 kJ/mol is very close to the reported sublimation energy of the compound. In the mixtures, the value for toluene is somewhat lower than that for its neat film, because of the influence of the presence of a high concentration of a dopant (i.e., the interaction dopant-toluene). This influence has also been reproduced by molecular dynamics simulations of these systems as shown in the Appendix I. Some influence of the dopant aggregation on the determined values is also plausible.

Table 3-3 Comparison TDS and Laser induced thermal desorption

Compound/System	E_{TDS} (kJ/mol)	E_{des} (kJ/mol)
$C_6H_5CH_3$/NeatToluene	41±2	30±3
$(CH_3)_2O$/Mixture	16±3	17±3
$C_6H_5CH_3$/Mixture	35±3	25±3
c-C_3H_6/Mixture	15±3	14±3
$C_6H_5CH_3$/Mixture	35±3	-
C_6H_{12}/Mixture	33±4	22±6
$C_6H_5CH_3$/Mixture	39±3	25±3
$C_6H_5CH_3$/Mixture	45±5	31±2
$C_{10}H_{22}$	77	-

In the case of laser desorption E_{des} are extracted from the fitting of the experimental integrated Yields in the 50-120 mJ/cm^2 range using the equation 3.8 . For the cyclohexane, because of the small signal, the determined value is not as accurate.

Overall, there is rather good correspondence between the activation energies determined for the laser-induced desorption process and for the thermal one. Certainly, discrepancies between the values do exist. Yet, the good correspondence for so many systems is quite reassuring. As for the discrepancies, these may be partly ascribed to the employed multipulse protocol employed in the laser experiments as well as in the inaccuracies for the

various parameters in the calculations (á,ñ,Cp). Another reasonable explanation for some of the discrepancies can also be given. Namely, the TDS values are determined from heating of the substrate over a rather small temperature range (typically from 160-180 °K). In contrast, as indicated in Table 3.3, the E_{des} in the laser-induced process represent desorption from a melt heated considerably above 200 °K. As the temperature is raised to higher and higher values, the effective ΔH_{vap} decreases. Thus, the discrepancy between the thermal and laser values may be fully acceptable. The very good correspondence establishes that the determining parameter in the desorption in the low fluence range is the binding energy of the species in the matrix.

3.4. CONCLUSIONS

In the present chapter, desorption dynamics in the irradiation of van der Waals solids has been examined in the 20 - 100 mJ/cm^2 fluence range through the comparative examination of the desorption efficiencies of non-absorbing dopants incorporated within a $C_6H_5CH_3$ matrix. In this fluence range, the desorption efficiencies of the various dopants is shown to correlate exclusively with their binding energy to the matrix. The thermal nature is further demonstrated by the observation of a solid restructuring which is consistent with a transformation of the solid to liquid phase during irradiation.

The occurrence of this phase transformation is crusial, because as shown in the next chapter, the threshold for ablation for all systems is observed at fluences well above the indicated point of slope changes in Fig. 3.2 Thus, this demonstrates that ablation is initiated from a liquid well-overheated above the melting point, consistent with the “explosive Boiling” model.

4. THE DIFFERENT EJECTION MECHANISM AT HIGH LASER FLUENCES -ABLATION

4.1. INTRODUCTION

In the preceding chapter, desorption dynamics at low and intermediate fluence regimes was examined. It was shown that all observables are consistent with a thermal, evaporation-type process. In this chapter, the study is extended to higher laser fluences and is shown that the ejection process above a specific fluence value deviates significantly from that observed in the previous chapter. No correlation of the ejection efficiencies of the dopants with their binding energies is found. Thus, ejection dynamics at these fluences is demonstrated to be a qualitatively different phenomenon from the vaporization / desorption process at low fluences. Consequently, this higher fluence range is the one that should be identifiable with UV ablation. The observables in this fluence range accord to the idea of explosive boiling. The experimental criteria defining ablation are also specified.

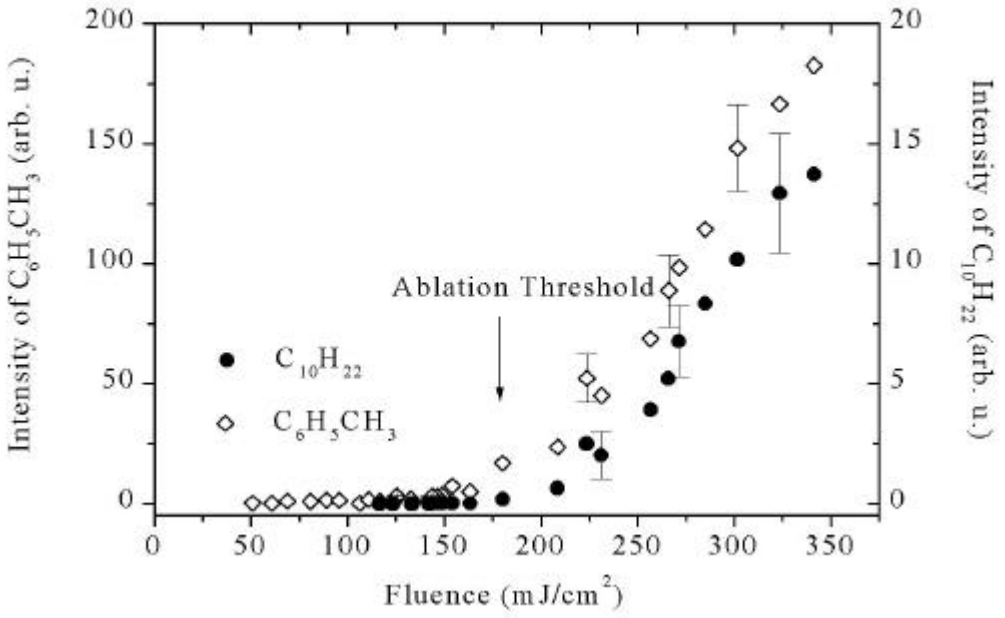

Figure 4-1 Desorption intensities in the irradiation of $C_6H_5CH_3/C_{10}H_{22}$ (5:1 molar ratio) as a function of the incident laser fluence. The data depicted at fluences below 250 mJ/cm^2 for $C_{10}H_{22}$ represent generally averaging over 5-10 pulses.

4.2. RESULTS

As shown in the previous chapter, in the 20-100 mJ/cm^2 range, desorption yields scale with the binding energy of the dopants in the matrix. Consequently, only weakly bound dopants are observed in the gas-phase. However, at higher fluences, the relative desorption efficiencies clearly deviate from the ones described above. Thus, for the volatile dopants, (Fig. 3.9), with increasing laser fluence, the toluene signal is observed to overtake the dopant signal and becomes significantly larger, with the relative intensity ratio assuming a value close to the film stoichiometry (Fig. 3.10). Furthermore, above a specific laser fluence, even dopants for which no signal is detected at lower fluences, are observed to be ejected efficiently, independently of their size, mass or binding energy. This is illustrated in Fig. 4.1, which depicts the ejection efficiency of the $C_{10}H_{22}$ dopant, along with that of toluene, as a function of the laser fluence. Reproducible and well-defined signal for $C_{10}H_{22}$ is detected at fluences $\geq$180 mJ/cm^2. In fact, ejection has been observed for even higher organic molecules, such as the highly involatile adamantine and pentadecane, although the full dependence of their desorption signals on F_{LASER} could not be determined, because of experimental problems in their reproducible deposition mixing with $C_6H_5CH_3$.

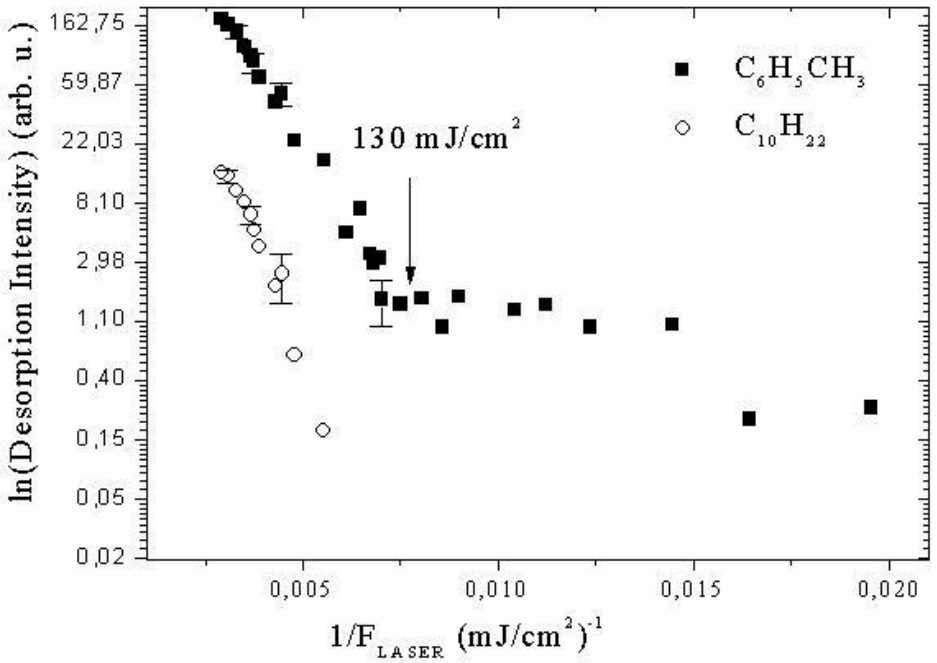

Figure 4-2 Semilogarithmic plot of the data of Fig. 4.1 as a function of $1/F_{LASER}$.

The fluence value necessary for the detection of these species coincides always with the threshold, as this is determined by the conventional way of plotting etching depth of the *matrix* as a function of laser fluence (using the formulas (3.1)). Analysis of the data in the (Fig. 3.9, Fig. 4.1) according to this formula shows that the value of the threshold differs according to the employed dopants. Evidently, the nature of the dopant affects also the ejection efficiency of toluene. In fact, the exact value of the threshold F_{Thr} is found to increase with increasing "involatility" (binding energy) of the solute in the mixture (Table 4.1). Second, in parallel, the slope of the $C_6H_5CH_3$ as a function of laser fluence changes. However, if the data are plotted in terms of a "reduced fluence" (i.e., F/F_{Thr}) then all curves essentially superimpose. Third, the maximum toluene signal at the plateau is found to differ depending on the particular dopant. Thus, for the $C_{10}H_{22}/C_6H_5CH_3$ system, the maximum total (i.e., toluene+dopant) intensity is nearly half of that attained in the irradiation of $(CH_3)_2O/C_6H_5CH_3$ system.

Table 4-1 The ablation thresholds for the various systems

System	F_{thr} (mJ/cm^2)
Neat-$C_6H_5CH_3$	105±5
$C_6H_5CH_3/(CH_3)_2O$	110±5
$C_6H_5CH_3/C_6H_{12}$	120±5
$C_6H_5CH_3/C_{10}H_{22}$	180±10
$C_6H_5CH_3$/c-C_3H_6	80±5

As argued in the next section, the change in the threshold is due to the fact that the incorporation of dopant in the solid at concentrations as high as 16 % affects the thermodynamic properties of the system (cohesive energy and heat capacity) (Chapter 3) and this is reflected in the observed increase of the threshold. As a result, ejection of material occurs at different fluences for the various dopant systems. For the purposes of the arguments developed subsequently, it is important to show that "involatile" dopant ejection is also possible at lower fluences. To this end, for the D_2O / $C_6H_5CH_3$ systems dopant ejection from solids of lower concentrations was examined. Reproducible signals just above the S/N ratio could be detected for a solid concentration of 1%. At this concentration, the influence of the mixing on the ejection process is much weaker and the threshold is just 5% higher than that of the neat solid. Dopant ejection is clearly observed at 120 mJ/cm^2 and thus it can be argued that if higher S/N, then ejection of dopant could be observed right at 110 mJ/cm^2 for even lower dopant/matrix stoichiometry.

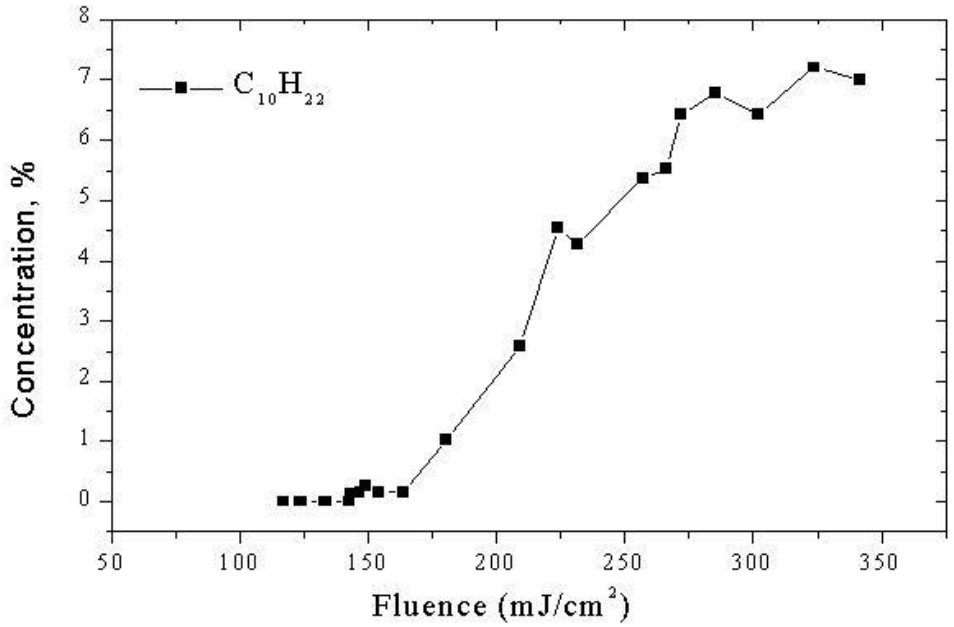

Figure 4-3 The graph depicts the concentration of $C_{10}H_{22}$ in the plume as a function of laser fluence.

Besides the influence on threshold, there are several other important differences between the mixtures (Figs. 3.9 and 3.10). For all volatile dopants $(CH_3)_2O$, c-C_3H_6), desorption signals are observed to "saturate" (reach a limiting value) at fluences just above the ablation threshold, whereas in contrast the $C_6H_5CH_3$ signal continues to increase. In sharp contrast, for D_2O and $C_{10}H_{22}$, there is clearly a close correspondence between the F_{LASER} – dependence of their signals and that of the matrix molecule.

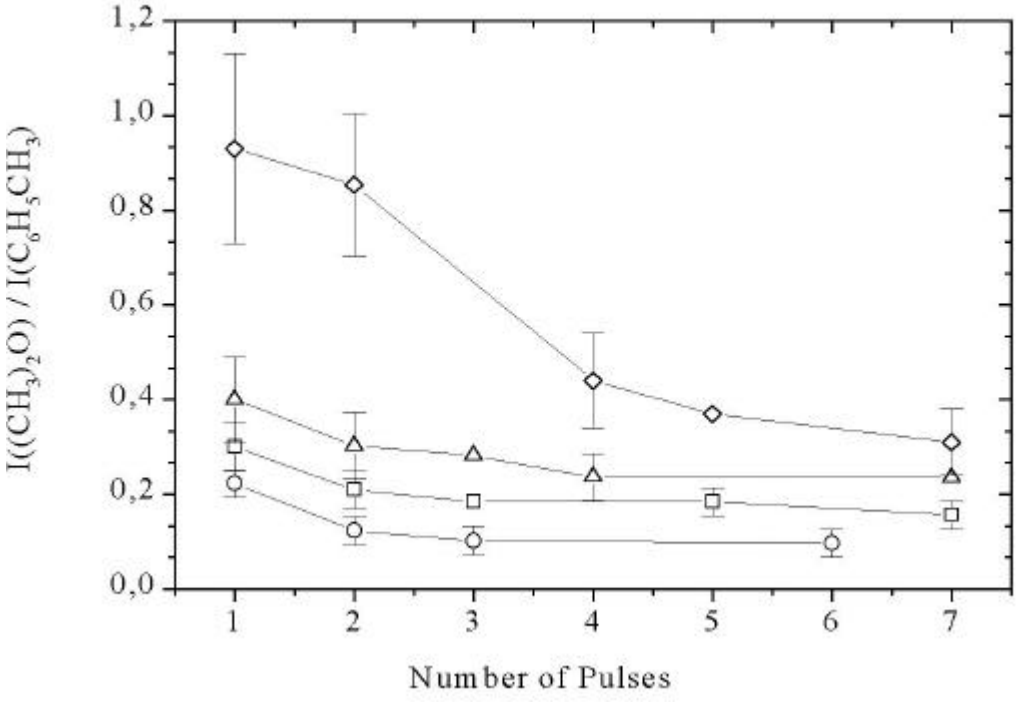

Figure 4-4 Pulse evolution of the relative desorption intensities of the dopant to the matrix recorded in the irradiation of freshly deposited mixture of $C_6H_5CH_3/(CH_3)_2O$ (5:1 molar ratio) films at various laser fluences, 240 mJ/cm^2 ( ), 220 mJ/cm^2 ( ), 160 mJ/cm^2 ( ), 130 mJ/cm^2 ( ).

Second, the relative value of the desorption intensities of the dopants vs. that of $C_6H_5CH_3$ differs for the various dopants. In the case of the volatile $(CH_3)_2O$ and c-C_3H_6, their relative intensity vs. that of $C_6H_5CH_3$ reaches above threshold nearly the initial solid stoichiometry. In fact, for the very first laser pulse from freshly deposited films, the relative gas-phase dopant concentration is found to exceed somewhat the film stoichiometry (0.2) (f.e., for $[(CH_3)_2O]/[C_6H_5CH_3]$ @1-0.4 i.e., 5-2 higher the film stoichiometry). In sharp contrast, for the "involatile" species, the gas-phase concentration appears to be systematically lower than the film stoichiometry ($[C_6H_{12}]/[C_6H_5CH_3]$@0.2, $[D_2O]/[C_6H_5CH_3]$@0.15, $[C_{10}H_{22}]/[C_6H_5CH_3]$=0.03-0.12).

Finally, there is a clear-cut difference between strongly and weakly bound dopants also as pulse dependence of their signals is concerned. The desorption intensity of the "nonvolatile" dopants relatively to that of $C_6H_5CH_3$ remains, within experimental

error, nearly constant for successive laser pulses that irradiate a given deposited solid (Fig. 4.5). The only deviation is observed for the very first laser pulse, for which the ratio is much enhanced in favor of toluene. This discrepancy is probably due to desorption from toluene-rich areas formed during deposition. However, from the second pulse onwards, the relative signals stabilize at a constant value, which as mentioned above is nearly by a factor of 2 than the solid stoichiometry.

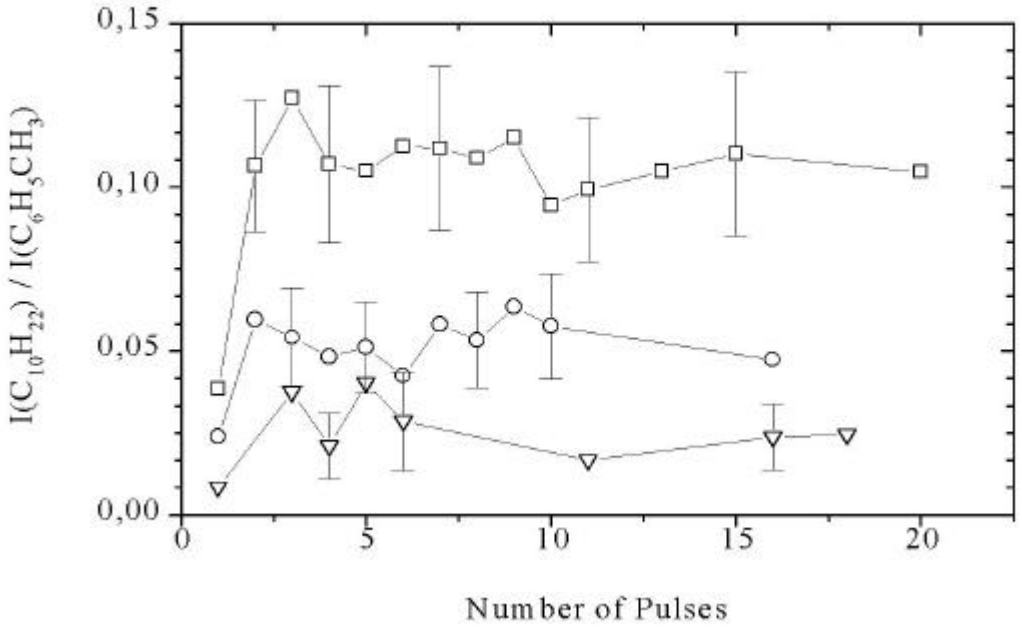

Figure 4-5 Pulse evolution of the relative desorption intensities of the dopant to the matrix, recorded in the irradiation of freshly deposited mixture $C_6H_5CH_3/C_{10}H_{22}$ (5:1 molar ratio) films at various laser fluences, 300 mJ/cm^2 ( ), 270 mJ/cm^2 ( ), 210 mJ/cm^2 ( ).

In sharp contrast to the ejection dynamics described for $C_{10}H_{22}$, the relative desorption signal of $(CH_3)_2O$, c-C_3H_6, decreases sharply from the first to the second pulse (Fig. 4.4). The decrease reflects mainly the change in the dopant absolute signal, whereas the changes in the toluene signal are much less significant. The extent of the discrepancy observed in the first pulse becomes less pronounced with increasing laser fluence, with

the determined dopant/toluene ratio nearly equaling the solid stoichiometry at high enough fluences.

4.3. DISCUSSION

In the present chapter, we have extended the study of the ejection dynamics of dopants incorporated within a $C_6H_5CH_3$ matrix to high laser fluences (>100 mJ/cm^2). At these higher fluences ejection, observables of the dopants are found to differ in distinct and many respects from those observed at somewhat lower laser fluences:

A. In contrast to the findings at low laser fluences, here the relative ejection efficiencies of the dopants seem to be independent of their binding energy to the matrix. Furthermore, in all cases the intensity of $C_6H_5CH_3$ vs. dopant reaches a ratio representative of the solid stoichiometry, thereby illustrating the nonselective nature of ejection in this regime.

B. A close correspondence of the pulse evolution of the "non-volatile" dopants with matrix molecule is observed. A different dependence is observed for the "volatile" dopants, which in addition differs from that observed for the same dopants at low fluences.

C. Finally, the fluence at which this change in ejection dynamics is observed to differ for mixtures of 16 % concentration in the dopant. In fact, it scales with the binding energy of the dopant to the $C_6H_5CH_3$ matrix (and thus, with the cohesive energy of the system).

In the following, we first demonstrate that a different mechanism of material ejection must operate in this fluence range and this is representative of UV ablation. The main characteristic of this mechanism/process is the nonselective ejection of a volume of material. Finally, plausible mechanisms responsible for the ejection are discussed and

shown that an “explosive boiling” consistent with overheating of the material is strongly suggested.

4.3.1. Demonstration of the non-evaporative nature of UV Ablation

The most clear feature of ejection dynamics in this fluence regime, as compared to that studied in the previous chapter, is the efficient ejection of the strongly bound to the matrix $C_{10}H_{22}$ (n-Decane), $C_{10}H_{16}$ (Adamantane) and $C_{15}H_{32}$ (n-Pentadecane). These molecules to interact strongly with $C_6H_5CH_3$, indeed in the TDS experiments, these species do not desorb well after $C_6H_5CH_3$ has desorbed (T>250 K), while the $C_6H_5CH_3$ desorption signal is also much affected. From cluster studies, the $\Delta H_{binding}$ ($C_{10}H_{22}$ to $C_6H_5CH_3$) is estimated at 0.8 eV/molecule (» 77 kJ/mol). By formulas 3.2 and 3.3 it is found that the evaporation of these species would require fluences ³250-290 mJ/cm^2, which is well above the experimentally observed threshold. The fact that ejection of these species is not due to a simple evaporation process is also indicated by the fact that, the Arrhenius-type analysis (ln(signal) vs $1/F_{LASER}$) of their signals yields a value close to that of toluene. The efficient ejection of these species at fluences ≈ 180 mJ/cm^2 cannot be ascribed to a thermal process.

The ejection of these species could in principle, be explained if energy deposition in the solid is higher than indicated. To this end, transmission measurements on thin $C_6H_5CH_3$ solids (~5μm) were undertaken. A one photon absorption is strictly indicated (1.1±0.2 from plot) even as fluence reaches the ablation threshold. Thus the percentage of absorbed energy does not change, to within a 10% accuracy. The negligible contribution of multiphoton excitation process at the employed fluences is also suggested by the literature values of excitation cross-sections reported for toluene and related aromatics.

The previous considerations establish that the efficient ejection of the “involatile” species at higher fluences signifies a change in the mechanism of material ejection from the evaporative one established at low laser fluences. Thus, it represents a new phenomenon and this is the regime that should be identified with UV ablation. In

particular, the ejection of the involatile molecules demonstrates that *ablation is a collective process, entailing the nonselective expulsion of a given depth of material, i.e. quite different from the surface-mediated evaporation.*

First, at all fluences, the TOF distributions of the heavy involatile analytes are nearly identical with that of the matrix TOF curve (i.e., exactly same velocity distribution). The most direct way of accounting for this observation is that the "heavy" analyte is entrapped in the desorbing jet of the matrix molecules and is accelerated by collisions with the desorbing matrix molecules to nearly the same radial velocity. This aspect is discussed in detail in chapter 5.

Direct and strong evidence for the entrainment/volume character of ejection comes from the close correspondence of the ejection efficiency of the "involatile" dopants to that of $C_6H_5CH_3$. This correspondence is observed both in relationship with the laser fluence (Fig. 4.1) and on number of successive laser pulses (Fig. 4.5). With increasing laser fluence, the transmitted fluence is sufficient to cause the ejection of a higher film thickness according to

$$N = n_m \cdot L_p \cdot \ell n\left(\frac{F_L}{L_p(E_v^* - CT_o)}\right),\ F_L \geq F_{thr} \Rightarrow l_{ejected} \propto \ell n\left(\frac{F_L}{L_p E_v^*}\right) \quad (4.1)$$

where L_p represents the optical penetration depth and E_v^* represents the critical energy density (J/cm^3) required for material ejection. Both toluene and dopant signals in Fig. 4.2 follow a logarithmic dependence and can be described by the same $F_{thr} = L_p \cdot E_v^*$ (=180±10 mJ/cm^2). This results is fully consistent with the suggestion of ejection of an entire film volume unselectively.

According to the previous arguments, all observations strongly suggest that at these fluences, a volume of material is unselectively ejected. The only observation that is not directly compatible with this "volume" ejection suggestion is the systematic deviation of the relative dopant/matrix desorption yields from the solid stoichiometry for dopants strongly bound to the matrix[28]. However, this systematic deviation cannot be ascribed to

[28]The discrepancy cannot be ascribed to problems in the deposition of the compounds (f.e. that smaller quantities of the dopant is condensed than introduced), because the other observables (f.e., toluene intensity, ablation threshold, etc.) are severely affected. Furthermore,

a much lower ejection efficiencies of the involatile dopants vs. toluene because in that case the solid should, within few laser pulses, become excessively rich in the dopant at the expense of toluene. However, as shown in Fig. 4.5, the relative dopant/toluene ejection yields remains quite constant with successive laser pulses, thereby indicating that film stoichiometry is not much modified from its initial one.

An explanation for these deviations has been advanced through a complementary study with molecular dynamics simulations. Simulations on the particular systems studied here indicate that the involatile species such as $C_{10}H_{22}$ are ejected preferentially bound within clusters of the matrix molecules[29]. Some of them may shed their $C_6H_5CH_3$ molecules through evaporation when they are in the gas phase, but given the relative strong interaction between dopant-solvent, a good number of the clusters would survive on their way to the mass spectrometer. The incorporation of the involatile dopants within clusters should modify significantly their ionization efficiency. Since the ionization potential of toluene is lower than that of the dopants, toluene ionization will take place preferentially over that of the dopant, thereby accounting for the low "apparent" yield/signal of the involatile species (As indeed observed in photoionization experiments on clusters of toluene with polar solvents). In sharp contrast to the involatile dopants, the simualtion indicate that the volatile dopants desorb largely as monomers. In this case, no deviations like the ones evidenced for the involatile species should be observed. Indeed,

---

these systematic deviations cannot be accounted by different angular distributions for the different dopants. According to all theoretical models, collisional effects in the plume result in the focusing of the "heavy" (higher-mass) species towards the center of the ejected beam. Thus, since our detection angle is close to the normal to the substrate, "heavy" species should be detected preferentially over the lighter dopants. Gas-phase effects could thus explain only the deviations observed in the case of the "light" (compared to toluene) D_2O, but not the ones observed for the high molecular weight $C_{10}H_{22}$.

[29] The MD Simulations did not provide any explanation for this finding. This finding, however, can be given a simple physical explanation within the assumption of a explosive boiling. Although the thermodynamics of superheated mixtures is complex [72], to a first approximation (the ratio of rate of evaporation corrected for the relative concentration of the two species $\propto \frac{P(T)}{\sqrt{2p\, mk_B T}}$ for toluene and decane is estimated to be 0.02 i.e., nearly exclusive presence of the volatile component.

the relative yield for the volatile dopant vs. toluene reflects closely the solid stoichiometry.

In the present study, there is no direct evidence for the ejection of clusters (the high electron-impact value will result in their fragmentation). Evidence for the presence of clusters in the plume was provided some time ago by Knutzer et al. in the UV irradiation of condensed CH_3I films [63]. By employing state-resolved resonant multiphoton ionization for the detection of the desorbates, they noted changes in the TOF signals, indicatively of the presence of clusters in the explosive photodesorption. Analogous spectral changes have been observed in the laser ablation of films of a polyaromatic hydrocarbon. [64] Further evidence for cluster ejection has been obtained in recent trapping plate experiment by Handschuh et al. Based on this circumstantial evidence, cluster ejection appears quite probable and provides a consistent rational for the observed discrepancy between gas (plume) and solid stoichiomtery observed for the involatile dopants.

In all, the study unequivocally establish that the nature of material ejection above the 100 mJ/cm^2 value differs from the thermal surface evaporation one at lower laser fluences. Thus the 100 mJ/cm^2 value represents a physically-significant parameter, i.e. an actual threshold. In contrast, the operation of different mechanisms is difficult to be evidenced in the corresponding examination of the dependence of the $C_6H_5CH_3$ desorption signal vs. F_{LASER}, as already illustrated by the discussion on chapter 3 (3.2.1 section). Furthermore, the present work introduces a simple experimental criterion for the identification of ablation regime, namely the ejection of strongly bound species which exactly reflects the volume, nonselective ejection of material. Though still not proven experimentally, this criterion appears to be initimately interrelated with the criterion advanced through the MD simulations of the onset of cluster ejection.

4.3.2. Implications for MALDI and related Applications

The present results has important implications for MALDI work. First, they can account for the fact that the detection limit for the matrix is lower than the threshold fluence for the detection of the heavy proteins. In the MALDI studies[30], the delineation has been difficult to establish because ions are detected and the difference between the two detection limits have been plagued by arguments about the contribution of the ionization processes. However, here, this issue is all together avoided by detecting neutral desorbates. On the basis of our results, the difference between the detection limits of matrix and protein is due to the fact that the matrix can desorb thermally already at low fluences whereas protein is ejected only at higher fluences, i.e. in the ablative regime. The observation of the biopolymers only above some fluence value is due to the existence of an actual, physically significant threshold and not to detection limitations as usually suggested.

The different fluence dependencies of the volatile vs. involatile species clearly indicates the dangers in the interpretation of Arrhenius-fitting of the ejection efficiencies. An Arrhenius-type of analysis in the present case indicates the same activation energy of ejection for the involatile species as for toluene. It is clear from the previous that this activation energy does not relate to the binding energy of the specific molecules, but rather to the activation energy of the process (identified with the bubble nucleation energy within the "explosive boiling model"). The coincidence of the fitting in MALDI may suggest that the ionization process is not a rate limiting step in the detection of the biopolymers but rather the rate limiting step must be the ejection process. On the other hand, it is rather difficult to apply an Arrhenius-type analysis to the volatile species (because of the signal saturation at fluences above the threshold).

Finally, a most serious consideration for the study of UV ablation/desorption processes is raised by the suggestion that the "involatile" species are ejected within clusters. It is highly likely that this feature is closely related/responsible for the stability of the ejected thermaly labile proteins. The ejected clusters should undergo very fast and efficient vaporative cooling, before thermal decomposition of the protein becomes

[30] Evidently, according to our results the Desorption/Evaporation in the acronyms of MALDI and MAPLE is clearly misleading.

significant. Thus, this would result in a "stabilization" of the ejected protein in a much more physically acceptable way than the model of Vertes and Levine[10].

On the other hand, the ejection of clusters introduces serious considerations for the analytical uses of ablation. As already discussed, this presence of clusters may seriously modify the quantitative measurement of the ejected species. Calibrating the spectroscopic techniques for their relative sensitivity towards clusters vs. monomers is in most cases very demanding or even practically imposible, especially since the distribution of cluster sizes is not known. Therefore the work indicates that because of this, experimental results of gas-phase measurements tend to be "artifactual".

4.3.3. Mechanism of UV ablation.

Finally, we address the question of the nature of the mechanism(s) of the UV ablation process that results in this massive, unselective material ejection. The entrainment process can in fact be a result of different mechanisms. At least three major types have been considered in the literature, namely photochemical, photomechanical and explosive boiling. All of them in one way or another are able to account for the ejection of involatile species, but they differ considerably in the exact mechanism by which this is achieved. In the present case, the data strongly support the possibility of an explosive boiling, as suggested recently by simualtions [19] and thermodynamic considerations [23]. To this end, we consider first the possibility of a photochemical mechanism and show that this mechanism does not operate in the present case.

4.3.3.1. The case against a photochemical mechanism

This mechanism has been advanced by Masuhara and coworkers [33] in the case of the UV ablation of aromatic compounds in liquid condition. (section 1.2).

However, in the present case, the photochemical mechanism can be rejected first on the basis of the observation that were made in the previous chapter (3.2.2) for no particular influence of preirradiation on the desorption observables (no induction effect ch. 7). For addressing the possibility of photoproduct formation in the irradiation of toluene neat condensed solid, a search for peaks with masses above that of the parent

peak (m>100 amu) was performed[31]. Examination of the 100-300 amu mass range showed no signal, except for $(C_6H_5CH_2)_2$ at fluences > 250 mJ/cm^2 where all evidence suggests ionic processes taking place (probably multiphoton ionization in the ejected plume). For examining further if plausibly $(C_6H_5CH_2)_2$ is not detected because of its inefficiency of desorption, pump-probe experiments were performed in which the solid was first irradiated for 50 or more pulses at low fluences (35 mJ/cm^2) and subsequently the signal at the mass setting for $(C_6H_5CH_2)_2$ was probed in the irradiation of the film at 150 mJ/cm^2. Again no signal could be detected, thereby establishing minimal if any product formation in the irradiation of neat $C_6H_5CH_3$ solids. Photodissociation of $C_6H_5CH_3$ results in the highly reactive $C_6H_5CH_2$ radical, which either upon addition to $C_6H_5CH_3$ or by reaction with another radical should give $(C_6H_5CH_2)_2$. Thus, we have to disagree with previous suggestions about the photochemical nature of ablation of molecular substrates ($C_6H_5CH_3$) at 248 nm, at least as far as $C_6H_5CH_3$ is concerned[32].

In spectroscopic studies of $C_6H_5CH_3$ within benzene matrices at low temperatures [65], no phosphorescence from the triplet state of toluene is detected upon UV irradiation at 77 °K, though such phosphorescence is detected at lower temperatures (10 °K). The negligible phosphorescence at 77 °K was suggestive to be indicative of the oparetion of efficient electronic energy transfer via excitonic interactions. It is thus, plausible that these processes result in electronic energy dissipation without fragmentation. Similarly, in the gas phase, recent experiments have reported the photolysis yield of toluene upon excitation at 248 nm to be » 6% and to be further reduced by collisions. A detail study of the influence of the photochemistry under ablation conditions is presented in chapter 6.

---

[31] A search for masses in the 0-100 amu range was not performed, because this examination is hampered by the complicating contribution of the peaks due to the e-impact cracking of $C_6H_5CH_3$. Thus formation or not of $C_6H_5CH_2$ itself cannot be ascertained directly.

[32] Interestingly a similar discrepancy between liquid and solid studies has been also observed in the case of the C_6H_6 ablation at 248 nm. In the ablation of liquid C_6H_6, Srinivasan and Ghosh [77] observed the formation of biphenyl, whereas in the mass spectoscopic study of condensed C_6H_6 solids [49], Hess reported the failure to observe any biphenyl formation.

4.3.3.2. The case in support of "explosive boiling"

The results provide strong support for a "explosive boiling" type process. It was shown in the previous chapter that at fluences higher than ~ 45 mJ/cm^2, changes in the morphology/structure of the films are observed that are consistent with melting and subsequent superheating. On the other hand, we have demonstrated here that the features that are clearly identified with ablation become important only at fluences above ~ 110 mJ/cm^2. Thus, there is an overheating of the toluene film of about , $\Delta T_{overHeat} \approx 180$ K well above its melting point[33].

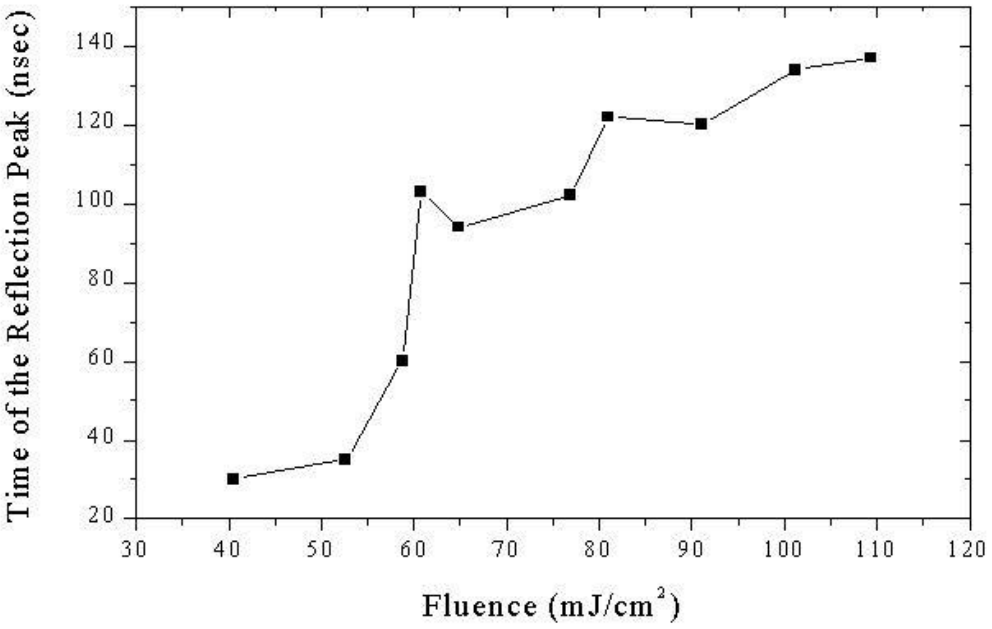

Figure 4-6 The figure shows the time of the maximum in the reflection peak from Fig. 3.7 as a function of laser fluence.

According to the thermodynamic treatment

$$J = Jo \times \exp(-W_{cr} / k_B T) = Jo \times \exp\left(\frac{-16ps^3}{3k_B T (P_V - P_L)^2}\right) \quad (4.2)$$

[33] An overheating in a temperature of twice the melting point is attained at the threshold. This finding agrees with the results of the MD simulations [18-20].

[66-74] where ó is the surface tension of the compound and P_V and P_L is the pressure inside the nucleous and superheated liquid respectively, increase in the superheating is accompanied by a sharp increase of J due to the sharp decrease of ó and sharp increase of $(P_V-P_L)^2$ factor. In the present case, these values are not known with sufficient accuracy and especially the effective P_L (pressure above the liquid) during the irradiation is ill-defined. Yet, a calculation of J values relatively to arbitrarily fixed J value (at reference value of 200 °K) clearly shows the exponential, almost "threshold like" nature of the process. Independently of modeling inaccuracies, the optical experimental results presented in chapter 3 provide a wealth of information for the process.

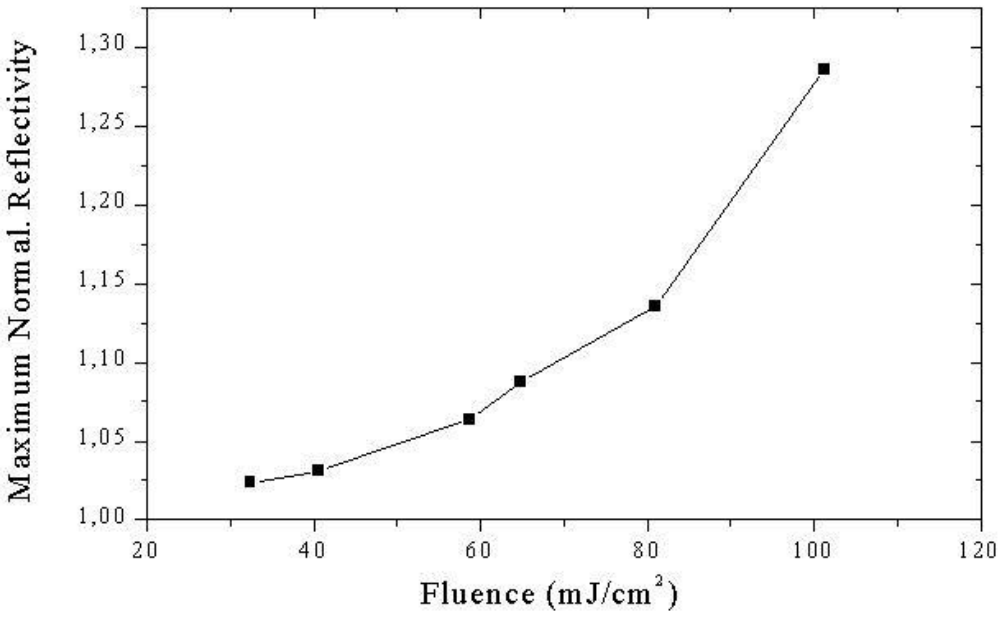

Figure 4-7 The graph illustrates the maximum normalized reflectivity from Fig. 3.7 as a function of laser fluence.

At low fluences, the temperatures are not sufficient to substain growth and sufficient number of bubbles, which quickly collapse (Figures 3.6 and 3.7). With increasing laser fluence, the time of attaining the maximum reaches a plataue (Fig. 4.6), most probably because of the competing effect of the fast temperature drop after 100 ns

(Fig. 3.13). However, the rate of bubble size/number growth is found to increase, thus resulting in the nearly exponentially dependence observed in the optical intensity maxima (Fig. 4.7). It is reasonable to consider that this optical change reflects a corresponding increase in the number and size of the bubbles. The total number of nucleous is proportional to the volume V superheated by ΔT_s.

$$Z = V \times \int_{T_{\max}(30\,ns)}^{T(100\,ns)} \frac{J(T)}{dT/dt}\,dT \quad \text{where } V \propto l_{eff} = \frac{1}{a} \times \ln\left(\frac{a F_{LASER}}{\Delta T_s\, r C_P}\right)$$

Since dT/dt is negative, the observed exponential increase is due to a sharply increasing of the J(T) function.

At a critical value, their development results in material ejection, as clearly illustrated by the transmission curve at 110 mJ/cm^2 (Fig. 3.6). This observation clearly establishes that the ejection process must be due to a explosive boiling-like process where material ejection is initiated near the maximum of bubble growth [72].

A explosive boiling is also strongly suggested by the observation of the pulse dependence of the desorption signals of the volatile dopants (Fig. 4.4). Their high signal in the first pulse and the subsequent sharp decrease in subsequent pulses shows that dopant molecules from much deeper than the ejected volume are able to diffuse, reaching the receeding surface from where, they can desorb. Indeed, the ratios determined at fluences close to the threshold suggest diffusion of dopant from depths at least 3-4 times higher than the ejected solid thickness (»5nm). The observed high dopant mobility strongly suggests melting of the *underlying* (non-ejected) layers, exactly as expected from the “explosive boiling” model.

The suggestion for the "explosive boiling" is also consistent with the observation that the ablation threshold increases sharply with decreasing “volatility” of the solute. Despite any uncertainties, it is clear that the change in Cp is insufficient to account for the increase in the ablation threshold (Table 4.2). The trend can be fully explained by the fact that the absorbed energy must exceed a minimum critical energy value for explosive boiling to occur. As shown in the previous chapter, the average cohesive energy of the substrate increases with increasing dopant involatility. A higher cohesive energy of the

system results in an increase of the surface tension and an increase of P_B. Thus, for the same J to be achieved, a higher T is needed to be attained. Generally, the limit of a superheat of a mixture can be approximated as the molar-weighted linear function of the superheat limits of the two components (Table 4.2) [73-74]. In the table, the difference between superheating expected for the mixtures and that of neat toluene is presented, along with the temperatures estimated at threshold for the various mixtures. Given the uncertainties in the estimation the temperatures are considered to be approximate. Nevertheless, they are in rather good correspondence with the estimated differences in the limits of superheats in the literature [68].

Table 4-2 Heat capacities of the mixture systems

System	Molar average[34] Cp(J/molK) (178-360 °K)	Estimated Temperature at the Threshold (°K)	$\Delta\Theta_{superheating}$ $(T_{mixture}-T_{toluene})$[35] (°K)
$C_6H_5CH_3$/c-C_3H_6	130	310	-29
$C_6H_5CH_3$/$(CH_3)_2O$	148	350	-10
$C_6H_5CH_3$/C_6H_{12}	157	355	-6
Neat-$C_6H_5CH_3$	154	375	0
$C_6H_5CH_3$/$C_{10}H_{22}$	180	420	+6

[34] The heat capacity of the doped systems can be approximated by the molar average of the heat capacities of the dopant and $C_6H_5CH_3$. In this case, the change in the heat capacity results in the fluence values given in Table 4.2. Since this estimation assumes weak interaction between dopant and matrix the T for $C_{10}H_{22}$/$C_6H_5CH_3$ represents a very rough estimate.

[35] Ts : spinodal decomposition temperature, approximated for the neat compounds as 0.8Tc (critical temperature) or from experimentally derived maximum overheats [68,74].

4.4. CONCLUSIONS

The present chapter has extended the previous study of the ejection dynamics in the UV irradiation of condensed molecular solids to high laser fluences. It was shown that at some specific fluence, a clear change in the ejection dynamics is observed. In particular no correlation between the efficiency of ejection of a species and its binding energy to the matrix is found. It was demostrated that this change can not be ascribed to a change in the amount of energy absorbed in the film. Thus, the change in ejection dynamics has to reflect a change in the ejection mechanism. Thus, UV ablation constitutes a physically different phenomenon from the thermal desorption process observed at low laser fluences, entailing the unselective, volume expulsion of material. A clear unambiguous criterion for defining experimentally the regime of UV ablation has been established, namely the ejection of strongly bound to the matrix species.

As for the nature of the mechanism responsible for this massive, unselective material ejection, a photochemical one is shown to be of no importance for the studied system. Instead, all data are compatible with a “explosive boiling” mechanism. In particular, ablation is found to occur at fluences well above the melting point reported in the previous chapter thus suggesting that ejection is initiated from an overheated liquid. Additionally, the ablation threshold is found to scale with the cohesive energy of the system exactly as expected from a “explosive boiling” mechanism.

5. EXAMINATION OF DESORBATE TRANSLATIONAL CHARACTERISTICS

5.1. INTRODUCTION

The examination of the translational distributions of the ejected particles in laser ablation is important for understanding the characteristics of the material ejection/flow in the gas phase during ablation. Furthermore the knowledge of the parameters that affect the translational distributions can help in the optimization and improvement of analytical and technological applications (for example, in laser deposition techniques, the desorbate velocity distributions affect critically the structural quality and the properties of the grown films, in MALDI, the resolution of the recorded spectra, etc)

In the case of photodesorption from surfaces at very low laser fluences the desorbate translational distributions can be correlated with the energy dissipation processes that result in desorption. (f.e, for a fragment ejected upon dissociation of an adsorbate, the maximum translational energy can be related (i.e. $E_{trans}^{\max} = hn - e_{bind}$). However, in laser ablation, because of the high quantity of ejected material, the desorbates suffer a substantial number of collisions and their initial translational distributions are severely modified. As a result, it is very difficult to correlate the observed translational distributions with the initial processes[36]. It is clear that the description of the plume evolution where the particles start with an initial (unknown) velocity and then suffer an (unknown) time-varying number of collisions along the flow axis, is a very complex problem of hydrodynamics.

The purpose of the present thesis was not to study the translational features in ablation. Nevertheless, in the previous examination, of ejection mechanisms a number of interesting features, have been noted in relationship with translational distributions. These results are summarized in this chapter as a basis for future theoretical/modelling and experimental work. In the 248 nm ablation of in neat solids, (toluene, chlorobenzene,

[36] In fact, this problem had not been realized in a number of studies so that, on the basis of desorbate translational distributions, they claimed unphysically high temperatures to be reached in the solid during irradiation. It is now clear that these are in error.

iodomethane, benzene, etc.) importantly, the attainment of the threshold is found to result in a rather abrupt increase of the desorbate most probable translational energies ($E_{TRANS,mp}$), and distinctly different F_{LASER}-dependences in the ablative and the subablative regimes are observed. Finally, the comparison of the translational features of mixtures with dopants of various desorption efficiencies "simulates" experimentally the effect of gas phase collisions when the desorption mechanism is known, Our results indicate that existing model can not describe consistently all desorbate translational features.

5.1.1. PostDesorption Processes

5.1.1.1. Supersonic Expansion Model

As described in the introduction, the translational distributions can be generally fitted to sums of "full-range" Boltzmann distributions (i.e., with a stream or drift velocity υ_{drift} superimposed) (Chapter 2). The question then refers to the physical origin and significance of the determined T and $\tilde{o}_{drift}$ fitting parameters.

As described in the introduction, the high translational energies (E_{TRANS}) and the low energy in the internal degrees of freedom have been suggested to indicate the supersonic-like expansion of the material, with the random thermal energy of the desorbates transferred into directed translational energy [42,79]. However, as the number of collisions in the plume cannot be established, the analogy may be not fully justifiable.

A wide number of Monte Carlo Simulations and hydrodynamic calculations have been presented [80,87]. These indicate that the laser-induced desorption of molecules can be likened to an adiabatic expansion. However, others empasize the density of material ejected to be the determining factor for the translational distributions [87], while others the short time scale (duration) of the ejection [85-86].

5.1.1.2. Knudsen layer fromation

Analytical models rely on the concept of knudsen layer [81-84]. For moderate densities of desorbed particles (f.e., monolayer) a Knudsen layer forms, within a few mean free paths of the target surface, in which the velocity distribution evolves from "half-range" Maxwellian to a "full-range" one in a center-of-mass coordinate system

(chapter 2). In this case, the relation $k_B \times T_s = \frac{\hat{E}}{2}$ is shown to be replaced by $k_B \times T_s = \frac{\hat{E}}{n_K}$, with n_K ranging from 2.52 for a mono-atomic particle to 3.28 for a polyatomic molecule and T_s is the surface temperature. Thus even few gas-phase collisions can lead to a severely overestimated value of Ts, but on the other hand, this model does not go to the extreme of assuming a "fully-developed" supersonic expansion.

Finally, others emphasize that the main features of the desorbate translational distributions relate to the initial dynamic "impulse" of the phenomenon, thus accounting for the high observed desorbate velocities.

5.2. RESULTS

5.2.1. Neat Systems

Fig. 5.1 illustrates the desorbate most probable Translational energy E_{TRANS} as a function of laser fluence, in the 248 nm laser irradiation of neat $C_6H_5CH_3$ and C_6H_5Cl solids (the corresponding for CH_3I and CD_3I are presented in chapter 6). Clearly, two laser fluence ranges can be defined with different dependences. In all cases, the change from the one range to the other is abrupt and take place close to the ablation threshold of the compounds as this established by the conventional approach from the dependence of the desorption signal on fluence. Most interestingly, the E_{TRANS} below the threshold remain nearly constant. In contrast, in the ablative regime, they increase with increasing laser fluence, in good agreement with previous studies. Table 5.1 presents for all examined systems the laser fluence where the velocity gap take place and the $ÄE_{TRANS}$ i.e. the change in the most probable translational energy. The observation of the abrupt change in all examined systems indicates that this effect is a general characteristic of the ablation process. Furthermore the observation in the case of the photo-inert $C_6H_5CH_3$ demostrates that this change relates to photophysical, rather than chemical, processes.

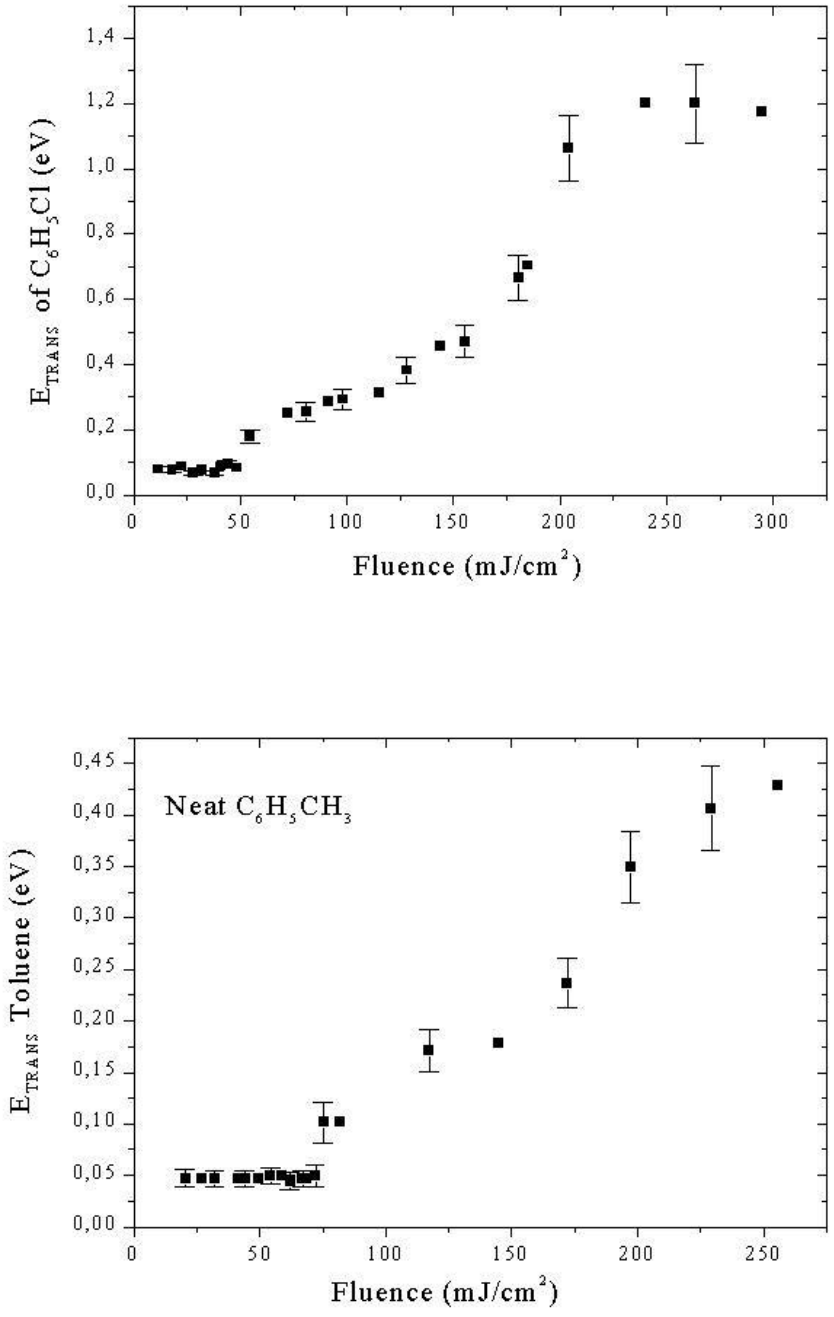

Figure 5-1 Most probable Translational energy (E_{TRANS}) of the (up) C_6H_5Cl and $C_6H_5CH_3$ (bottom) as a function of the incident laser fluence (F_{LASER}). The errors bars represent 2ó, as determined from at least 4-5 measurements.

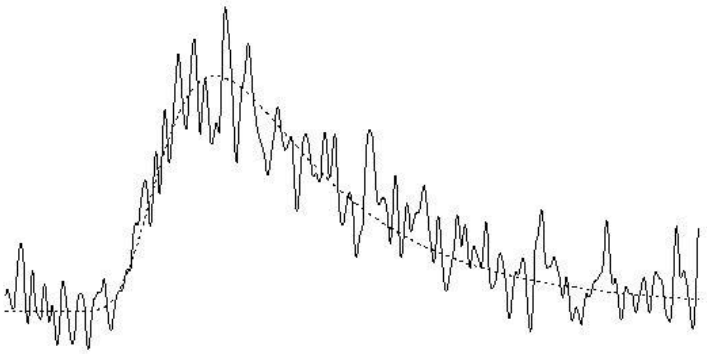

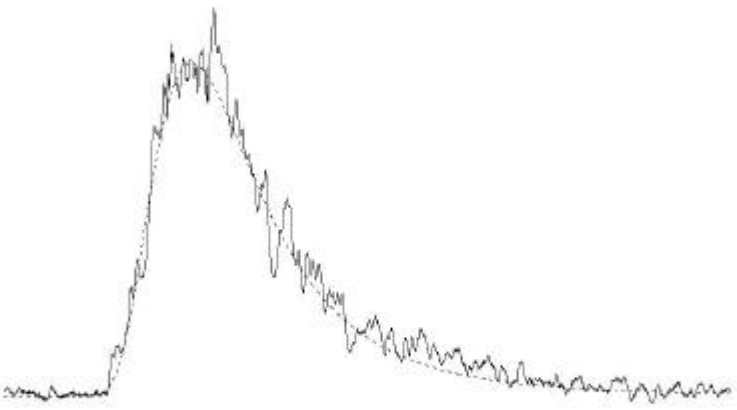

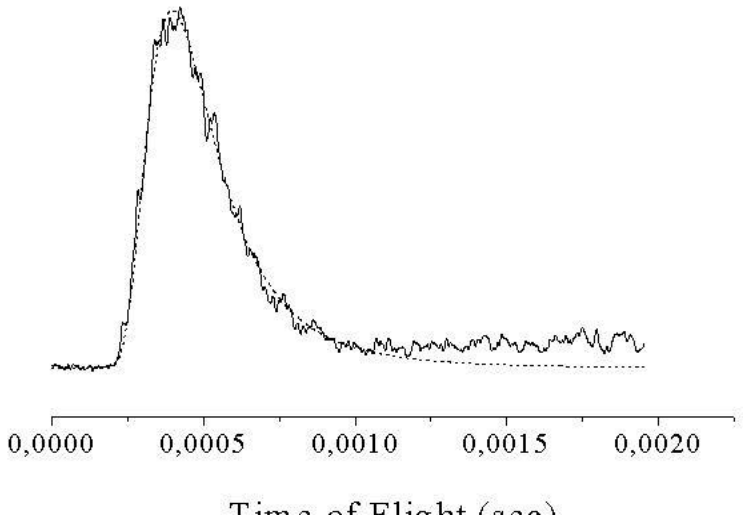

Figure 5-2 Time-of-flight spectra of C_6H_5Cl recorded in the irradiation of neat films of the compound at $F_{LASER} \approx 45$ mJ/cm^2 (top), $F_{LASER} \approx 80$ mJ/cm^2 (middle) and $F_{LASER} \approx 150$ mJ/cm^2. (The spectra are not to scale.). For the spectrum at 45 mJ/cm^2, the fitted Boltzmann has $\upsilon_{drift} \approx 20$ m/sec and T≈500 K; for the one at 80 mJ/cm^2, $\upsilon_{drift} \approx 300$ m/sec and T≈470 K; and for one at the highest fluence, $\upsilon_{drift} \approx 375$ m/sec and T≈800 K.

In parallel with the energies values change, the shape of the TOF spectra changes. As shown in Fig. 2 the spectra recorded at low fluences are broad and are generally modeled by Boltzmann distributions with temperatures in the range 300-500 and zero or small drift velocities ~ 20 m/sec. In contrast, the spectra recorded above the threshold are sharp and are better described by "shifted" Boltzmann distributions with high $\tilde{o}_{drift}$ and T values. The dependence of $\tilde{o}_{drift}$ and T on laser fluence is shown in Fig 3 for the case of $C_6H_5CH_3$. It is clear that the changes observed correspond very closely to those observed in the study of desorption from NO.[37]

[37] At very high fluences the spectra are found to exhibit long "tails" (Fig. 2). Such tails have been observed in previous studies [42] and have been ascribed to thermal desorption after the end of the laser pulse. Since in our case, these tails are observed at high fluences, we consider them to artifacts due to limitations in pumping the high amount of material that is ejected at these fluences.

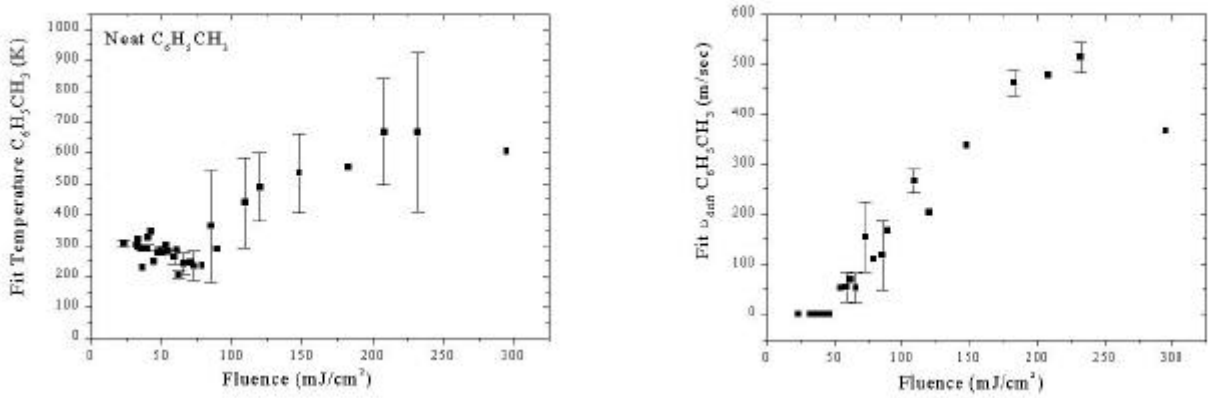

Figure 5-3 The plot illustrates the time-of-flight curve fit (half range Maxwellian) results, (right) drift velocity (v_d) and (left) temperature (T) as a function of laser fluence in the irradiation of neat $C_6H_5CH_3$ solids.

Table 5-1 The velocity gap

System	Fluence at the gap (mJ/cm^2)	ΔE_{TRANS} (%)	E_{TRANS} (Below Threshold) (eV)	E_{TRANS} (Above Threshold) (eV)
$C_6H_5CH_3$	85	50	0.05	0.1
C_6H_5Cl	50	55	0.1	0.2
CH_3I	20	30	0.046	0.066

5.2.1.1. Mixture Films

Fig. 3.5 illustrates the most probable E_{TRANS} of toluene as a function of laser fluence in the case of its mixture with dimethylether (5:1 molar concentration). For this system, there is no evidence for an abrupt change in the E_{TRANS} at the ablation threshold of the system (120 mJ/cm^2) (chapter 4). Furthermore, in contrast to the constant value of E_{TRANS} in the neat toluene case, at low fluences (20-100 mJ/cm^2), E_{TRANS} of both matrix and solute is found to increase with laser fluence. However, their kinetic energies are not equal (as would be expected for a thermal desorption mechanism with E_{TRANS} $(CH_3)_2O$ < E_{TRANS} $(C_6H_5CH_3)$). Above the threshold, E_{TRANS} increases in a manner comparable with

that determined in the neat toluene case. The same features are observed for c-C_3H_6/$C_6H_5CH_3$, CH_3OH/$C_6H_5CH_3$, i.e., in all mixtures that dopants desorb efficiently below the threshold.

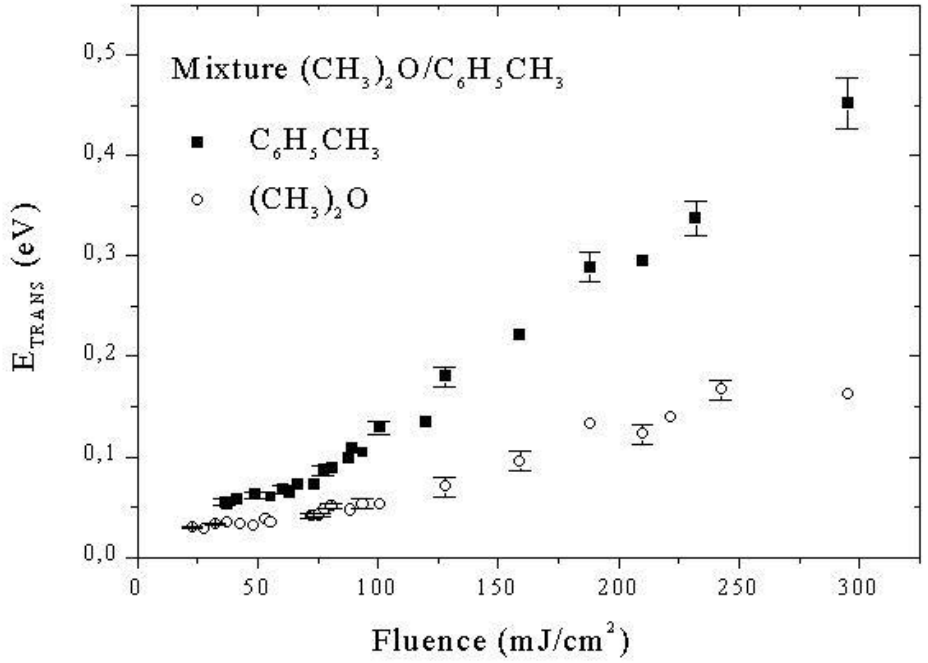

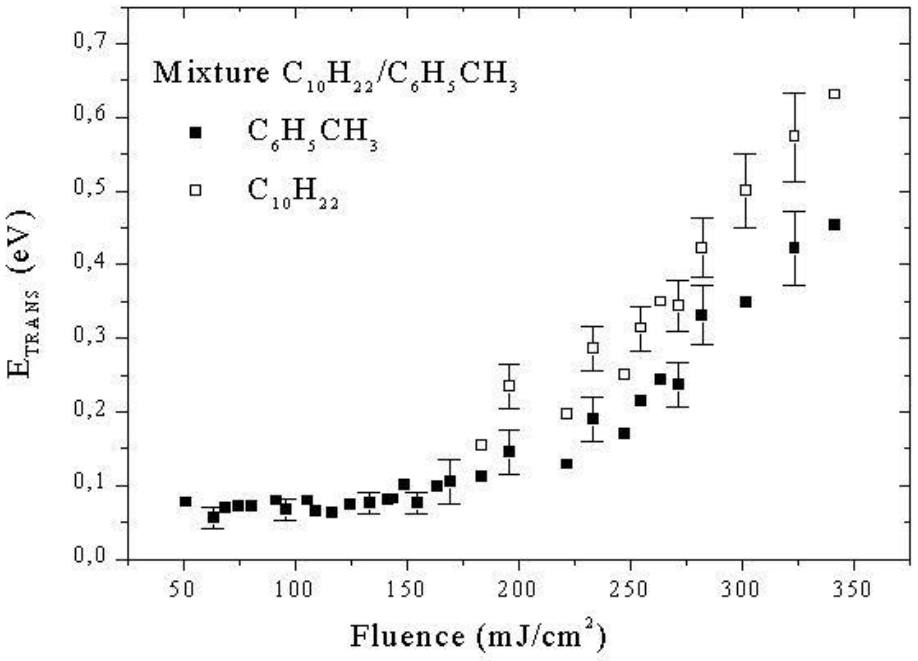

Figure 5-4 The figure depicts the E_{TRANS} of the $C_6H_5CH_3$ and the indicated dopants (up) $(CH_3)_2O$ (bottom) $C_{10}H_{22}$ as a function of the incident laser fluence in the irradiation of mixture solids of the compounds. The errors bars represent 2σ, as determined from at least 4-5 measurements.

In contrast, for the cases that dopants do not desorb below threshold, the F_{LASER}-dependence of the desorbate E_{TRANS} is qualitatively similar to that observed for neat films. In particular, below the ablation threshold, the $\tilde{o}_{mp}$ (E_{TRANS}) of the toluene are nearly constant, thus contrasting the dependence observed for volatile dopants. The difference establishes that the increase in the E_{TRANS} observed for the former systems is due to the fact that for these systems, the gas-phase collisions suffered by toluene are extensive and result in modification of its translational distribution. Most interestingly, the value E_{TRANS} observed at low fluences for the $C_{10}H_{22}/C_6H_5CH_3$ systems is higher than that specified for the neat toluene system, at the same fluence range. At fluences above threshold, (F_{LASER}> 190 mJ/cm^2), both the dopant and toluene attain equal values of $\tilde{o}_{mp}$, which are comparable to those determined for the neat $C_6H_5CH_3$ system.

5.3. DISCUSSION

An examination of the translational characteristics of the desorbed molecules in the UV ablation of cryogenic van der Waals neat and mixture solids has been presented. The results can be summarized as follow:

(1) In all examined neat solids, upon attainment of the ablation threshold, E_{TRANS} increase abruptly and distinctly different dependences on F_{LASER} are observed above and below threshold. Interestingly, the E_{TRANS} values below the threshold are nearly constant.

(2) In the irradiation of toluene/volatile dopant solids in the subablative regime the values of the E_{TRANS} of the toluene increase with increasing laser fluences. In contrast, in the case of mixtures (toluene+involatile dopants) the overall dependence is qualitatively similar to that of neat $C_6H_5CH_3$ system.

In the following, we account for the observed features in terms of the different ejection mechanisms and postdesorption collisional dynamics that may operate in the corresponding regimes. This examination uses for first time mixtures with dopants of various volatilities in order to simulate experimentally the effect of the gas phase collisions and separate it from the ejection mechanisms.

5.3.1. Ablation Regime

Considering first the translational features in the ablation range, the quite high E_{TRANS} values observed here would appear to be compatible with a supersonic-like expansion of the material, exactly as suggested by Natzle et al [40], Cousins et al [42] and also by simulations and analytical modeling of the postdesorption gas flow [80-86]. The influence of the gas-collisions is clearly indicated by the Monte Carlo study [87] of the time-dependent desorption of polyatomic molecules (Table 5.2). In our case, based on the callibration procedure discussed in chapter 2 it is estimated that at least 5-10 monolayers (in the irradiation of neat $C_6H_5CH_3$) desorb at fluences close to the threshold. On the basis of an approximate model (Appendix II) $\gg$ 100, postdesorption collisions are estimated, which can largely account for the high υ_{mp} values, especially for the studied polyatomic systems with a high number of internal degrees of freedom. With increasing

laser fluence, the higher amount of ejected material (Fig. 2(a)) results in a "tighter" supersonic expansion, with a consequent increase of the υ_{mp} values (Fig 2(b)).

Table 5-2 The results from the Collisional Models

System	Desorbing Quantity (ML)	Estimated Number of Collisions (N_{coll})
Valine [80]	0.1	2.5
	1	18.47
Indole [79]	0.1	2.54
	1	18.47
Toluene [this Thesis]	0.1	2.19
	1	19.4
	5	100

Yet, in detail, the desorbate translational features observed in the ablative regime are not fully compatible with the idea of a supersonic expansion. First, both the υ_{drift} and the T values are found to increase with increasing laser fluence, contrary to the characteristic of beams of decreasing T_z with increasing υ_{drift}. This trend is correctly predicted by the theoretical treatment emphasizing the time-dependent dynamics of desorption [86], but it is indicated (Tables III and IV in [80]) to be much weaker than the observed one. Furthermore, for a supersonic-like expansion, υ_{drift} should be given [80,86] by $M\,(\gamma kT/m)^{1/2}$, where M is the Mach number, $\gamma = Cp/Cv$ and T is the corresponding temperature of the TOF spectrum. Employing the known spectroscopic constants [57,62] for the estimation of γ for $C_6H_5CH_3$ and C_6H_5Cl, a Mach numbers of 2, at most is indicated (which is certainly not high enough for a "tight" supersonic expansion). This estimated value agrees with the Mach number determined by Levy in the irradiation of

aminoacids and Costa in the ablation of frozen aqueous solutions. On the other hand, others have claimed Mach numbers of 5 or higher. Finally, the most clear-cut feature in the determined F_{LASER}-dependence of the desorbate u_{mp} is the abrupt change at the ablation threshold in the case of the neat films. This sharp increase cannot be ascribed, at least fully, to the increase of the material ejected at the threshold. This is directly demonstrated by the plot of E_{TRANS} as a function of desorbing signal where it is seen that there is no gradual evolution of the E_{TRANS} as a function of the desorbing signal. Clearly, the correlation between the two parameters is much more complicated than any model appears to suggest.

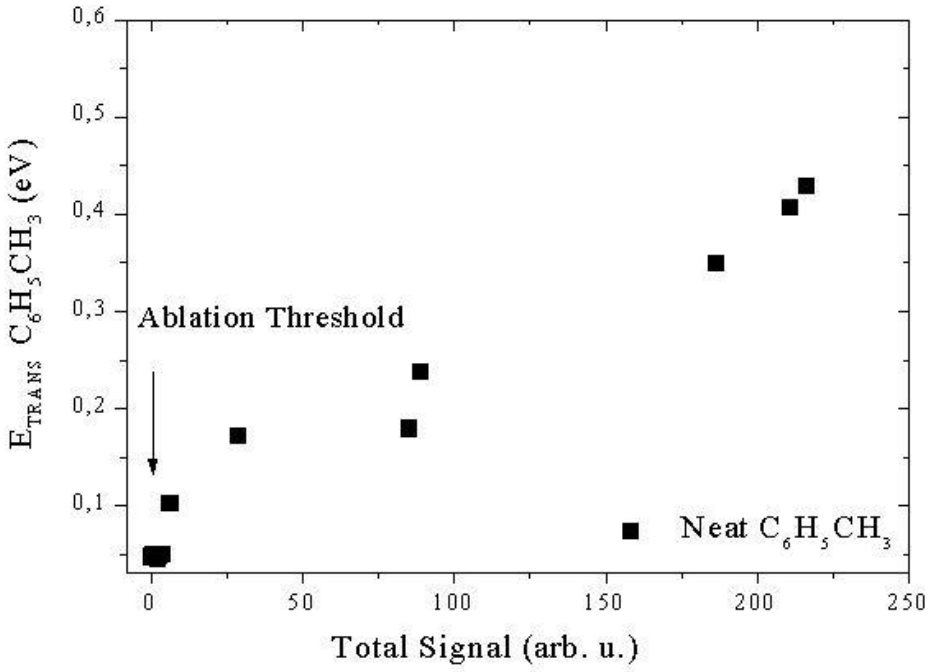

Figure 5-5 The figure illustrates the E_{TRANS} of $C_6H_5CH_3$ as a function of the total desorbing material in the irradiation of the neat solids of the compound.

The question then arises if the discrepancies are due to the nature of the gas-flow dynamics in the plume or due to some contribution by the processes in the solid (before material ejection occur). The importance of the gas phase collisions is directly indicated in the study of the $(CH_3)_2O/C_6H_5CH_3$ system. As shown in 5.2.2.1, the $\tilde{o}_{mp}$ below the

threshold increases with increasing fluence whereas in the case of the nonvolatile dopants, no such dependence is observed. Since it has been demostrated that at these fluences, the mechanism of desorption is the same for both systems (thermal evaporation), the high $\tilde{o}_{mp}$ observed for the volatile dopant/$C_6H_5CH_3$ system clearly relate to the gas-phase enhanced number of collisions resulting from the high amount of dopant desorbing. In fact, this is a unique example illustrating unequivocally the importance of the gas-phase collisions. We take advantage of this system in order to access the importance of the gas-phase (collisional) vs. processes in the solid in the abaltive regime.

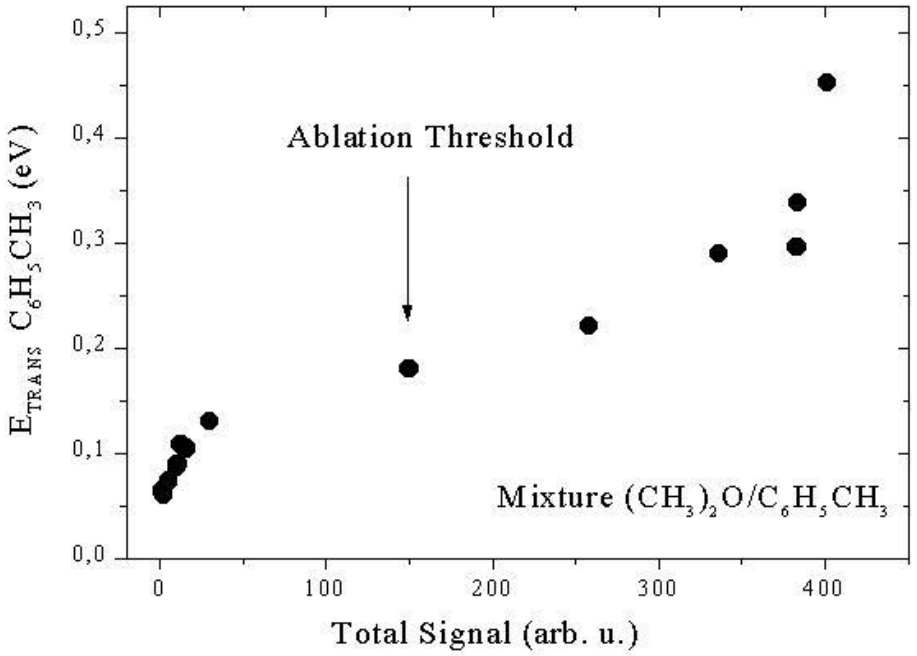

Figure 5-6 The figure illustrates the E_{TRANS} of $C_6H_5CH_3$ as a function of the total desorbing material in the irradiation of mixture $(CH_3)_2O/C_6H_5CH_3$.

Table 5-3 The results of the linear fit of E_{TRANS} vs Total Signal.

System	Slope (eV/Signal)	Intercept[38] (eV)	Signal[39] (arb.u.)
Neat $C_6H_5CH_3$ Above threshold	1.276×10^{-6}	0.106±0.005	5.8 - 216
$C_6H_5CH_3/(CH_3)_2O$ Below threshold	3.5×10^{-6}	0.05±0.003	1.9-30
$C_6H_5CH_3/(CH_3)_2O$ Above threshold	$5.4 \times 10^{-7}(\pm 1 \times 10^{-8})$	0.103±0.005	30-383

For this purpose, we plot the E_{TRANS} of $C_6H_5CH_3$ as a function of the total desorption signal in the irradiation of $C_6H_5CH_3/(CH_3)_2O$ below the threshold. The total desorbed signal is calculated by summing the toluene signal and the corrected to toluene signal of the dopant (dimethylether in this case). At low laser fluences, the E_{TRANS} of $C_6H_5CH_3$ (and of $(CH_3)_2O$) increases with desorbing amount, evidently due to efficient energy transfer from $(CH_3)_2O$ to $C_6H_5CH_3$. This is clearly shown by the observation that $E_{TRANS}((CH_3)_2O) < E_{TRANS}(C_6H_5CH_3)$ (Fig. 5.4), despite the fact that for the thermal desorption mechanism demonstrated at these fluences, E_{TRANS} of the two compounds would be expected to be equal[40]. However, with increasing desorbing amount, the E_{TRANS} ($C_6H_5CH_3$) reaches a plateau in an exponential way i.e., there is a maximum in the amount of "directional" translational energy as a function of desorbing signal. Most importantly, this plateau is reached below the ablation threshold of the system. At the ablation threshold, E_{TRANS} are observed to increase again. Evidently, this increase cannot be correlated to the desorbing signal, thereby indicating a new contribution. Furthermore,

[38] The intercept can be considered to be the velocity of the desorbates for zero collisions. Thus, the fact that this is nonzero, further indicates that desorbates in ablation are ejected with a forward velocity.

[39] Signal range in the Fit

[40] This is consistent with the findings of a Monte Carlo Simulation presented by Urbassek. For a thermal desorption mechanism, the light species is desorbed with a higher velocity than the heavy species, but accelerates the latter. This phenomenon influence the energy distribution of the desorbed particles.

the rate of increase of E_{TRANS} in the ablative regime is not as high as that below the threshold.

Thus, gas phase collisions are not as important in determining affecting the kinetic energies in the ablative regime, contrary to common belief. This can be understood by the fact that in ablation molecules already leave with a forward velocity so that in the center-of-mass framework of ejected material, collisions are much less significant. As has been proposed in the chapter 3 and 4 ablation is strongly indicated to be due to a "explosive boiling". As shown by MD simulations, the high pressures that develop in the film by the explosive boiling result in the strong axial acceleration of the desorbates. Evidently, these result in the extra, forward velocity component of the desorbates. Furthermore in an theoretical examination of the phenomenon by Chen et al on the basis of hydrodynamic they found that if the gas expansion front is accelarated by a dynamical effect, like a explosive boiling process, then the particles attained faster velocities than those predicted from conventional models of a gas collision theory.

5.3.1.1. Dopant Translational Characteristics in Ablation

Above the ablation threshold, considering first the involatile species, their TOF spectra are nearly "superimposable" with those of the matrix. (thus, their kinetic energies are higher than the matrix by the relative ratio of masses). Clearly, their description in terms of Maxwell-Boltzmann distributions requires either "wrong mass" or very different (T, udrift) sets. Once more, this demonstrates the pitfals of the studies relying on modelling the translational distributions of biopolymers in MALDI or in polymers for establishing mechanisms. On the other hand, the observed translational distributions are clearly compatible with the idea that the "involatile" species are ejected within clusters and are accelerated by the explosive boiling and the collisions with the ejected $C_6H_5CH_3$ molecules to the same velocity. As employed sometimes in molecular beams modelling the translational distributions can be in that case be attained by [130]:

$$dN(u,T,u_{\max}) = K \times \left\{ erf[\sqrt{\frac{m}{2k_BT}}u_z] - erf[\sqrt{\frac{m}{2k_BT}}(u_z - u_o)] \right\} du_x du_y du_z$$

$$\text{where } K = \frac{m}{4p\,k_B T u_{\max}} \exp\left\{ \frac{-m(u_x^2 + u_y^2)}{2k_BT} \right\}$$

Indeed, good fitting is attained for $C_{10}H_{22}/C_6H_5CH_3$ distributions, but evidently the formula is too cumbersome for quantitative comparison.

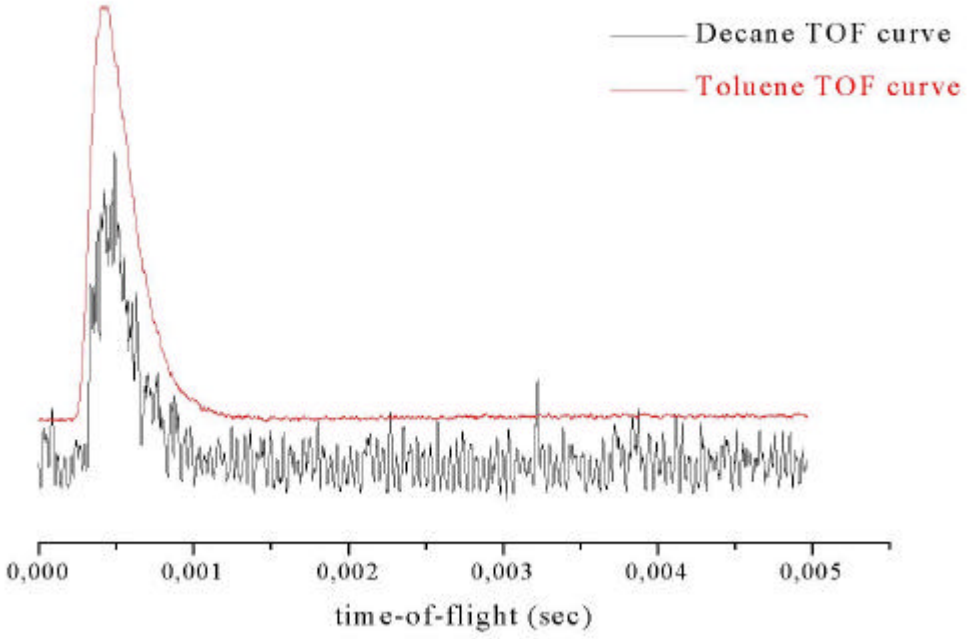

Figure 5-7 The figure illustrates two charatceristic TOF curves recorded in the irradiation of $C_{10}H_{22}/C_6H_5CH_3$ solids at fluences above the threshold.

The features of the "involatile" species are better appreciated when they are compared with those of the volatile species above the threshold. In sharp contrast to the "involatile" species, the translational energies of $(CH_3)_2O$, c-C_3H_6 etc. are much lower than that of the matrix, and in addition, their translational distributions can be approximated by swifted Maxwellian with well-defined ($\tilde{o}_d$, T). As described in chapter 4, for the volatile species, there is strong evidence that they are ejected as monomers, whereas the matrix desorbs also in the form of clusters (~60%). Collisions between the

light $(CH_3)_2O$ and the heavy clusters will thus result in a major translational energy loss of $(CH_3)_2O$. Furthermore as shown in chapter 4, for the volatile dopants, there is also contribution of molecules from underlying layers (via diffusion) in addition to the molecules ejected from the volume ejected layer. Since these molecules desorb essentially thermally with correspondingly lower temperatures, their contribution will result in the $(CH_3)_2O$ translational energies being lower.

5.3.2. Sub-ablation Regime in Neat Systems

The most surprising feature of the examination concerns the very weak dependence of E_{TRANS} or υ_{mp} on F_{LASER} at fluences below the threshold. As demonstrated in Chapter 3, a thermal mechanism of desorption is established to operate in this regime. The surface film temperature have been estimated, to be in the range of 200 – 400 K. Both the υ_{mp} velocities and the T derived from the fitting of the TOF spectra in this regime correspond to these temperatures, but most suprisingly do not scale as expected. In the framework of a simple thermal model, the desorbate υ_{mp} values should scale as $(3k_BT/m)^{1/2}$ (where T represents the film tempaerature) and since T is proportional to F_{LASER} (formula 3.2 and 3.3), a corresponding dependence between υ_{mp} and F_{LASER} should be observed. On the basis of the formulas (3.2) and (3.3), a dependence of $\approx 17F^{1/2}_{LASER}$ is calculated for toluene and chlorobenzene, which is certainly stronger than the experimental one.

One possibility that may be responsible for the near constant δ_{mp} value is an "apparent" broadening of the translational distributions. First, even for these systems, some collisions may occur with the result that any differences in the initial δ_{mp} are "smoothed" out[41]. Alternatively any structural inhomogeneities of the films will result in different distributions of the desorbate velocities, and as a result, the TOF spectra may be a convolution of different populations. In either case, the consequent broadening of translational distributions may be responsible for an "apparent" constant δ_{mp} value. These

[41] However, it can be counter-argued that the effect of gas-phase collisions should result in the opposite trend, i.e., in an increase of δ_{mp} with increasing laser fluence and desorbing amount. In fact, this effect is seen in the $C_6H_5CH_3$ distributions at fluences approaching the threshold, where desorbing quantity starts becomes significant.

possibilities cannot be ruled out at present though, the possibility should be noted that the molecules may indeed desorb with constant $\tilde{o}_{mp}$ from the film, despite the fact that different temperatures are attained at different fluences.

A further indication that the observation of constant $\tilde{o}_{mp}$ may be an important result is provided by the fact that its value appears to relate to the cohesive energy of the system, as the comparison between neat $C_6H_5CH_3$ and involatile dopant/$C_6H_5CH_3$ seems to suggest: *$\tilde{o}_{mp}$ is higher for systems of higher cohesive energy*. One most interesting possibility would be that the observation of constant $\tilde{o}_{mp}$ may be intimately related to properties of superheated liquids. The proportionality $u_{mp} = \sqrt{\frac{3k_BT}{m}}$ relates to the principle of microscopic reversibility and assumes equilibrium between the adsorption and the desorption process. In the case of superheated liquids, the principle of equilibrium is not fully fulfilled and thus a priori there is no reason why $\tilde{o}_{mp}$ should follow the above relationship. Instead, velocities may be determined by the barrier that they may have to overcome in order to be released into the gas-phase. For $(C_{10}H_{22})/C_6H_5CH_3$, this barrier is higher, thereby accounting for the higher $\tilde{o}_{mp}$ of $C_6H_5CH_3$ desorbate in this case as compared with the case of $C_6H_5CH_3$ desorbates in the irradiation of neat $C_6H_5CH_3$ solids.

Certainly, this is a most tentative explanation and further experiments on a number of systems of different cohesive energies must be studied for establishing the validity of this proposition. Furthermore, theoretical work is necessary for justifying this proposition. Thus far, the issue of velocity distributions of molecules desorbing from overheated liquids has never been addressed.

5.4. CONCLUSIONS

The study illustrates a number of interesting trends concerning the desorbate translational features in the UV irradiation of molecular solids. In the irradiation of neat solids (and mixtures with "involatile" dopants) E_{TRANS} increase abruptly at the ablation threshold with distinctly different dependences on F_{LASER} above vs. below the threshold. It is strongly indicated that the change is not only due to the gas-phase collisions but it reflects also the "impulse" of the processes responsible for material ejection. An interesting observation is the near constant E_{TRANS} values below the threshold, which may relate to the desorption from superheated liquids. Finally, the study of the toluene/volatile dopant mixtures provides the means for experimentally "simulating" the effect of gas-phase collisions. These can provide the basis for detailed modelling and theoretical examination of desorbate translational features.

6. PHOTOCHEMICAL PROCESSES IN THE UV ABLATION CRYOGENIC SOLIDS

6.1. INTRODUCTION

In previous chapters we examine the desorption/ejection processes factoring out any effect of the electronic/chemical processes that take place. Yet, the issue of photochemical modifications effected to the substrate and the desorbates is crucial both for the optimization of the analytical and technological capabilities of the techniques as well as for the elucidation of the underlying mechanisms. Most importantly the question is raised how photophysical and chemical processes differ in the ablative regime vs at low laser fluences. No satisfactory model exists for the description of electronic excitation and deexcitation processes and of the subsequent photoreactivity in the UV ablation of molecular solids. First, concerning excitation and deexcitation processes, novel processes have been indicated (f.e. as discussed in chapter 1). Furthermore, despite numerous studies, the nature of the photochemical processes that take place in the UV ablation of molecular substrates remains ill-understood. In particular, there is no consecusus if photoproduct formation differs from those formed at low laser fluences (where conventional photophysics/chemistry is applicable).

In this chapter, we present a study of the ablation of neat C_6H_5Cl films at 248 nm. Upon excitation at 248 nm, C_6H_5Cl dissociates exclusively by scission of the C-Cl bond [92-94] to yield C_6H_5 and Cl, which, in solution and static gas cell experiments, react with the precursor molecule to form a number of different products [95-96]. Thus, the study of the ablation of C_6H_5Cl films provides the possibility for examining the characteristics of reactivity that takes place in the UV ablation of molecular films, i.e. for establishing the factors that affect of photoproducts formation.

6.2. STUDY OF CHLOROBENZENE FILMS

6.3. RESULTS

6.3.1. Characterization of the Desorption of C_6H_5Cl

6.3.1.1. Fluence Dependence of the Desorption Signal

Chlorobenzene is a moderately strong absorber at 248 nm (á ≈ 1900 cm^{-1} in liquid phase[33]). Accordingly, upon irradiation of condensed solids of the compound, desorption is observed at fluences as low as ≈10 mJ/cm^2 (the lowest examined fluence). Fig. (6.1) illustrates the desorption signal of C_6H_5Cl as a function of the incident laser fluence. The curve is similar to that determined for the other systems studied in this work ($C_6H_5CH_3$, CH_3I etc.)

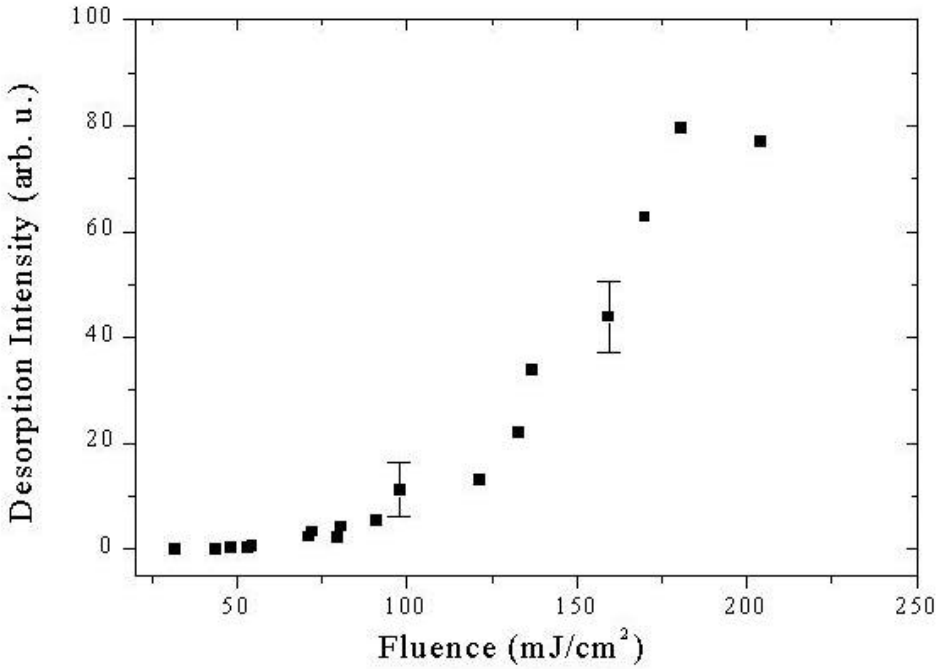

Figure 6-1 The figure depicts the intensity of C_6H_5Cl recorded in the first pulse from freshly deposited film as function of the incident laser fluence. The error bars represent 2ó.

All depicted data derive from spectra recorded in the first laser pulse from freshly deposited solids, except at low laser fluences (< 50 mJ/cm^2), where the poor S/N ratio

necessitated averaging of the spectra over 5 or more laser pulses. The need for minimum pulse averaging in the recording spectra comes from the fact that as shown in the next section, chlorobenzene's intensity of the spectra, as well as the shape of TOF curve, depend sensitively on the irradiation prehistory (indcution effect) of the solid. Following the practice described in the case of neat toluene, the ablation threshold of neat C_6H_5Cl films can be established at $\approx$ 50 mJ/cm^2. In parallel, at this fluence value, the dependence of desorbate most probable υ_{mp} values on F_{LASER} abruptly changes with quite different characteristics (chapter 5).

6.3.1.2. Induction Effect

A most interesting feature that was not observed in the study of the previous systems is provided by the examination of the C_6H_5Cl desorption efficiency from freshly deposited films as a function of successive laser pulses. At fluences above 50 mJ/cm^2, desorption of the parent molecule is observed to be significant from the very first pulse. At these fluences, the observed pulse dependence is similar to that described for neat $C_6H_5CH_3$.

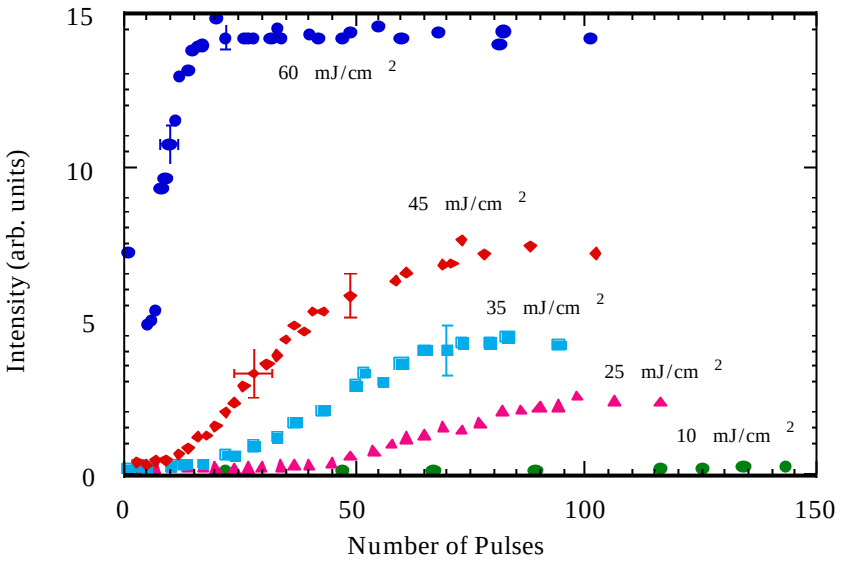

Figure 6-2 Pulse evolution of the C_6H_5Cl intensity in the irradiation of freshly deposited films at low F_{LASER}. For comparison purposes, the corresponding pulse evolution at a higher laser fluence is also illustrated.

However, at fluences below the threshold (50 mJ/cm^2), the intensity of C_6H_5Cl is observed to be initially low, but it rises with continuing irradiation until attaining a plateau (Fig. 6.2). This effect is observed not only in the mass spectrometer signal, but also in the desorption intensity measured by an open ionization gauge placed across the irradiated area. Consequently, the observed increase in the signal is not due to changes in the desorbate angular distribution, but instead reflects an actual increase in the total desorption efficiency. In parallel, the shape of the TOF spectra changes, with the E_{TRANS} increasing to a final constant value.

For elucidating the origin of this effect, the transmission of the film was monitored as a function of successive laser pulses. To this end, a second, probe 248 nm beam was employed for examining the transmission of the solid after each "pump" laser pulse (Fig. 6.3). Clearly film transmission decreases with successive laser pulses and the decrease is higher with increasing "pump" fluence. Consequently the changes in the

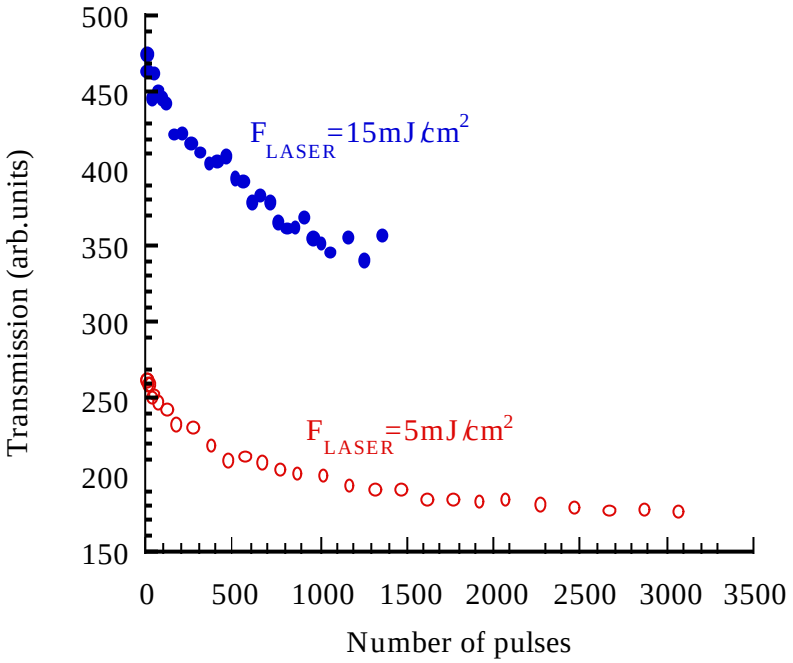

Figure 6-3 Probe transmission of the film following UV irradiation with successive laser pulses at the indicated fluences

desorption signal must be ascribed to the more efficient coupling of the laser light into the solid. The reason for the changes in the transmission will become apparent after the examination of photoporduct formation.

6.3.2. Photoproduct ejection

6.3.2.1. Pulse Evolution

In the irradiation of chlorobenzene films, we detect four new major species, namely HCl, $(C_6H_5)_2$, $C_6H_4Cl_2$ and C_6H_4Cl - C_6H_5. Free Cl is unambiguously observed at somewhat higher fluences (> 300 mJ/cm^2), while C_6H_4Cl - C_6H_4Cl is observed[42] with

[42] Because of the relatively low resolution of the mass spectrometer for masses above 100 amu, we can not exclude the possibility that the phenyl derivatives are actually the corresponding ipso-adduct radicals, i.e., $C_6H_5Cl_2$, C_6H_5Cl-C_6H_5. We consider, however, more likely the detected species to be the stable phenyl derivatives and we adopt this possibility in the subsequent

increasing intensity above ≈130 mJ/cm^2. Furthermore, we cannot exclude the possibility of C_6H_6 formation, since its detection is hampered by the contribution of the strong $C_6H_5^+$ peak deriving from the mass cracking of C_6H_5Cl.

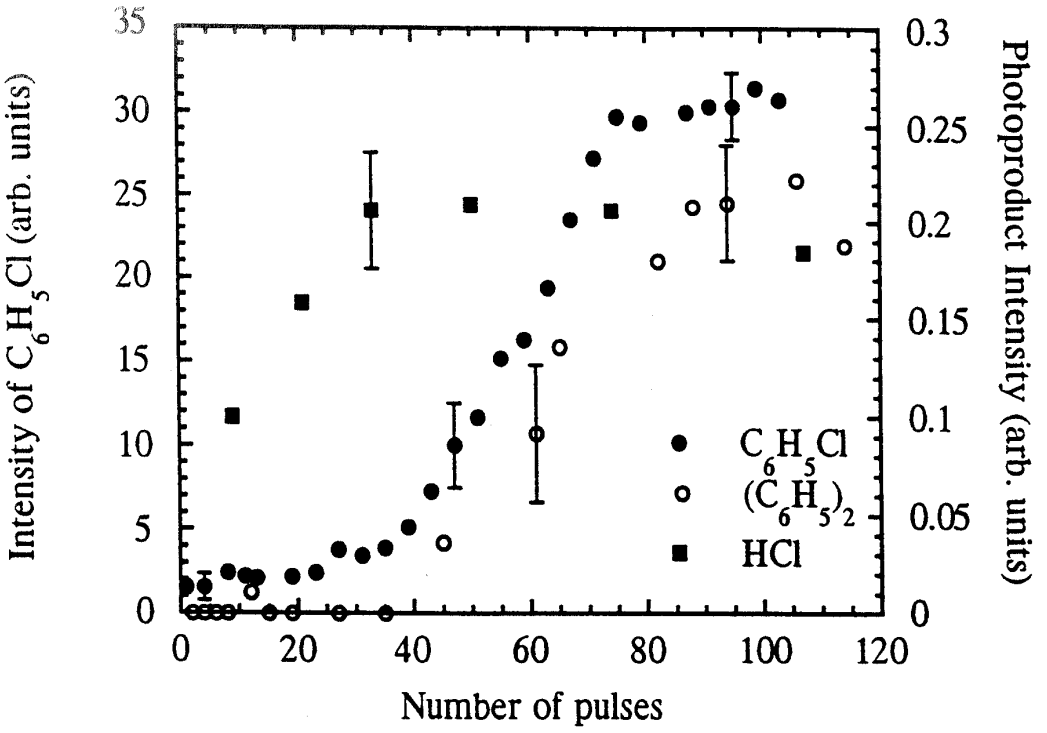

Figure 6-4 Pulse evolution of the intensities of C_6H_5Cl, HCl and $(C_6H_5)_2$ in the irradiation of freshly deposited films with ≈30 mJ/cm^2. The intensities have not been corrected for the different detection efficiencies of the various species in the mass spectrometer. Essentially the same pulse dependence as that for $(C_6H_5)_2$ is also observed for $C_6H_4Cl_2$ and $C_{12}H_9Cl$.

Of the various products, HCl is observed from the lowest examined fluence. At the lowest fluences, its detection required averaging over 30 or more pulses, evidently because of low S/N ratio. However, at somewhat higher fluences, signal for this species

---

discussion of this paper.

can be clearly detected from the very first pulse on freshly deposited films, with its intensity growing somewhat in the subsequent few pulses. (Fig. 4)[43].

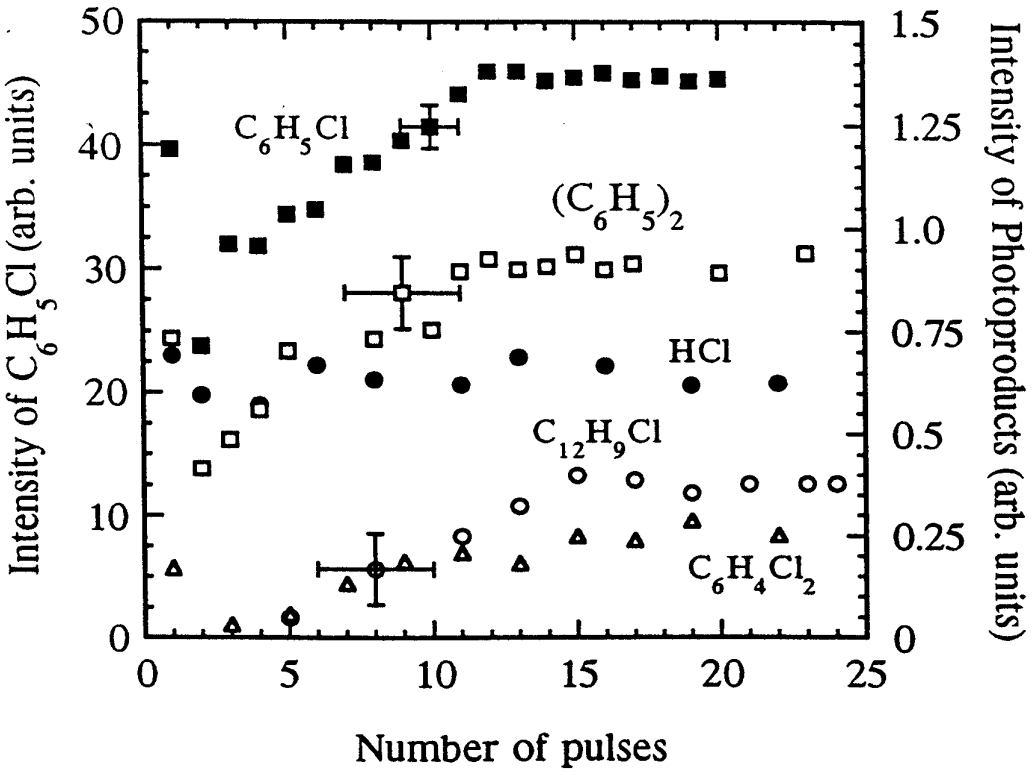

Figure 6-5 Pulse evolution of the intensities of C_6H_5Cl and of the various photoproducts in the irradiation of freshly deposited films with ≈100 mJ/cm^2. The intensities have not been corrected for the different detection efficiencies of the various species in the mass spectrometer. In fact, for clarity of presentation, the intensities of HCl have been scaled arbitrarily.

In contrast, at F_{LASER} ≤50 mJ/cm^2, phenyl photoproducts are detected only as parent signal induction becomes significant (Fig. 6.5). No signal (0.1% of the parent peak) was discernible for $(C_6H_5)_2$ or any other phenyl derivative in the first few pulses from freshly deposited solids. In sharp contrast, at fluences above 50 mJ/cm^2, signal for

[43] The HCl peak impurity in the initial sample, is after extensive purification is, at most, 0.5% as intense as the parent peak, which is small to interfere with the HCl signal that derives from the irradiation process in the solid.

these photoproducts is observed almost from the very first pulse. Furthermore, their relative intensity does not change with successive laser pulses, which strongly indicates that they are formed mainly via parallel rather than consecutive reactions. (i.e., the one product is not formed at the expense of others)

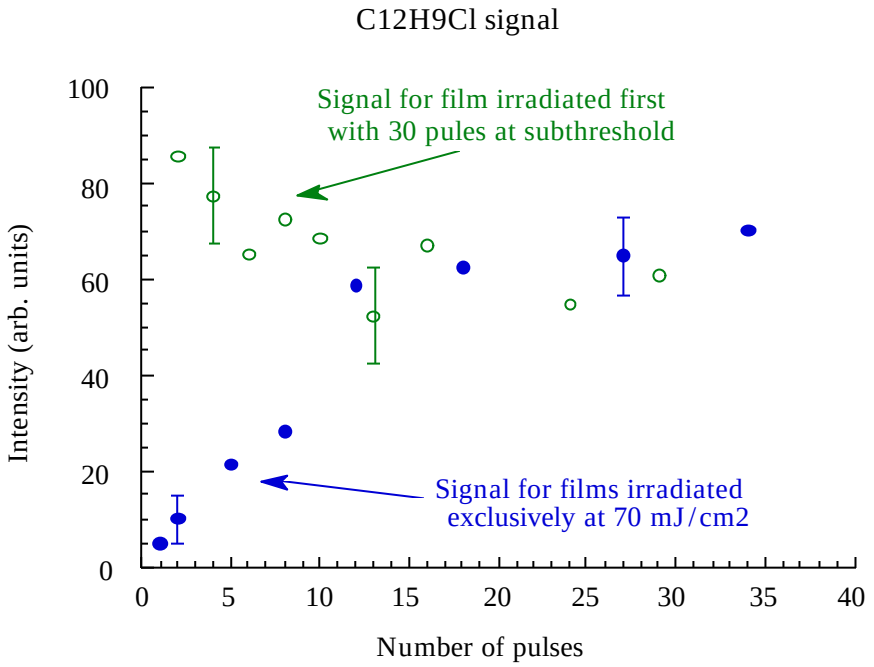

Figure 6-6 Pulse evolution of the $C_{12}H_9Cl$ intenisty recorded at F_{LASER}» 70 mJ/cm^2 for film that has been irradiated with 30 pulses at F_{LASER} » 35 mJ/cm^2. (•) Corresponding pulse evolution observed in the irradiation of freshly deposited films exclusively at F_{LASER} » 70 mJ/cm^2.

Importantly, even at the higher fluences, the pulse evolution of the phenyl photoproduct intensities is found to follow closely the corresponding one of the parent peak (Fig. 6.5), indicating that the ejection process of the phenyl photoproducts correlates closely to that of the parent molecule. Some degree of the observed pulse dependence must also result from the accumulation of these species in the film. To establish the degree of accumulation, we have examined the dependence of the ratio $I_{product}/I_{C6H5Cl}$, i.e., the ratio of the intensities of the various products vs. that of the parent peak, as function of successive laser pulses.

For HCl, accumulation in the film is indicated to be minor, even at fluences close to the ablation threshold, evidently because of its very high volatility. In contrast, for the phenyl photoproducts, this ratio is found to grow with successive laser pulses until reaching a plateau, where evidently equilibrium is attained between photoproduct formed per pulse and photoproduct desorbed. This effect is significant for fluences up to ≈150 mJ/cm^2. Thus, at least up to those fluences, a significant percentage of the products is produced in the film. Accumulation for these species is indicated to become progressively less important at higher fluences.

In contrast to HCl and the phenyl photoproducts, Cl is, within our S/N, observed only above ~90 mJ/cm^2, with little, if any, signal being detected at lower fluences even after extensive averaging. The Cl signal starts increasing sharply above ≈150 mJ/cm^2. It exhibits minimal, if any, pulse dependence.

Finally, C_6H_4Cl - C_6H_4Cl is detected with increasing intensity at fluences above ≈130 mJ/cm^2. We have not examined, its formation in any detail, because at these high fluences, multiphoton processes leading to ionization and ill-defined chemistry are expected to start becoming important, as indicated by the detection of an ion signal in the mass spectrometer (with electron impact turned off).

6.3.2.2. Fluence Dependence

In Fig. 6.7, we present the intensities recorded in the first pulse from freshly deposited solid of the various products as function of the laser fluence. Considering first the HCl photoproduct, its intensity over the 40-150 mJ/cm^2 range barely doubles, which sharply contrasts the strong increase observed for C_6H_5Cl in this range. The observation of different F_{LASER}-dependences for the two species suggests that HCl formation herein is decoupled from C_6H_5Cl desorption. Most interestingly, the HCl signal is observed to be very small in comparison with the parent peak. As illustrated in Fig. 6.8, the "apparent" yield, (i.e. the ratio $I_{HCl} / I_{C_6H_5Cl} + I_{HCl}$ remains well below 0.01 over the 40-150 mJ/cm^2 range. Assuming an excitation cross-section of 3.2 x 10^{-19} cm^2/molecule [12], the quantum yield of C_6H_5Cl photolysis is calculated to be, at most, ≈ 0.05, nearly an order

of magnitude lower than the 0.4 gas-phase value. Of course, the determined value constitutes only a rough estimate, since the angular distribution of the parent molecule and of the photoproduct is not taken into account. Nevertheless, it clearly illustrates the apparent inefficiency of molecular fragmentation under ablation conditions.

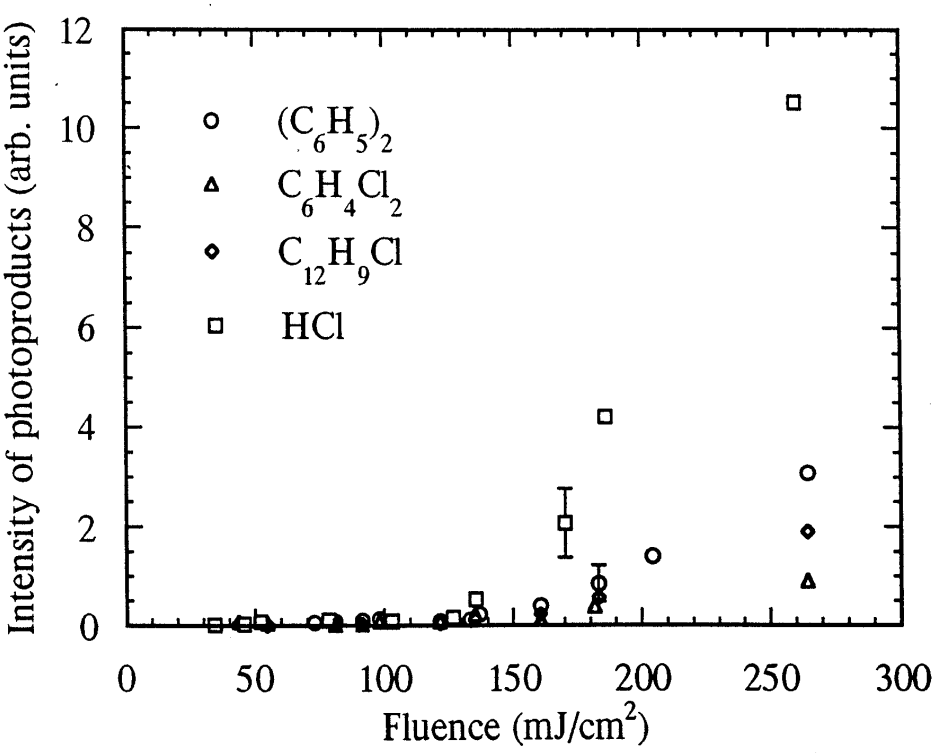

Figure 6-7 The figure depicts the intensities of the indicated photoproducts as function of the incident laser fluence. The error bars represent 2ó.

The branching ratio between the photoproducts does not change over the 50-150 mJ/cm^2 range. Thus, it appears that over this fluence range, the factors that affect the reactivity of the Cl and C_6H_5 fragments are not modified by the change in the laser fluence. The relative intensities of the products start changing only at higher fluences (F_{LASER} > 150 mJ/cm^2). Since the increase is observed for all products, the change is not due to the enhancement of the formation of one particular product over others, but due to an increase in the photolysis efficiency of C_6H_5Cl. In particular, HCl starts to grow drastically and at fluences above ≈200 mJ/cm^2, its growth evidently occurs at the expense of the C_6H_5Cl intensity. A log-log plot establishes the increase in the HCl yield to be

linear on F_{LASER} with a slope of 4±2 x 10^{-4} (in units of cm^2/mJ). However, this number underestimates somewhat the degree of photolysis, because at the higher laser fluences,

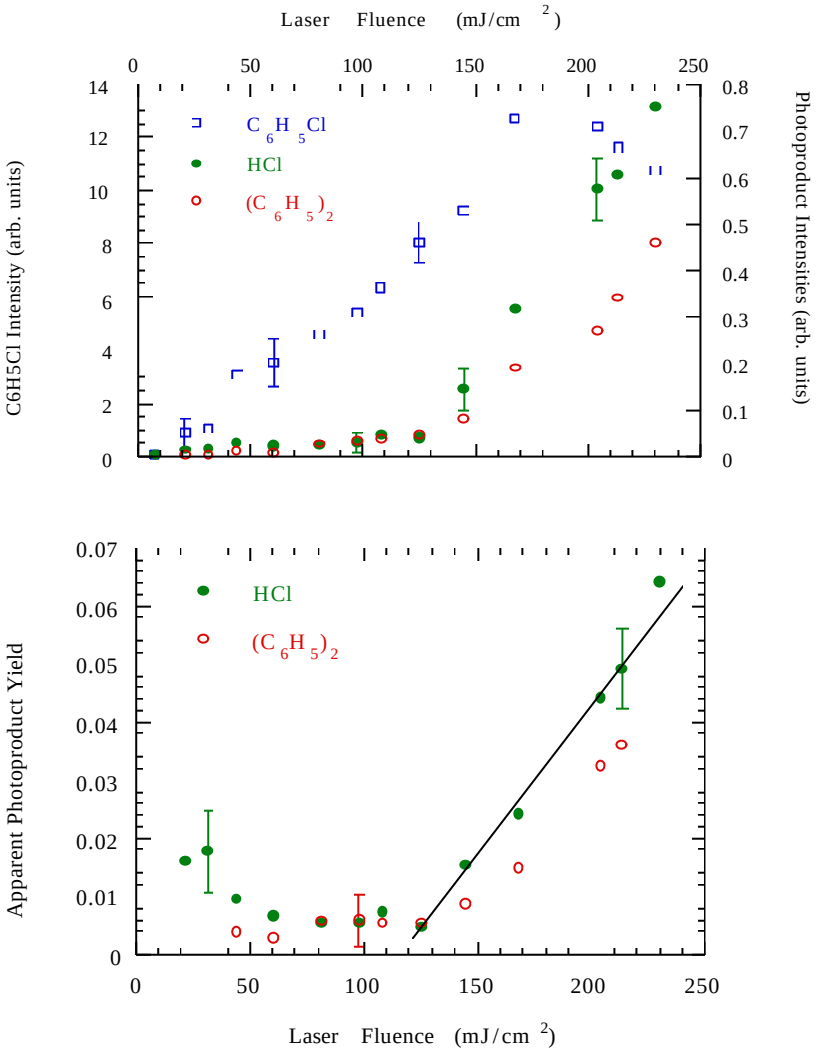

Figure 6-8 The figure depicts the HCl concentration as function of the incident laser fluence.

various new desorption peaks are detected, showing that the depletion of C_6H_5Cl in this range is not fully accountable by the HCl signal. Nevertheless, as HCl remains the most prominent signal in the desorbate mass spectra, the involved error is relatively small. Furthermore, as shown in Fig. 6.7 above 150 mJ/cm^2 there is also an increase of the phenyl-type products but with lower rate than the HCl. In the Discussion section, we will

argue that these differences relate to the different times of plume ejection in the different fluence ranges and as a result to the different relative contributions of the photolysis of C_6H_5Cl in the gas-phase (plume) vs. in the solid [97-98,65]

6.3.3. Photoproduct Translational Distributions

The observed photoproducts differ not only in their efficiencies of formation and of desorption, but also in their translational features. Specifically, the phenyl derivatives $(C_6H_5)_2$, $C_6H_4Cl_2$ and C_6H_5- C_6H_4Cl, as well as the Cl fragment that is observed at higher fluences, are generally characterized by essentially the same TOF distributions as the parent peak[44]. In sharp contrast to the phenyl photoproducts, HCl generally arrives at earlier times, which are suggestive of an "energetic accomodation" (equilibration) to the parent peak. At fluences higher than 130 mJ/cm^2, Etrans(HCl)≈Etrans(C_6H_5Cl). At lower fluences, its E_{TRANS} is somewhat lower than that of the parent peak, but still comparable.

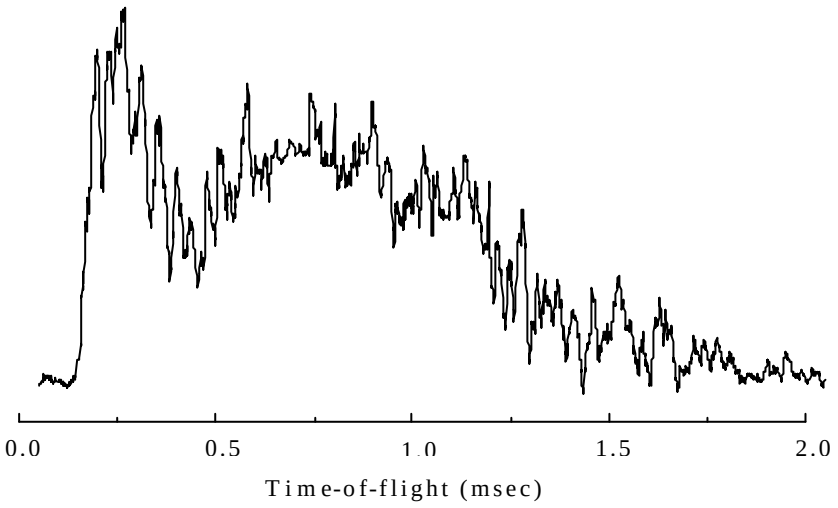

Figure 6-9 Illustration of the TOF curves recorded for HCl at low laser fluences, and exhibiting two well-defined components: the slow one that is observed from freshly deposited films at low fluences and the fast one that "grows in" as parent signal induction

[44] Deviations from this behavior are observed only at high fluences (F_{LASER}>200 mJ/cm^2) (observation of a slower TOF component (E_{TRANS} ≈ 0.1-0.2 eV)). These deviations are observed only at high fluences, at which several different pathways (processes in the plume as well as in the film, multiphoton processes, etc) may be responsible for these discrepancies.

becomes important. The depicted spectrum was recorded at F_{LASER} 30 mJ/cm^2 and has been averaged over ≈40 laser pulses.

In contrast to the translational characteristics just described, the HCl TOF curves recorded below ≈ 50 mJ/cm^2 are generally characterized by a bimodal distribution (Fig. 6.9). In addition to the fast peak observed at high laser fluences, there is a slow one with E_{TRANS} in the range of 0.02 - 0.06 eV. In fact, the HCl signal recorded from freshly deposited films is described almost exclusively by the slow component, but as parent signal induction sets in, there is a growing contribution by the fast HCl component[45]. Since the slow component is observed only below the ablation threshold, the desorption of HCl with this distribution may relate to the fact that no well-defined plume is formed in this fluence range.

6.4. DISCUSSION OF THE RESULTS

6.4.1. Desorption Dynamics of the Photoproducts

In the present chapter, the ablation of a photosensitive compound namely of C_6H_5Cl was studied with emphasis on the observed photoproduct patterns and characteristics. A number of different products have been observed. Significant differences between them were observed both in terms of detection efficiencies as well as in terms of translational characteristics.

The observations can be summarized as follows:

(a) A number of different phenyl products are observed in the ablative regime, whereas only HCl is observed below the ablation threshold.

(b) We delineate two fluence ranges in which C_6H_5Cl photolysis proceeds at very different yields. In the 40-150 mJ/cm^2 range the photolysis yield is found to be quite low and constant, nearly one order of magnitude smaller than that in the gas phase. On the other hand above 150 mJ/cm^2 the photolysis yield is found to grow drastically.

[45] It is important to note that this slow component appears only at low fluences at which as indicated by Fig. 6.7 , desorption is very low . Thus, we can clearly rule out the possibility that the slow HCl component is an “artifact” of slow pumping speed in the vacuum chamber.

(c) At all fluences, the phenyl derivatives are described by the same õ-distribution as the parent molecule. In contrast, HCl shows a much more complex behavior: at higher fluences, it is nearly energetically equilibrated to the parent peak, whereas at low fluences, it is characterized by a quite slow υ-distribution.

In principle it could be suggested that these differences reflect the unselective reactivity in the ablative regime. We first demostrate that this is not the case and in fact, all differences observed relate to the ejection mechanisms that were discussed in the previous Chapter 4.

First, as described in the first section of this chapter, irradiation at fluences below the threshold, film transmission is found to decrease with successive laser pulses, thus indicating the accumulation in the film of species that absorb stronger than the parent molecule. Indeed, biphenyl species are known to absorb[20] much stronger than the parent peak at 248 nm, and thus the decrease in the transmission can be ascribed to their accumulation. In a different type of experiments, films were first irradiated at low fluences and then signals for the phenyl products were recorded by irradiating the same spot at a fluence above the ablation threshold. The signal recorded in the first few pulses at the monitoring laser fluence is much higher than that observed in the irradiation of freshly deposited films exclusively at this higher fluence. The difference must be due to photoproducts that accumulated in the film during the irradiation at low fluence. Thus, even at fluences below 50 mJ/cm^2, phenyl photoproducts are strongly indicated to be formed and the main or exclusive reason for failing to observe them is their inefficiency of ejection.

The reason for the failure of desorption of the phenyl products species can be understood in the framework of the different desorption mechanims opearting below vs above the ablation threshold. Indeed, (formulas 3.2 and 3.3) the temperature of the film for F_{LASER} = 50 mJ/cm^2 is estimated to be ≈170 °K, which is sufficiently high for HCl desorption established by TDS (~150 °K), but still quite lower than the temperature (250 °K) necessary for the desorption of the phenyl derivatives. On the other hand, the efficient ejection of the phenyl species at fluences above 120 mJ/cm^2 is due to the nonselective volume expulsion of the matrix due to explosive boiling as that for the n-

decane dopant inside the toluene matrix. This is clearly shown by the close correlation of their ejection efficiency to that of parent (matrix) molecule both in pulse and fluence dependence.

Similarly, as for the photoproduct translational distributions, these appear to be mainly determined by the desorption mechanims and the plume dynamics. (i.e., the different amounts of nascent kinetic energies deposited on the species by their formation reactions do not appear to affect them). This is directly shown by the fact that at all fluences, the TOF spectra of the photoproducts perfectly overlap with the corresponding parent peak spectrum. Thus the photoproduct translational distributions, at least in the studied system, are well described in the framework of a volume expulsion model (explosive boiling) employed before for accounting for the translational characteristics of involatile dopants[46].

This "switching" from a fast to a slow translational distribution has also been observed, albeit for the parent desorbate peak, by Natzle et al [40] in the study of photodesorption from NO multilayers. They ascribed the appearance of the "slow" peak to the onset of the collisional regime, whereas the "fast" peak observed at higher desorption efficiencies to the development of the supersonic expansion.

6.4.2. Reactivity Considerations

We consider next the reaction paths responsible for the formation of the various products observed in the 248 nm irradiation of neat C_6H_5Cl films. Upon excitation with UV light, C_6H_5Cl dissociates in the gas phase and in solution by a process involving exclusively C-Cl bond scission to give phenyl radical and chlorine atom. We consider that a similar process takes place in the irradiation of the C_6H_5Cl films. Thermal

[46] In contrast, for HCl, given its relatively small collisional cross section, and the independent desorption path, its entrainment in the desorbing C_6H_5Cl jet is expected to be less efficient. Furthermore, for equal initial translational energies, its velocity is 1.8 times higher than that of C_6H_5Cl. Therefore, we do not expect velocity accomodation to be as efficient as that for the phenyl photoproducts. This agrees with the 3D Monte Carlo simulation of the desorption from binary mixtures [80] Evidently, the suggested explanation does not account for the very slow translational distribution observed for HCl at fluences below 50 mJ/cm^2. As shown in the results all available evidence indicates that the change from the fast to the slow distribution closely relates to the development or not of a well-defined plume.

decomposition can be safely discounted (for the C-Cl bond energy @3.6 eV, $-\frac{d[N]}{dt} = Ae^{-E_A/RT}[No] \Rightarrow [N]_{thermally}/[N]_o$ be $< 10^{-6}$ for msec time scales) , whereas other pathways (as for example, concerted reactions) are not known in either gas-phase or solution chemistry of the compound. Instead, all observed products can be consistently accounted for by well-known reactions of the C_6H_5 and Cl radicals, thus providing further support to our analysis.

$$Cl + C_6H_5Cl \rightarrow HCl \text{ or } C_6H_4Cl_2 \qquad (1)$$

$$C_6H_5 + C_6H_5 \rightarrow (C_6H_5)_2 \qquad (2)$$

$$C_6H_5 + C_6H_5Cl \rightarrow (C_6H_5)_2 \text{ or } C_{12}H_9Cl \qquad (3)$$

$$C_6H_4Cl + C_6H_5Cl \rightarrow C_{12}H_8Cl_2 \qquad (4)$$

Both modes of Cl and C_6H_5 reactivity (i.e., addition and H-atom abstraction) are observed in the solution and gas phase chemistry of benzene and chlorobenzene, with the relative importance of the two pathways depending on the temperature of the system.

In all, despite any kinetic ambiguities, all observed products can be consistently accounted for in terms of reactions known from the gas-phase and solution chemistry of C_6H_5Cl. Thus, it appears that reaction pathways under UV ablation does not present any peculiarities.

6.4.2.1. Kinetic Considerations

We consider next the kinetics of the reactions responsible for the observed products, since this can shed light on the temporal and energetic factors that may be important under ablation conditions. The discussion focuses on the reactions of the Cl photofragment, since there is insufficient kinetic information on the corresponding reactions of the C_6H_5 fragment.

Considering first the H-atom abstraction reaction (1), a recent examination [99] has reported its cross-section to be ~10^{-15} cm^3/molecule (at room temperature). Assuming that the film or plume density can be approximated with that of the liquid (1.1 gr/cm^3),

$$-\frac{d[Cl]}{dt} = k[C_6H_5Cl][Cl] \Rightarrow [HCl] = [Cl]_o(1-e^{-k[C_6H_5Cl]}) = [Cl]_o(1-e^{-Ae^{-(Ea/RT)}[C_6H_5Cl]t})$$

this rate constant suggests the half-life for HCl formation to be, at least, ~170 nsec , which is rather slow for competing with the time scale of plume ejection (~100 nsec), as this has been established by means of nanosecond imaging [106]. In that case, a significant percentage of the Cl photofragments would be expected to escape reaction, at variance with the observations. As described in the Results Section, HCl appears from the very first pulse (Fig. 6.7,6.8), while free Cl is observed only above ~90 mJ/cm^2 and at very low intensity.

The simplest explanation for the efficient formation of these species would appear to be that the irradiated film reaches temperatures high enough for promoting the reactions. For instance, in the case of the HCl photoproduct, approximating the temperature dependence of its formation rate constant to that for the corresponding reaction of Cl with C_6H_6 (log k = 9.35 - (30/RT) with the activation energy in kJ/mol) [104], its formation in few 10s nsec (i.e., on the time scale of plume ejection as established from the imaging study) would require remperatures well above 500 °K range, whereas temperatures at the threshold are expected (formulas 3.2 and 3.3) to be 400 K. Of course, this calculation is subject to the accuracy of the temperature dependence of the employed rate constant[47]. It is even more difficult to account for the efficient formation of HCl in the subthreshold regime.

Alternatively the "hot" reactivity may indicate incomplete "thermalization" of the C_6H_5 and Cl photofragments. Ichimura et al[14(b)] have shown that in the photodissociation

[47] Similarly, concerning $C_6H_4Cl_2$ formation in (2) the rate constant for the addition reaction has been reported to be negligible at room temperature. Presumably, because of the strong aromatic C-H bond, the reaction barrier is relatively high. Once more, the observation of $C_6H_4Cl_2$ herein suggests that the reactants have sufficient energy for overcoming the barrier. (i.e., suggestive of "hot" reactivity of C_6H_5 and Cl fragments)

of C_6H_5Cl, in the gas phase ≈46 kJ/mol are deposited on the liberated Cl fragment. In the case of the photodissociation in the film, some of this energy is expected to be collisionally dissipated. Still, sufficient may remain on the fragment for overcoming the ≈30 kJ/mol reaction barrier.

It is not possible at this moment to distinguish between these different mechanisms. However, since HCl is observed even at fluences well below the ablation threshold, we tend to favor the incomplete fragment thermalization case. In fact, there are by now several examples of reactivity between nonthermalized photofragments and coadsorbates in surface studies of monolayers and multilayers at very low fluences [102]. Studies on systems of simpler reactivity are required in order to establish in detail the kinetics of reactions in the irradiation of van der Waals films.

6.4.2.2. Plume Ejection Time and Photolysis yield

A most surprising result of the examination is the very low HCl yield (and of the other products) (Fig. 6.8). Generally, it is considered in the literature that photoproduct in the UV ablation derives largely from secondary reactions in the plume. As shown in the results section, the strong accumulation effect for phenyl photoproducts conclusively shows that photoproduct formation occurs mainly in the film (before material ejection). The low photolysis yield could, in principle, be accounted by the fact that a large C_6H_5Cl percentage is ejected without having absorbing themselves a photon, whereas HCl and the other photoproducts derive exclusively from photoabsorption events. However, if this factor was the only responsible one then:

$$\frac{N_{HCl}}{N_{C_6H_5Cl}} = \frac{q\Phi_{LASER} \times (1 - \exp(-a\,x))}{r\,x N_a / MW}$$

(where á = 1900 cm^{-1}, $Ö_{LASER}$ is the incident photon flux in units of photons/cm^2, ñ = 1.1 gr/cm^3 , N_a the Avogadro number and MW=112 the molecular weight of the compound). The estimation shows that this contribution can be appreciable in decreasing the yield

from the gas-phase value, but for reasonable values of x, it definitely can not account for the observed order-of- magnitude reduction.

A plausible explanation can be advanced on the basis of the recent finding that material ejection occurs mainly after the end of the laser pulse. Accordingly, photolysis occurs exclusively or mainly in the film so it can be suggested that limited by the operation of recombination processes. Indeed, photodissociation yields in condensed phases are generally quite low, as a result of "cage effects" [97] promoting recombination of the photofragments. (Ultrafast deactivation of the photo-excited state can also play a role. These values are of the same order as the apparent dissociation yield determined in the low fluence range, thereby providing strong support to our suggestion that photolysis takes place in the film.

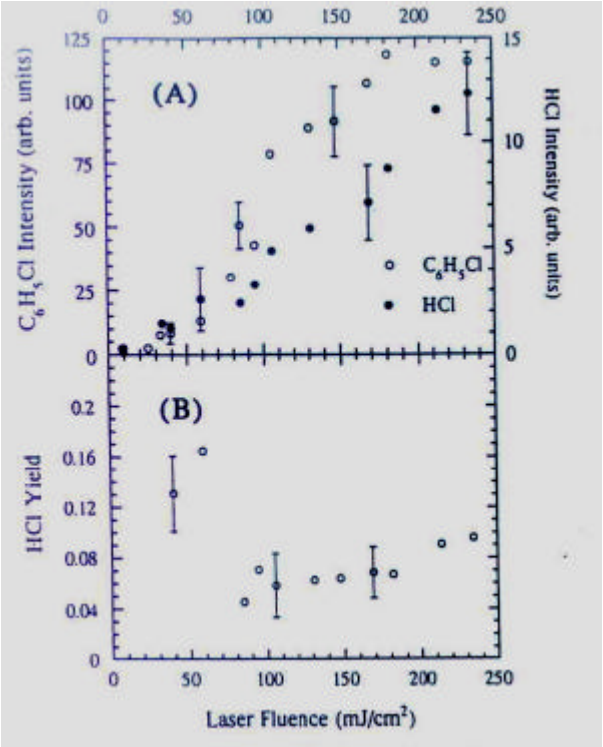

Figure 6-10 (a) Fluence dependence of the C_6H_5Cl and HCl intensities in the ablation of C_6H_{12}/C_6H_5Cl films with a 10-to-1 molar concentration in the two compounds. The error bars represent 2ó, as determined from 4 at least measurements of each datum.

(b) Plot of the HCl yield in the ablation of the C_6H_{12}/C_6H_5Cl film.

To demonstrate the operation of "cage effects", the HCl yield in the irradiation of C_6H_{12}/C_6H_5Cl mixtures was examined. Cl is much more reactive towards C_6H_{12} than C_6H_5Cl and thus according to the above, its yield should be enchansed. Indeed, in the ablation of the mixture, the intensity of C_6H_5Cl is generally ≈ 1/15 of that in the neat film, but, very good agreenment to the above prediction, the HCl yield is ≈10 times higher.

Because Cl reacts with C_6H_{12} in ≈10-20 collisions (in liquid [128], but presumably with comparable efficiency in matrices, as well), HCl formation in the mixture is much enhanced over recombination to C_6H_5Cl. In contrast, H-atom abstraction from C_6H_5Cl is a much slower process [104,127] and as a result, in the case of the neat C_6H_5Cl films, radical recombination can compete efficiently with HCl production. Evidently, if the chromophore was incorporated in a chemically inert substrate, the apparent photofragmentation yields would be even further reduced. Preliminary results on the ablation of C_6H_5Cl in freon matrix are fully consistent with this suggestion.

Further support of the importance of photolysis in the film, derives from the comparison with the increasing slope at higher fluences. The slope of 4 x 10^{-4} determined for the linear dependence (Fig. 6.7) in the 150-300 mJ/cm^2 range corresponds well to the 1.6 x 10^{-4} value calculated for dissociation of the compound in the gas phase:

$$N_{HCl} / N_{(C_6H_5Cl+HCl)} = 0.125\times10^{16} qs\, F_{LASER}$$

(the equation holding under the assumption that $\sigma \cdot F_{LASER} << 1$), where q is the photolysis efficiency of the compound at 248 nm (0.4), σ is the gas-phase absorption cross-section (=3.2$\cdot 10^{-19}$ cm^2/molecule) and F_{LASER} is the fluence in mJ/cm^2. The fact that the experimental value is somewhat higher than the calculated one could be due to a number of factors. Plausibly, differences in the angular distributions of the species are responsible. Alternatively, contribution by multiphoton processes at these high laser fluences cannot be excluded.

According to the above, the weak Cl signal that is observed for F_{LASER} > 90 mJ/cm^2 represents fragments formed by photolysis of C_6H_5Cl in the gas phase (i.e., by the fragmentation of the compound that has desorbed during the laser pulse)[48]. This suggestion can rationalize how this Cl photofragment "manages" to avoid reaction for the formation of HCl or $C_6H_4Cl_2$. Plausibly, the detected Cl is liberated in the early stages of the plume ejection, before this has been fully developed. As a result, the density of C_6H_5Cl in the plume may not be sufficient to "trap" the Cl photofragment atoms.

6.5. ISOTOPE EFFECTS

Deuterium substitution is a well-known method in organic chemistry and photochemistry for establishing reaction pathways [110] and in surface science, deuteration is employed for characterizing the desorption kinetics of adsorbates [111-112]. In the case of UV laser induced desorption and ablation of condensed van der Waals solids, deuteration may affect the processes in several ways. First, deuteration may affect the rates and the yields of intramolecular radiationless energy decay. In this way, questions such as raised by the MD study of Dutkiewicz et al [25] are amenable to experimental examination. Most importantly, deuteration may be particularly useful in examining reaction pathways and rates under ablation conditions. Unfortunately, through its influence on the phonon modes of the solid, deuteration may also modify the heat capacity of the molecular solid, thereby complicating somewhat the interpretation of the results. In this chapter, we examine the potential of this approach in the comparison of laser-induced material ejection from CH_3I and CD_3I films at ë=248 nm.

6.5.1. Results

Fig. 6.11(A) illustrates the intensities of the CH_3I and CD_3I parent peaks as a function of laser fluence (F_{LASER}) in the irradiation (ë=248 nm) of the corresponding

[48] Cl certainly does not derive from the photolysis of the desorbing HCl, since the photodissociation cross-section of HCl at 248 nm is [102] rather small (10^{-21} cm^2/molecule). The observation of different υ-distributions for Cl and HCl constitutes further support for this conclusion. Furthermore, Cl does not appear to derive from the photolysis of $C_6H_4Cl_2$, since Cl shows essentially no pulse dependence, which sharply contrasts the pronounced one observed for this species.

condensed solids. Desorption is observed at quite low fluences, consistent with the fact that methyl iodide is a strong absorber at 248 nm ($\alpha \approx 5700$ cm^{-1}) [-]. From a semi-logarithmic plot of the intensity vs. F_{LASER}, the ablation threshold is established to be 22 ± 3 mJ/cm^2 for CH_3I and 27 ± 4 mJ/cm^2 for CD_3I. Thus, deuteration results in a moderate increase of the ablation threshold. In addition, at a given laser fluence, the parent peak intensity from the CD_3I system, is lower than its preprotonated analogue. This holds both below and above the ablation threshold.

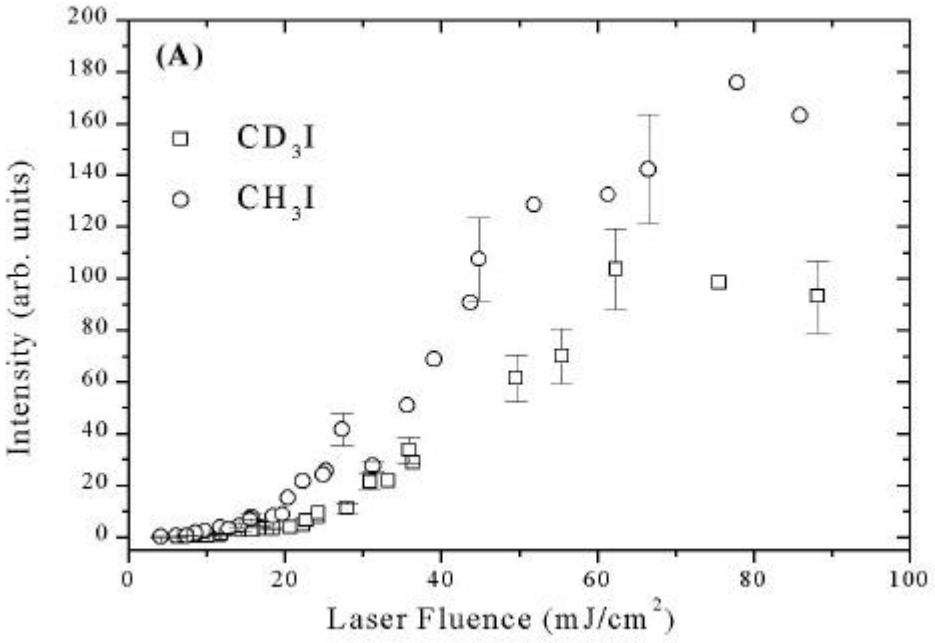

Figure 6-11 Desorption intensities of the parent molecules CH_3I and CD_3I recorded in the irradiation of thick films of the corresponding compounds as a function of the incident laser fluence (F_{LASER}). The lower figure (B) depicts in higher detail the data below the thresholds. The error bars represent 2ó, as determined from 4 measurements.

Fig. 6.12 illustrates the desorbate most probable velocities $\tilde{o}_{mp}$ for the two systems. As already observed for C_6H_5Cl and $C_6H_5CH_3$ (chapter 5), the dependence on F_{LASER} at low fluences is very weak and the slope changes abruptly at the ablation threshold. The present results indicate the generality of this finding for non-aromatic systems. The importance of the features observed in the F_{LASER}-dependence of $\tilde{o}_{mp}$ are

discussed in detail in chapter 5 For the purpose of the present examination, we focus on the comparison between the two systems.

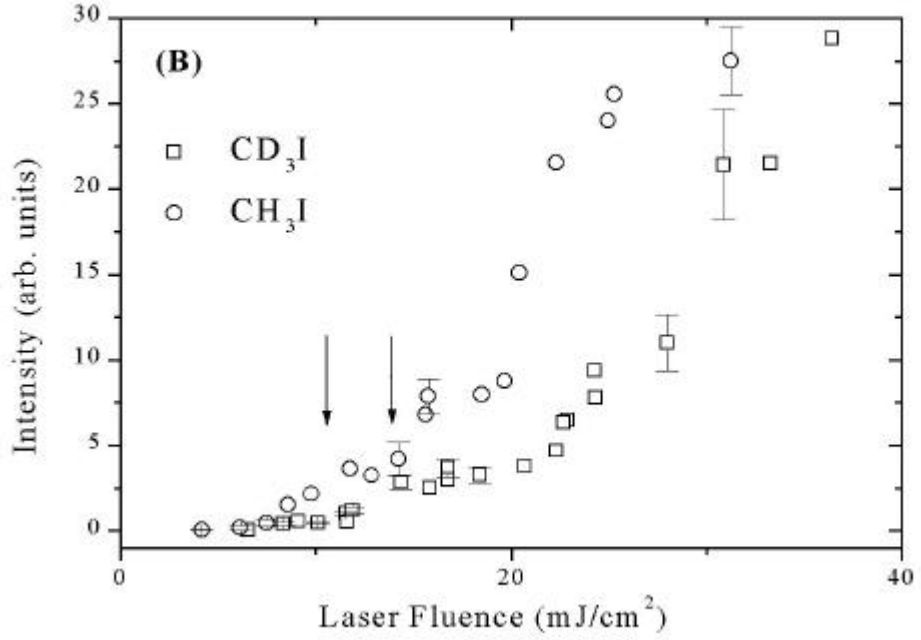

Below the ablation threshold, the desorbate $\tilde{o}_{mp}$ are approximately equal for the two systems, within the admittedly large error, due to photoproduct accumulation in the film. In any case, for both systems, the $\tilde{o}_{mp}$ correspond to translational temperatures in the 300-360 K range.[49] In contrast above the threshold, there is clearly a displacement of the CD_3I data to lower values. If, however, the velocities are plotted as a function of the amount of ejected material, the two dependences are nearly identical. Thus, the effect of deuteration on the translational distributions appears to be a secondary one, i.e. through the influence of the desorbing amount.

---

[49] At fluences ≤ 3 mJ/cm^2, electronically-mediated photo-ejection of CH_3I from surfaces has been reported [110-112], resulting in somewhat higher $\tilde{o}_{mp}$. Features of the CH_3I time-of-flight spectra recorded herein at the lowest fluences correspond closely to those reported in the previous studies. Thus, the variation in the $\tilde{o}_{mp}$ observed at the low fluences (Fig. 2) may be partly due to the competing contribution of different processes. Accordingly, the study appears to provide an illustration of the evolution from electronically-mediated to thermal-induced desorption to ablation.

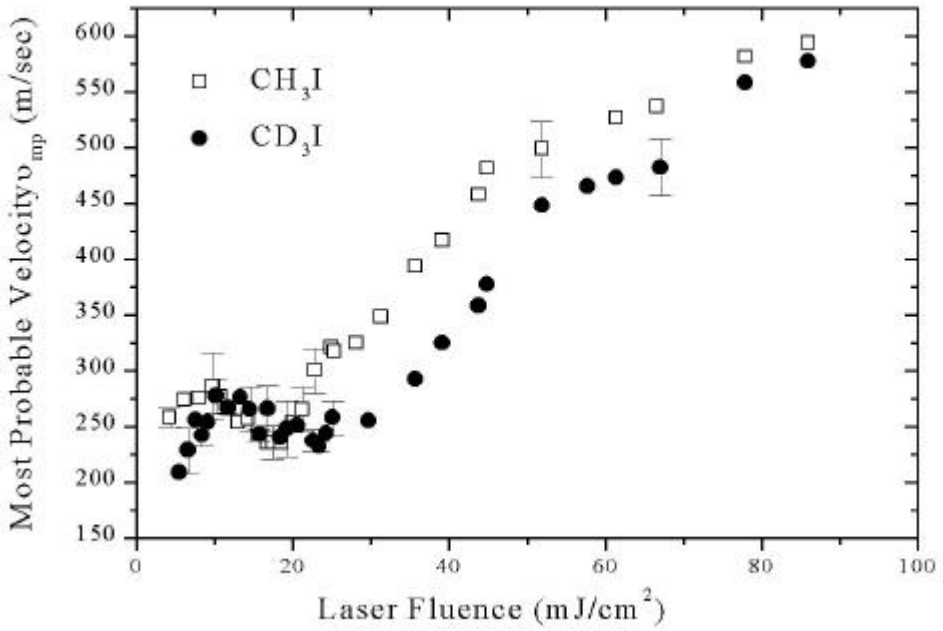

Figure 6-12 Most probable velocities ($\tilde{o}_{mp}$) of the CH_3I and its deuterated analogue (CD_3I) as a function of the incident laser fluence (F_{LASER}). The data at very low fluences (F_{LASER} < 10 mJ/cm^2) are recorded by the averaging over 30 pulses. The errors bars represent 2ó, as determined from at least 4-5 measurements.

6.5.2. Discussion of the results

In all, the effect of deuteration is mainly confined to a higher ablation threshold for the deuterated species and to lower absolute desorption yields at corresponding fluences. We first consider these differences within the "explosive boiling" model. To this end, we examine the influence of deuteration on the thermodynamic properties of the solid. Deuteration does not affect much the cohesive energy of the system [117], but it can have a significant effect on the heat capacity. Because of the lack of information on the heat capacity of solid CD_3I, its value has been estimated from spectroscopic constants. For temperatures $T \geq \Theta_D$ (Θ_D»110 K, Debye temperature of the compound [118]) the heat capacity C_v is estimated by $Cv = 3R + \sum_{i=0}^{i=s-6} R\frac{x_i^2 \cdot e^{x_i}}{(e^{x_i}-1)^2}$ with $x_i = \hbar w_i / k_B T$

where w_i are the representative vibrational modes of the molecule in crystal phase (80°

K) [119-120]. C_P is estimated from C_V via the Lord-Ahlberg formula $C_p - C_v = 0.0214 \times (\frac{T}{T_m}) \cdot C_v^2$ where Tm the melting point of the compound. The C_{P_D} / C_{P_H} ratio is calculated to range from 1.14 (150 K) to 1.42 (300 K). Accordingly for the difference in C_P, in $\Delta T = \frac{a \cdot F_{LASER}}{Cp \cdot r}$ (under the assumption of 1-photon excitation chapter 3)[50], brings the desorption curves of two systems in quantitative agreement. Consequently, the increase in the ablation threshold (given within this model by $F_{thr} = L_p(E_v^* - CT_o)$ where L_p represents the optical penetration depth, E_v^* the critical energy density required for material ejection, $C = Cp \times r$ and T_o (=120 K) the initial temperature of the solid) seems to be largely accounted by the difference in the heat capacity.

The previous suggestion is supported by the observation of a change in the F_{LASER}-dependence of the signal at low laser fluences (≈10 mJ/cm^2 and ≈14 mJ/cm^2 CH_3I and CD_3I, respectively) (Fig. 6.11(B)). This appears to correspond to the change has been observed before in the irradiation of $C_6H_5CH_3$ films, (Fig. 3.2)[51]. Based on the similarity of the F_{LASER}-dependences of the desorption intensities, it seems reasonable to suggest that the change observed in Fig. 6.11(B) is indicative of the same phase-transformation. This possibility is also supported by the fact that at ≈11 mJ/cm^2, the surface film temperature is estimated to be ~ 205 K, which corresponds closely to the melting point (T_m=206.5 °K). Accordingly, even for the photolabile CH_3I, ablation (at $F_{LASER} \geq 20$ mJ/cm^2) is indicated to be initiated from a heated liquid, i.e. ablation is due to "explosive boiling". Thus, at the present level of analysis, there is no evidence for the influence of the deuteration on electronic processes is found.

In the irradiation of CH_3I solids, we have already detected ejection of I, I_2, CH_3, CH_4, CH_2I_2. For I and CH_3, contribution directly from the film has been verified after

[50] Cp=35 J/mol K in the 100-200° K range [118], ñ=0.0208 mol/cm^3 at 150° K [121]

[51] Monitoring is feasible because of the formation of a highly smooth and transparent in the visible glass under the employed deposition conditions. In contrast, the vapor-deposited CH_3I films are highly light scattering (due to a high degree of polycrystallinity), thereby hindering optical monitoring.

substracting from the time-of-flight spectra the contributions to these signals due to the electron-impact fragmentation of CH_3I. Based on previous studies [119], it is suggested that 1-photon photolysis of CH_3I yields CH_3 and I fragments, which are partly ejected in the gas-phase and partly react with CH_3I molecules to produce the other indicated species. Furthermore, in clusters, direct formation of I_2 from the excited state(s) has also been demonstrated. A similar pathway may also operate in the irradiation of films. By using single-photon ionization of the desorbates, Feldman et al [63] observed intense emission of clusters under conditions of "explosive desorption" (F_{LASER} > 1.5 mJ/cm^2 at 266 nm). Thus far, we have not been able to detect unambiguously the presence of such signals. Plausibly, the use of high electron-impact energy results in the fragmentation of these clusters. Furthermore, the limited mass range (0-300 amu) of the quadrupole mass spectrometer precludes detection of clusters higher than dimers. At any rate, the dependence of the signals on F_{LASER} appears to differ for the different observed products (iodine increasing as a power of 1.5, whereas I_2 grows nearly as a power of 2), which indicates that different reactions contribute to the formation of the various species. Furthermore, the pulse dependence of the relative desorption yields is rather complicated, suggesting that a number of products remain trapped in the film. In all, the initial study demonstrates extensive photoreactivity in the system. Currently, the corresponding photoproducts in the irradiation of CD_3I films are examined as a function of F_{LASER}. Comparison of the relative yield of photoproducts ejected in the ablation of the two systems is expected to be more sensitive to deuteration effects than the F_{LASER}-dependences of the parent molecule desorption signals.

6.6. CONCLUSIONS

The study of the ablation of neat C_6H_5Cl films at 248 nm illustrates a number of interesting features about reactivity in the UV ablation of photosensitive molecular systems. First, the delineation drawn before for distinctly different desorption characteristics above vs. below the ablation threshold is illustrated here in an interesting, though indirect way, by the observation of strong induction effect for the parent peak. This is shown to be a result of the fact that below the threshold, any "heavy"

photoproducts formed by the UV photolysis of the parent molecule remain in the film, thereby resulting in an enhanced absorption of the laser energy.

The ejection characteristics (yields and translational distributions) of the photoproducts are shown to be exclusively determined by the desorption /material ejection mechanisms. Thus, it appears that the initial reactivity steps have no influence on these observables.

Finally, the observed photoproducts are fully consistent with the known gas-phase and solution chemistry of the compound. Thus, in this respect, ablation does not seem to involve any particularities of the involved chemistry. However, the observation of these products on the time scale of a single ablation event is inconsistent with the available room-temperature rate cross sections. The discrepancy suggests "hot" reactivity of the fragments of the C_6H_5Cl photolysis. This aspect may be addressed in the future via the study on systems of simpler reactivity are planned for addressing this question.

Finally, an initial study on the comparison of the laser-induced material ejection from deuterated vs protonated species has been presented for CH_3I at ë=248 nm. Deuterium effects" may turn out a particular useful way of studying aspects of UV laser-induced desorption and ablation processes.

7. EJECTION DYNAMICS IN THE UV FEMTOSECOND IRRADIATION

7.1. INTRODUCTION

Femtosecond-pulse laser systems have opened new possibilities for fundamental investigations in various fields of chemistry and physics. An area where this potential of femtosecond laser appears most promising is in the laser ablation [88-90]. The possibility of "instantaneous" excitation of a very high number of chromophores with an ultra short pulse can have a crucial effect in the mechanisms of material ejection/desorption.

In all previous chapters, we have examined the ablation of cryogenic solids due to the irradiation with nanosecond laser pulses. In this chapter we present a first examination of the effect of the pulse width on the laser ablation of cryogenic molecular solids. Specifically, ejection dynamics is examined for irradiation with 500 fs pulses (ë=248 nm) of a bicomponent solid consisting of toluene $C_6H_5CH_3$ and $(CH_3)_2O$ as the second compound (dopant). The idea behind this choice has already been explained in chapter 3. For studying the photochemistry that takes place in the ablation effected with ultrashort laser pulses we have chosen chlorobenzene that has been studied in chapter 7 with nanosecond pulses.

7.2. RESULTS

7.2.1. Toluene/Dimethylether Mixture

Fig.7.1 illustrates the desorption signals of molecules ejected from the $(CH_3)_2O/C_6H_5CH_3$ mixtures upon laser irradiation at 248 nm with 500 fs laser pulses. The examination of the graph directly indicates substantial differences from the corresponding ns case. First, toluene signal is observed from the lowest examined fluence ca. 10 mJ/cm2. In the nanosecond case we could not observe any toluene signal at such low fluences. At low fluences, the signal of the toluene

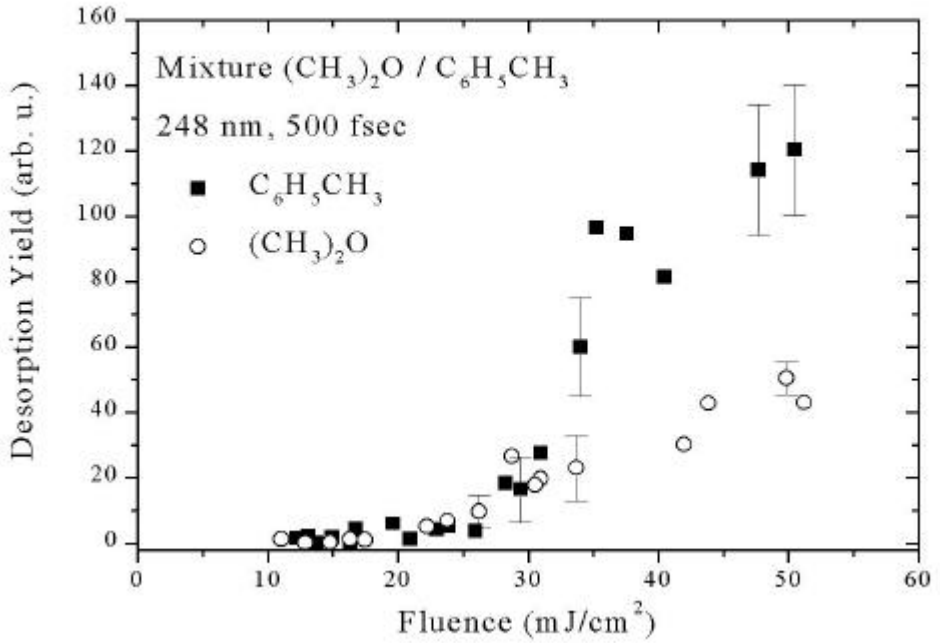

Figure 7-1 The desorption intensities of $(CH_3)_2O$ and $C_6H_5CH_3$ from a 1:5 (molar) mixture of the two compounds as a function of the laser fluence. The intensities are corrected for the different relative ionization efficiencies of the two compounds in the mass spectrometer. The error bars represent 2σ.

increases with increasing fluence, with the dependence becoming much more pronounced at 25-30 mJ/cm^2. At 30 mJ/cm^2 a steep increase of the signal is observed. From the ln(signal) vs. F_{LASER} the ablation threshold is found to be ca. 30 mJ/cm^2 the fluence value where the toluene signal becomes larger than that of dimethylether. So the ablation threshold in the fs irradiation is much lower than the one that we have found in the case of 30 ns laser pulse (~125 mJ/cm^2).

As shown in the graph, $(CH_3)_2O$ desorbs efficiently at all examined fluences and its signal increases with increasing laser fluence. In the 10 – 25 mJ/cm^2 fluence range, its desorption signal is almost equal to the $C_6H_5CH_3$ signal, although the concentration of the solute in the matrix is 1/5 of the latter. The desorption signal of $(CH_3)_2O$ remains close to that of toluene up to 30 mJ/cm^2, beyond which $C_6H_5CH_3$ ejection is much enchanced

over the dopant. In comparison with the nanosecond case, the signals of ether is found to be in general less intense, especially at low fluences (F_{LASER} < 25 mJ/cm^2). Importantly, above the indicated threshold, the ether signal is observed to increase with increasing fluence, in contrast to the nanosecond case where the ether signal reaches a limiting value.

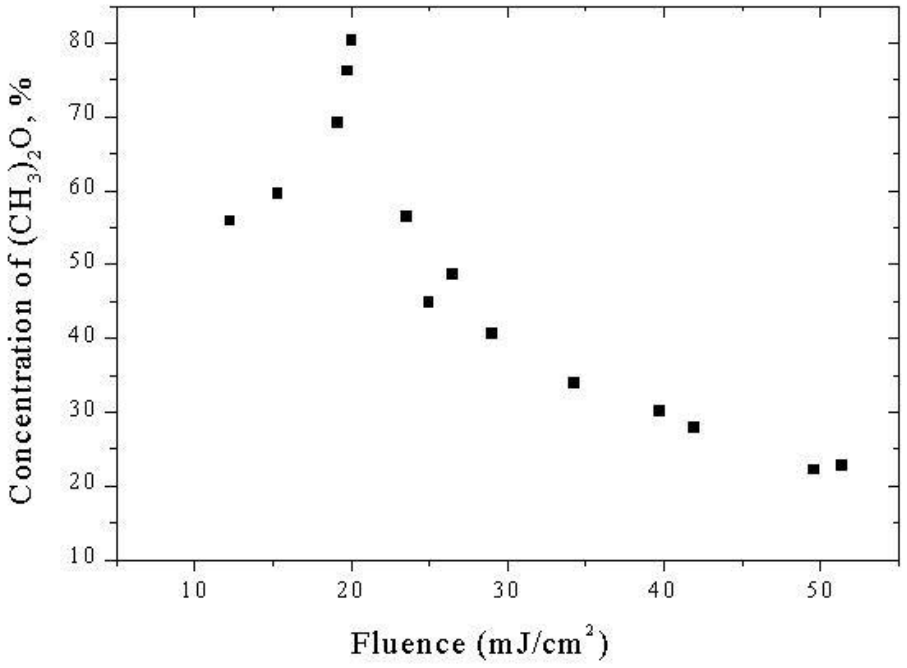

Figure 7-2 Concentration of $(CH_3)_2O$ in the plume as a function of the incident laser fluence in the irradiation of the mixture of the compound with $C_6H_5CH_3$.

The data of Fig. 7.1 are replotted in Fig. 7.2. Given is the percent concentration (apparent yield $\frac{I_{(CH_3)_2O}}{I_{(CH_3)_2O} + I_{C_6H_5CH_3}}$) of the dimethylether in the plume as a function of laser fluence. In the low fluence regime, the observed concentration for dimethylether is found to be ca. 55 % of the plume, while as the fluence increases this value increases at a maximum value of 75 % just below threshold (30 mJ/cm^2). At higher fluences (i.e., in the

ablative regime) the concentration of dimethylether drops with fluence, reaching (F_{LASER} > 30 mJ/cm^2) an almost constant value close to 25-30 % at the highest fluences.

Finally, the dependence of the most probable velocities of the two molecules on laser fluence has been determined (Fig. 7.3). The dependence is, whithin the admittedly high S/N error, qualitatively similar to that determined in ns case. Below 25 mJ/cm^2 the õmp of the dopant was found to be larger than that of the matrix. At higher fluences the velocities for

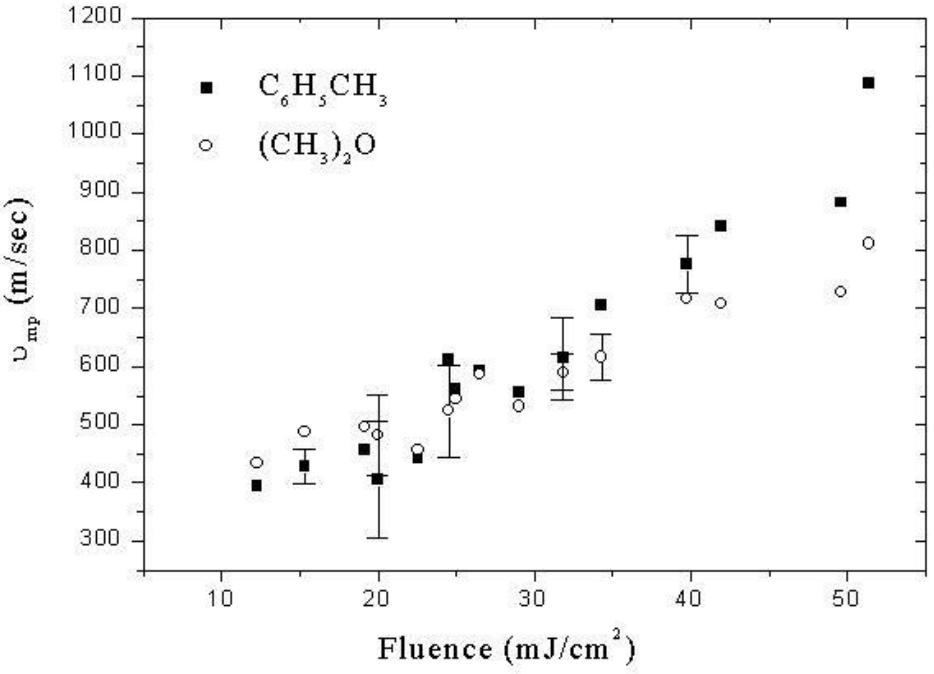

Figure 7-3 Plot of the dependence of õ$_{mp}$ of $C_6H_5CH_3$ and $(CH_3)_2O$ as a function of laser fluence.

both molecules, increase with fluence, the toluene velocity value is always larger than that of dimethylether.

7.2.2. Neat Chlorobenzene

7.2.2.1. Ejection Dynamics of C_6H_5Cl

Fig. 7.4 depicts the intensity of C_6H_5Cl recorded from freshly deposited solids as a function of the incident laser fluence (Fig. 7.4). From the fiitting of the signal vs ln(Fluence) we estimate the ablation threshold for neat C_6H_5Cl solids in irradiation with 500 fs laser pulses to be ca. 34 mJ/cm^2 which is nearly 2 times lower than that determined for nanosecond ablation.

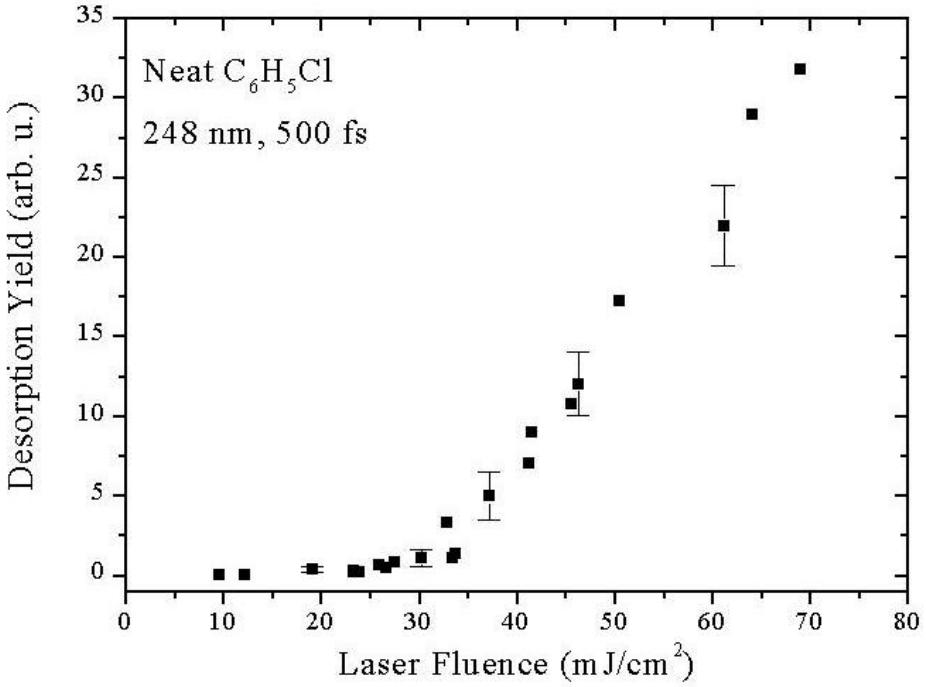

Figure 7-4 Desorption intensity of C_6H_5Cl recorded in the first pulse from freshly deposited solid as function of the incident laser fluence.

Upon irradiation of freshly deposited solids of the compound at F_{LASER} < 30 mJ/cm^2 the intensity of C_6H_5Cl is observed to rise somewhat with continuing irradiation, attaining a plateau after 400 pulses (Fig. 7.5). On the basis of the nanosecond study, we believe that this small increase of the signal with successive laser pulses is due to an "induction effect". However, the large number of laser pulses that is required for signal increase shows that the induction in the fs case is less "efficient" than nanosecond study.

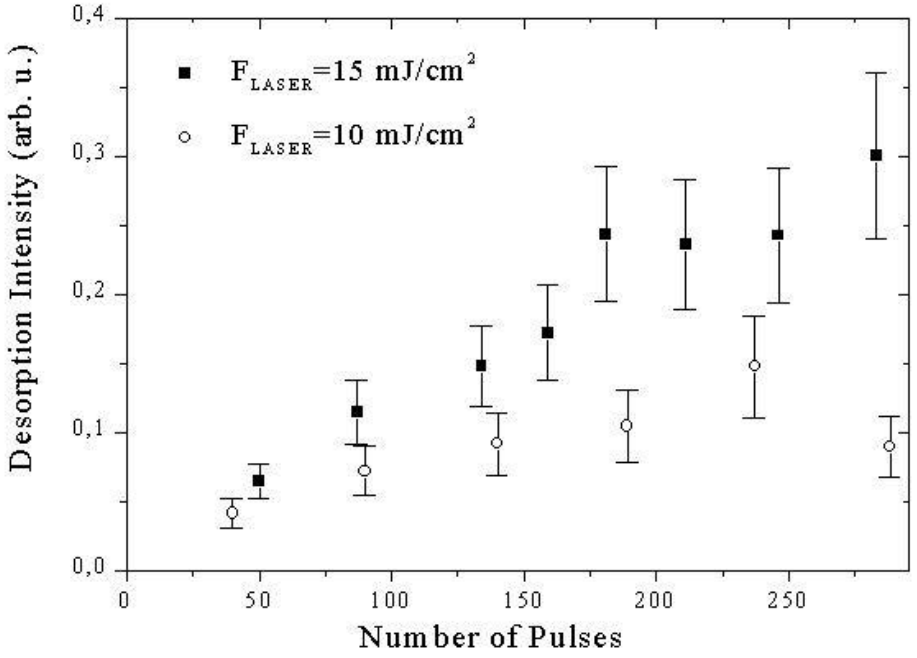

Figure 7-5 Pulse evolution of the C_6H_5Cl intensity in the irradiation of freshly deposited solids at the indicated fluences.

In contrast at fluences above 30 mJ/cm^2 desorption of the C_6H_5Cl from freshly deposited solids is observed to be significant from the very first pulse. The pulse dependence of the desorption signal at these fluences is, at least qualitatively, similar to that observed in the nanosecond case.

7.2.2.2. Ejection Dynamics of Photoproducts

In the irradiation of chlorobenzene solids with 500 fs laser pulses, we detect relatively intense signals at masses 35, 36, ca. 154, 188 and 223 amu. These peaks can be attributed, respectively, to Cl, HCl, $(C_6H_5)_2$, C_6H_4Cl-C_6H_5 and $(C_6H_4Cl)_2$. Despite this given the relative low resolution of the mass spectrometer for masses above 100 amu, we cannot exclude the possibility that the 223 mass peak represents the C_6H_5Cl-C_6H_5Cl dimer. Furthermore, we cannot exclude the possibility of C_6H_6 formation since its detection is hampered by the contribution from the strong C_6H_5+ peak deriving from the mass cracking of C_6H_5Cl.

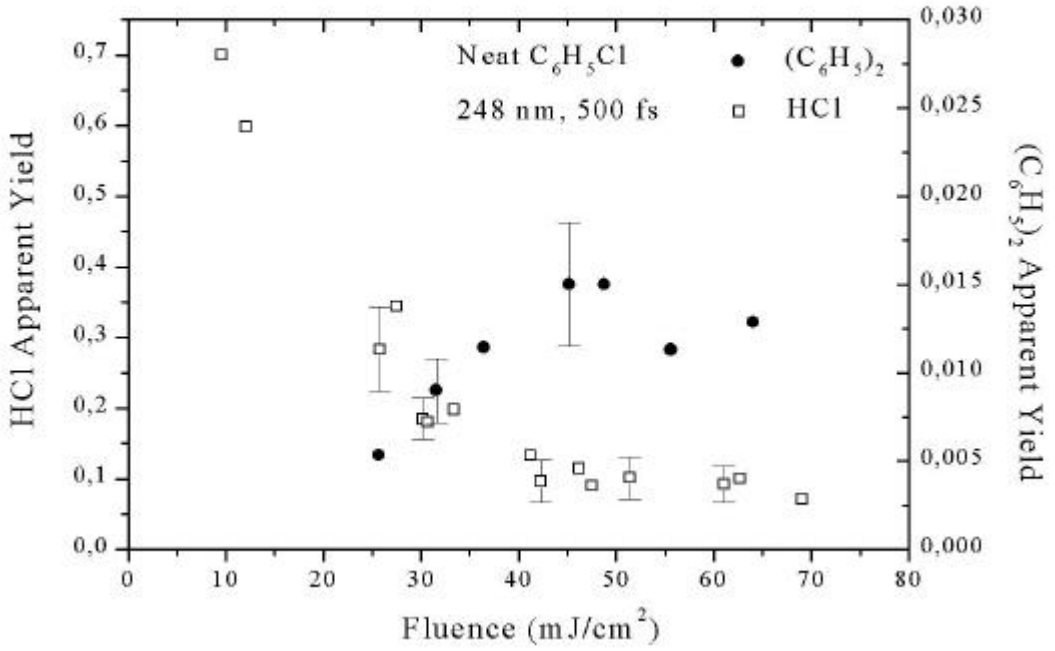

Figure 7-6 The HCl and $(C_6H_5)_2$ concentrations in the plume as function of the incident laser fluence in the irradiation of neat C_6H_5Cl solids.

Of the various products, HCl is observed from the lowest examined fluence (ca. 10 mJ/cm^2). At the lowest fluences, its detection required averaging over at least 20 or more pulses, but at somewhat higher fluences, it can be clearly detected from the very first pulse on freshly deposited solids (Fig. 7.6). At low fluences (F_{LASER}< 15 mJ/cm^2) the yield of HCl (i.e., $\frac{I_{HCl}}{I_{HCl} + I_{C_6H_5Cl}}$) is large ca. 0.7, but it decreases with increasing laser fluence to a value of ~ 0.1, (» 40 mJ/cm^2).

In contrast to HCl, Cl is observed immediately above ca. 30 mJ/cm^2, whereas little, if any signal, is detected at lower fluences even after extensive signal averaging (Fig. 7.8). Its signal starts increasing above 34 mJ/cm^2 until reaching a nearly constant value at 45 mJ/cm^2. Similarly, for the phenyl products, at low fluences (F_{LASER} < 30 mJ/cm^2), no signal is detected, even after extensive irradiation with over 300 pulses. These are detected only above ca. 30 mJ/cm^2 (ablation threshold). Ejection signal from the phenyl products is observed from the very first pulse [Fig. 7.7]. Their desorption

signals differs in absolute values i.e., I[$(C_6H_5)_2$]>I[C_6H_4Cl-C_6H_4Cl]>I. Except for the differences in absolute values, there are different rates of the signal increasing with laser fluence.

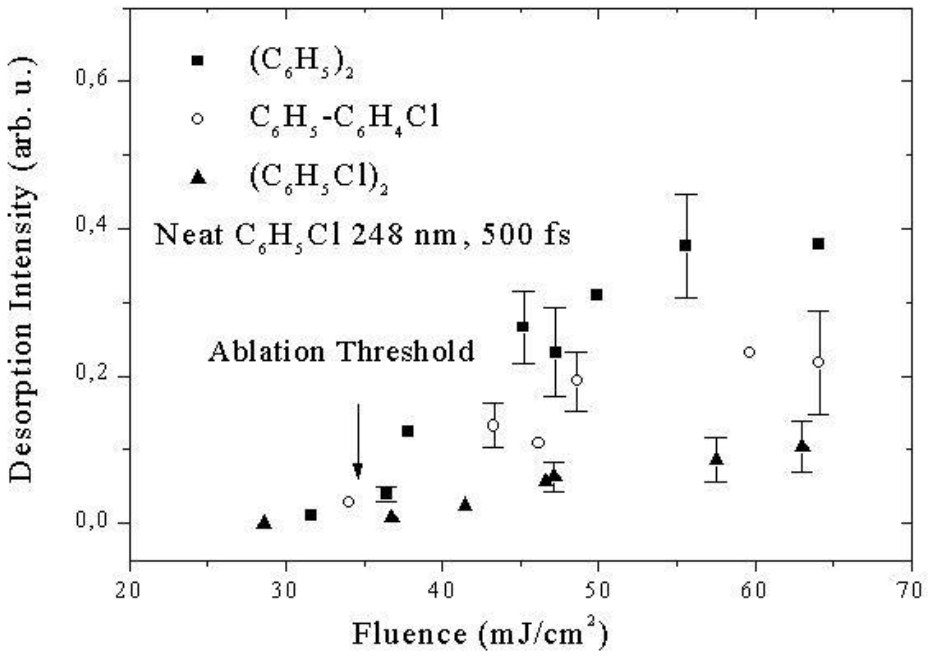

Figure 7-7 The figure depicts the intensities of the indicated photoproducts as function of the incident laser fluence. The error bars represent 2ó.

7.3. DISCUSSION

Considering first the examination of the mixture film, the major observations can be summarized as follows. (a) The ablation threshold has been found to be ~ 4 times lower than the nanosecond case, both for $(CH_3)_2O/C_6H_5CH_3$ and for C_6H_5Cl solids studies. Thus, the decrease in the threshold appears to be general (b) the dopant $(CH_3)_2O$ is found to desorb below threshold but with reduced efficiency as compared with the low fluence regime of the nanosecond induced desorption. Furthermore, above the threshold its signal is found to increase with laser fluence rather than to saturate as in the nanosecond examination (c) $C_6H_5CH_3$ is observed at very low fluences with intense

signal, in contrast with the nanosecond-case where its desorption was found to be minimal.

The decrease in the threshold may be either due to a higher energy deposition, (as for example if multiphoton processes become important) and/or due to the operation of material ejection mechanisms that differ from those operative in the nanosecond case. Multiphoton processes that could explain the decrease in the threshold, are expected to be enhanced in the irradiation with fs pulses, but in the present case, they cannot account for some critical features of the experimental results[52].

An important feature concerns the ejection efficiency of the dopant, e.g. dimethylether at high laser fluences (F_{LASER} > 30 mJ/cm^2). As shown in chapter 4, in the irradiation with nanosecond pulses, the signal of dimethylether "saturates" at laser fluences close the threshold, due to the efficient desorption of dopant from the heat-affected volume (below that ejected by the explosive boiling process). In sharp contrast, in the fs case, (Fig. 7.1) the signal of $(CH_3)_2O$ continuously increases, in close correspondence with the $C_6H_5CH_3$ signal at laser fluences above the threshold. This correlation is observed also in the most probable velocities of the two species (Fig. 2). Therefore, it appears that in the femtosecond ablation, even the volatile dopants, i.e. $(CH_3)_2O$ are ejected "in uniform" with $C_6H_5CH_3$. This correspondence illustrates that only a specific volume of material is ejected with no contribution of dopant from non-ejected film. The result directly indicates that the temperature below the ejected film never becomes high enough (as the case is in the nanosecond ablation) to enable significant diffusion of the dopant or if there is a temperature increase, the time scale is such that does not enable significant diffusion. Consequently, material ejection in the femtosecond irradiation cannot be due to a explosive boiling mechanism as that advanced in the nanosecond case.

That mechanisms of material ejection changes from that in nanosecond case is in fact even more directly indicated by the findings below the ablation threshold. At low fluences (F_{LASER} < 30 mJ/cm^2) (below threshold), it is evident from Fig. 2 that the

[52] Preliminary optical examination of the changes induced upon fs irradiation of $C_6H_5CH_3$ solids (similar to those described in chapter 3) shows very different temporal evolution than in ns. Transmission changes are observed at £ 5ns, too fast to be compatible with bubble formation.

concentration of $(CH_3)_2O$ in the plume is much lower than that in the nanosecond study (Fig. 3.1 in chapter 3). On the other hand, at these low fluences the desorption signal of toluene in absolute value is found to be very intense, compared with that in the nanosecond irradiation, although the experiments have been performed under the same detection conditions[53]. The observation of ether in the desorbing material (plume) indicates that thermal effects may still be present, but on the other hand, the efficient desorption of toluene shows that an additional to the thermal vaporization desorption pathway may exist. At present, the most reasonable possibility for compromizing these contradictory observations is that desorption occurs from local "hot" spots around photoexcited toluene molecules. In other words, the time scale is not sufficient to establish a uniform temperature.

The formation of these "hot spots" must be related to electronic processes. For instance, MD simulations similar to these described in nanosecond case, show that below the threshold, desorption processes are identical independently of the laser pulse duration (5 ps vs. 150 ps). Their results evidently disagree with the experimental results. The reason for the discrepancy must relate to electronic processes, since it is exactly the electronic degrees of freedom that have been neglected in the MD simulations.

The electronic processes taking place in the femtosecond case do not concern only the possibility of multiphoton processes. Another aspect is the high number of electronically excited states induced upon irradiation with fs pulses. Given this high number, singlet-singlet annihilation processes are going to be much more important. We propose, therefore, that the differences are due to the different mode of electronic energy decay. Such a phenomenon has been described by Fain and Lin [24] some time ago. In the femtosecond case, such a mechanism can be expected to be more efficient than in the nanosecond. In the case of irradiation with 30 ns pulses, this mechanism is not important because of the lifetime of the excited state being comparable (34 ns). According to the advanced explanation, with increasing laser fluence, the number of excited states is high

[53] Unusual and perplexing differences between ns and fs-induced desorption have also been reported by the Oxford group [91] in the irradiation of C_6H_6 multilayers (150 fs, 600 nm). A "molecular candle" effect was advanced as a plausible explanation.

enough that a process similar to that described by Fain and Lin or by Vertes et al. results in the "explosive desorption".

Alternatively, ikt has been suggested that in the use of ultrashort pulses, a photomechanical mechanism should becomes important. Due to the very fast deposition of energy, the substrate is heated under constant volume (stress confinement) and as a result a very high thermoelastic stress develops. (This suggestion is supported by recent Molecular dynamics simulation based on the breathing sphere model [].) The criterion for the laser-pulse duration tp that enables confinemnet of stress energy within the optical zone L_p is given by $t_p < L_p/C_s$ where L_p (» 3.3 ìm) is the optical penetration depth and C_s (» 1818 m/s at 190 K [59]) the velocity of sound inside the solid[54]. In the present case $5 \acute{} 10^{-13}$ s < $1.8 \acute{} 10^{-9}$ s.

Some of the experimental results presented herein seem to agree with the photomechanical mechanism. For example, the decrease in the ablation threshold for the examined systems and the high particle velocities for the same laser fluence in femtosecond vs the nanosecond case, the indication for clusters of chlorobenzene $(C_6H_5Cl)_2$. On the other hand, in other aspects, the experimental findings appear to deviate much from the predictions of molecular dynamics simulations. The most critical one appear to be the discrepancies between MD simulation and experimental results below the threshold. As argued, the failure must relate to the neglect of the electronic degrees of freedom. Thus, is reasonable to suggest that these processes will be also of importance in determining the ablation threshold and the material ejection processes in the ablative regime. It appears that addressing the nature of these processes will require different experimental techniques than those employed in the present study. The use of temporally-resolved fluorescence monitoring would be the most likely to provide information about the contrasting role of electronic processes in the fs vs. ns cases.[55]

---

[54] Dingus and Scammon [] point out that the confinement of stress falls according to a simple first-order exponential: stress confinemnet factor $A = \frac{1 - \exp(-t_p C_s / L_p)}{t_p C_s / L_p}$. For very short pulses A is unity and stress is confined; for longer pulses A decreases and stress dissipates.

[55] In fact, in the case of neat $C_6H_5CH_3$ solids a long-decay emission is observed at fluences close to the threshold upon irradiation. This long-lasting emission is observed in the visible and

7.3.1. Reactivity Patterns

Considering the femtosecond ablation of neat chlorobenzene solids, the observations can be summarized as follows: (a) below threshold, HCl is observed from the lowest examined fluences (ca. 10 mJ/cm^2) whereas at these fluences the phenyl photporducts are not observed even if the parent peak induction becomes important (b) above the threshold, the HCl yield (ca. 10^{-1}) is found to be one order of magnitude higher than the nanosecond yield (ca. 10^{-2}) and additionally intense signal of Cl is observed.

The fact that HCl is observed below the threshold, whereas the phenyl species are not, would seem to parallel the observations in the ns. (i.e., HCl thermally desorbs, whereas the phenyl species do not). Yet, the observation that induction effect of C_6H_5Cl below the threshold is very weak as compared with the ns case may indicates that further factors may involved (less efficient formation of the phenyl species as compared with the ns case).

To address this question we have performed pump-probe experiments (Fig. 8), in which the solid in the first case was first irradiated with 200 pulses at F_{LASER} = 15 mJ/cm^2 and then the signal of $(C_6H_5)_2$ was recorded by irradiating the same spot at fluences above the threshold ca. 45 mJ/cm^2.) Then this signal was compared with the signal of $(C_6H_5)_2$ without preirradiation. The results (Fig. 7.8) shows that within the S/N of the experiment, pre-irradiation of a freshly deposited solid with low laser fluence pulses doesn´t results in any enhancement of $(C_6H_5)_2$ formation. The efficient formation of HCl without the parallel formation of phenyl products, indicates the very different constraints in the fs irradiation of molecular solids as compared with ns case. *Plausibly* since as explained in the previous section, the thermal "component" appears to be low (or at least estimated solid temperatures are well below the melting point), the reactivity of the C_6H_5 fragments produced upon Cl liberation is much reduced due to the environmental

---

differs from the literature-reported fluorescence of toluene in the UV. Examination of this emiision should thus provide usefull information about the electronic processes in metastable liquid conditions. The important point is that usually the emission in the fs irradiation differs in color from that observed upon ns irradiation.

restriction (in contrast in nanosecond, due to the melting, C_6H_5 radical have a high mobility thereby having a high chance to encounter other radicals).

Differences become even more interesting when photoproduct formation is examined above the ablation threshold. Most interestingly, HCl yield is found to be nearly 1-order of magnitude higher than in ns case, whereas phenyl species $(C_6H_5)_2$, $C_6H_4Cl_2$ etc) nearly 1-order lower. (in the nanosecond ablation of C_6H_5Cl films, HCl and $(C_6H_5)_2$ to be formed with a yield of $\sim 10^{-2}$. Indeed, as shown $(C_6H_5)_2$ is produced at $\sim 10^{-3}$. Furthermore, the photoproduct intensities closely follow the intensity of the parent molecule, which indicates that it is formed with nearly constant yield over the fluence range examined herein.

The increased dissociation yield cannot be ascribed to multiphoton processes that could be enhanced by the use of the shorter laser pulse width. First, a two-photon excitation would promote ionization (I.P of the compound being 9.6 eV) over fragmentation but no ions could be detected by switching off the electron impact. However, this process should produce in parallel a number of other species, in particular $(C_6H_5)_2$, at variance with the experimental observations. Most importantly, if a two-photon process was responsible, then the HCl yield should increase with increasing laser fluence, which is at variance with the near constant value observed. Finally, it is not clear how multiphoton processes can account for differences HCl and $(C_6H_5)_2$ yields. Thus, the contribution of multiphoton processes cannot explain the increase in the fragmentation yield observed in the fs experiments, as compared with the nanosecond ones[56].

We instead advance the following explanation. The explanation is tentative and further experiments are needed for its verification, but at least it accounts for our observations in consistent way. Specifically, we suggest that the reason for the enhanced fragmentation is due to the faster plume ejection, plausibly on the picosecond level, for

[56] Interestingly, in a recent study [30] of the ablation of liquid $C_6H_5CH_2Cl$ with 300 fs pulses at 248 nm, the ablation threshold was found to be the same as in the corresponding ns process (≈30 mJ/cm^2). The authors indicate that a two-photon process does not become important at fluences close to the ablation threshold. They consider the invariability of the ablation threshold to be indicative of a photochemical ablation mechanism (i.e., ejection of material as a result of the formation of gaseous products).

ablation effected with femtosecond pulses. In the case of simple organic systems, the time scale of plume ejection has not been studied experimentally, but in the case of polymers the first studies indeed have shown that material ejection in fs ablation is already significant at ³ 100 ps. Accordingly, in the irradiation of C_6H_5Cl films, it can be suggested that before condensed-phase deactivation has proceeded, the excited molecules are ejected in the gas-phase where they dissociate in high yields, characteristic of their gas-phase. From fluorescence measurements, the lifetime of the S_1 (the state excited at 248 nm) of C_6H_5Cl is indicated to be ≈100 psec in the gas-phase[14]. However, in condensed phases, this lifetime may be considerably reduced due to the influence of efficient deactivation processes, in the analogous $C_6H_5CH_2Cl$, dilution of the molecule in hydrocarbon solution results, magnitude decrease of the photolysis yield. The decrease is paralleled by a corresponding shortening of the excited state lifetime, demonstrating that efficient deactivation, rather than recombination processes ("cage effects") are responsible for the low photolysis yield [14-15]. It is highly probable that a similarly fast deactivation mechanism operates also in the case of C_6H_5Cl. Thus, if photolysis of the compound occurred in the film, the yield would be expected to be of the order of 10^{-2}. Indeed, such values were obtained [9] in ablation with nanosecond pulses at 248 nm, where imaging studies have shown [16] that over the fluence range 40-150 mJ/cm^2, plume ejection occurs well after the end of the laser pulse.

The previous suggestion is supported by the observation of a high Cl signal just above the threshold. This high Cl signal strongly indicates that C_6H_5Cl density must be rather low at the time of Cl formation. Similarly the low $(C_6H_5)_2$ formation is consistent with fragmentation occuring mainly after plume ejection. The probability of $(C_6H_5)_2$ formation through interaction of two C_6H_5 radicals in the rarefied part of the plume is very low.

If, as suggested, dissociation occurs in the gas-phase, then its yield should be largely independent of the medium from which C_6H_5Cl is ablated. Indeed, the yield of HCl in the ablation of C_6H_5Cl mixed in C_6H_{12} in molar ratio of 1 to 10 turns out to be nearly equal to that determined in the previous case of neat C_6H_5Cl films. In sharp contrast, in the corresponding nanosecond experiments, the yield of HCl in the ablation

of C_6H_{12}/C_6H_5Cl is approximately 10 times higher than what for C_6H_5Cl neat films. This difference constitutes strong evidence for the fact that photolysis of the compound in the femto case must occur in the gas phase. Evidently, the above explanation is tentative. Future work for establishing this mechanism will require (a) establishing the time scale of plume ejection.

7.4. CONCLUSIONS

In conclusion, the study clearly illustrates that the laser pulse width has major effect both on the desorption dynamics of the molecules as well as the nature and the efficient of the formed products. Well-defined and most interesting differences from the nanosecond case are observed both below and above the ablation threshold. Tentative explanations have been advanced for these differences, but their verification calls for extensive experimentation, in particular via directly monitoring techniques.

Although this mechanism has to be established, it is specifically the observation that, the observed higher fragmentation, by-product yields may be considerably reduced, interesting to note the analytical possibilities that fs irradiation appears to offer (i.e., reduced significance of side-reactions) suggests that femtosecond ablation holds considerable merit for the study of the primary fragmentation patterns of "large-sized" desorbates f.e.of the biomolecular systems in Matrix Assisted Laser Desorption techniques.

8. APPENDIX I: MOLECULAR DYNAMICS SIMULATIONS

In this appendix we present the basic features of the breathing sphere model developed for MD simulations of laser ablation of organic solids. Then we describe some results of MD simulations that have been done on the bicomponent systems $(CH_3)_2O/C_6H_5CH_3$ and $C_{10}H_{22}/C_6H_5CH_3$.

8.1. BREATHING SPHERE MODEL

The model assumes that each molecule can be represented by "breathing" spheres. This model accurately describes the translational degrees of freedom but only aproximately the internal degrees of freedom. The internal (breathing) mode allows one to reproduce a realistic rate of the conversion of internal energy of the molecules excited by the laser to the translational motion of the other molecules. The parameters of interparticle interaction are chosen to reproduce the properties of the material, in this case a molecular solid. The parameters of a potential function ascribed to the internal motion can be used to change the characteristic frequency of the breathing mode and to affect the coupling between internal and translational molecular motions. The rate of the vibrational relaxation of excited molecules is an input parameter in the model and can be either estimated from experimental data or modeled with atomistic or ab initio molecular dynamics simulations.

For the excitation of the breathing sphere (molecule) is assumed that the initial electronic energy in the system, after photon absorption, is converted rapidly (1ps time scale) by internal conversion to vibrational energy. The effect of laser irradiation is thus simulated by vibrational excitation of random molecules during the time of the laser pulse, with the probability decreasing exponentially within the penetration depth (Beer's law).

Additionally, photofragmentation and reactions can be simulated within the breathing sphere model. The photofragmentation event is simulated by replacing the sphere representing a molecule to be excited with smaller spheres representing the resulting photofragmented molecules. The fate of fragments can be followed during the course of MD simulation and their role in the ablation process can be analyzed.

8.2. EXPERIMENT VS. MD SIMULATION

In this section we present the results of the Molecular dynamics Simulations in our model mixture systems described in chapters 3 and 4, namely $(CH_3)_2O$ / $C_6H_5CH_3$ and $C_{10}H_{22}$ / $C_6H_5CH_3$. In the simulation the dopants molecules are introduced and homogeneously mixed with matrix molecules at a 10 % concentration. The mass of all molecules is 100 amu. Adjusting the well depth of the intermolecular pair potential (Lennard-Johnes) controls the volatility of the dopant molecules.

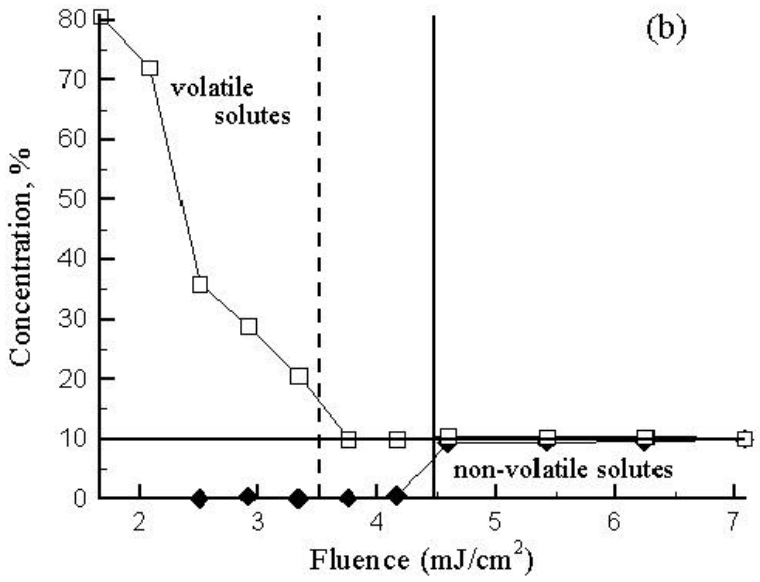

Figure 8-1 Concentration of volatile and nonvolatile dopants in the plume vs laser fluence from Molecular Dynamics simulations based on experimental data presented in chapter 3 and 4. The horizontal lines indicate the initial concentration of dopants in the sample. The vertical lines indicate the approximate position of the ablation threshold.

For the $(CH_3)_2O$ and $C_{10}H_{22}$ dopants, the binding energy in the matrix are 0.45 and 0.92 eV respectively, corresponding to an average cohesive energy of the systems of 0.57 and 0.66 eV/particle, respectively. Excitation is induced with 5 eV photons (ë=248 nm). The size of the system (10x10x180 nm), and penetration depth (55 nm) are chosen. The results of the simulations are presented in a similar form (as that presented in chapter

3 and 4) in Fig. 8.1. The computational results qualitative agree with the experimental observations and show the difference in desorption intensities and ablation thresholds for the mixtures with volatile and nonvolatile dopants. Both the experimental and computational results show that the ablation thresholds vary with cohesive energy of the system. Quantitatively, the fluence values in the simulation differ by an order of magnitude from the experimental ones due to differences in the optical penetration depth, specific heat capacity, no reflection losses in the simulations, etc.

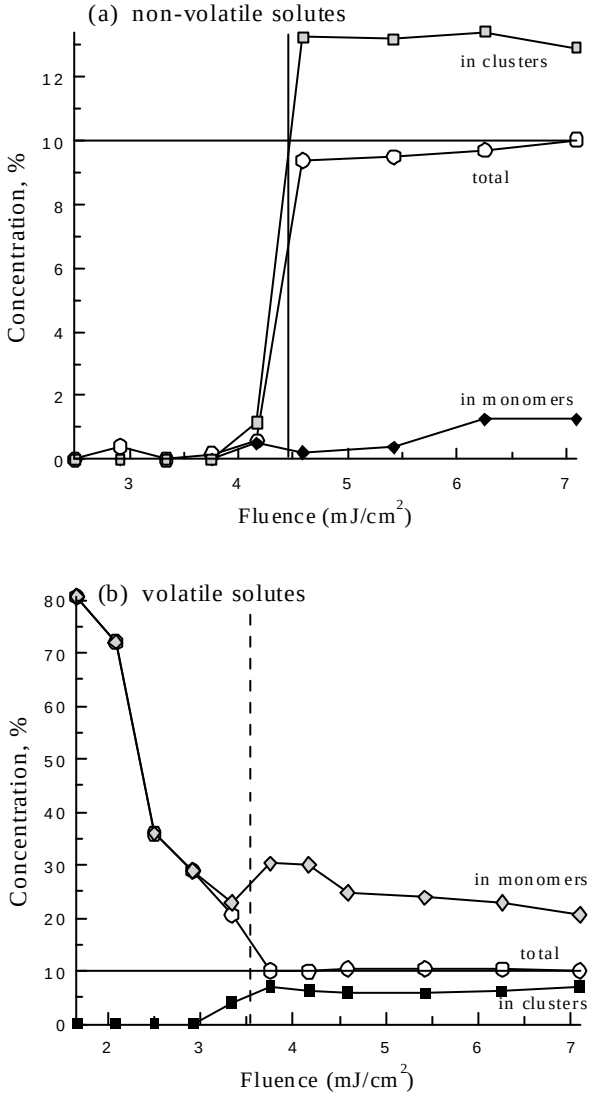

Figure 8-2 Concentrations of (a) nonvolatile and (b) volatile dopants ejected as monomers and as a part of the clusters vs laser fluence calculated in Molecular dynamics Simulations

Another features of the simulations are shown in Fig. 8.2. As shown the simulations predict that the nonvolatile dopants preferentially incorporate into the clusters that ablate. In contrast, the volatile dopants preferentially ablate as monomers. In the experiments, the existance of the clusters is difficult to be shown because of the e-impact cracking.

Very recently, Garisson has published simulation studies on the photochemical processes in C_6H_5Cl solid [31].

The main conclusion of the work is that the simulation very well describe the experimentally determined photoproduct ratios. Indeed, they observed all products reported in chapter 6 differences in the relative intensities of the various products can be traced to the fact that the phenyl "involatile" species are ejected within clusters.. Yet, a carefull examination of their results vs. experimental results indicates various interesting consistencies, but also differences.

- The accumulation of phenyl photoproducts below the threshold is well reproduced.
- The "cage effects" as suggested by this thesis could not be followed in the simulations. Thus this suggestion has not yet received theoretical support.
- The issue of "hot" reactivity is alltogether avoided. Presumably, they rely on more recent data concerning the reactivity of Cl and C_6H_5 radicals. However, it is clear that they have scaled their rate constants and their rate constants are quite high, while in our case comparison relied on a solution studies.
- Finally, a most interesting proposal that may eventually result in the compromosive of the "explosive boiling" and photochemical mechanism: the simulation shows that during the laser pulse, the formation of the volatile photoproducts HCl resulting in the decrease of the system cohesive energy.

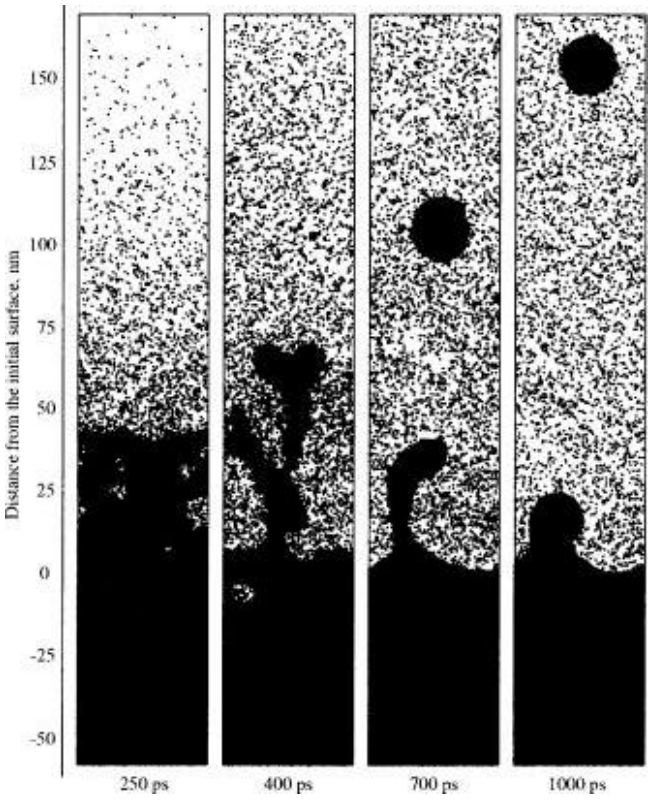

Figure 8-3 Snapshots of ablation regime in molecular dynamics simulations

9. APPENDIX II: MODEL FOR ESTIMATION OF NUMBER OF COLLISIONS

In this Appendix we use a simple (essentially geometric model) as a way of estimating, the number of gas phase collisions suffered by particles following desorption.

Table 9-1 The parameters of the collisional model

No (molecules/cm^2)	Nc	ó (cm^2)	î	Ó	w (cm)	V (cm/sec)	õ (cm/sec)	ô (nsec)	á
3.07×10^{14}	$N_{ML} \times No$	10^{-14}	0.67	0.363	0.1	$\sqrt{2}u$	$\sqrt{\frac{8RT}{pMB}} \times 10^{-2}$	30	$\frac{p}{18}$

The number of collisions N_{coll} suffered by a particle following desorption process from a surface can be estimated by integrating the collision rate over an appropriate time dependent density. The density of particles at time t is given by:

$$n(t) = N_c w / (w + 2ut \tan a) \times (ut + 2\Sigma ut)$$

where N_c is the desorbed coverage (molecules/cm^2), á is a parameter which governs the angular divergence of the beam, Ó is the standard deviation in the velocity distribution around the mean velocity õ, and ô is the duration of the desorption process.

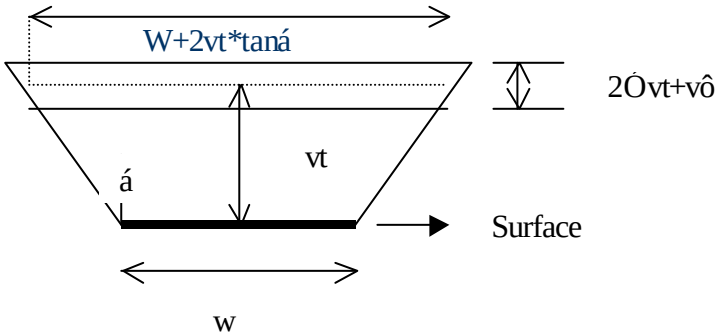

Figure 9-1 Schematic picture of the geometry of the problem

The geometry of the problem is determined by surface width w and length l where l>>w. The average number of collisions suffered by a typical particle which left the surface at ô/2 is:

$$N_{coll} = \int_{t/2}^{t} n(t')s\,ux\,dt'$$

î corrects for the collision rate within an effusive stream of particles is somewhat reduced from that in a bulb of gas due to the directionality of the stream [126]. Lubman et al. have derived the collision rate within a thermal, effusive stream far from its source as $Z = ns\,Vx$ where n is the gas density, ó is the collision cross section, $V = \sqrt{u_1^2 + u_2^2} = \sqrt{2}u$ where $u = \sqrt{\frac{8RT}{p\,MB}}$ is the mean velocity of the stream, and î=0.67 is the fraction of the bulk gas collision rate. In our case, the factor î may vary from ~ 1during the initial desorption to the effusive stream limit 0.336 far from the surface. In our case typical values of the various parameters are shown to the Table 9.1. In the Table N_{ML} is the number of monolayers desorbed per pulse. In the Fig. 1 we present an example plot for the case of toluene in the desorption of 0.1 ML of the compound.

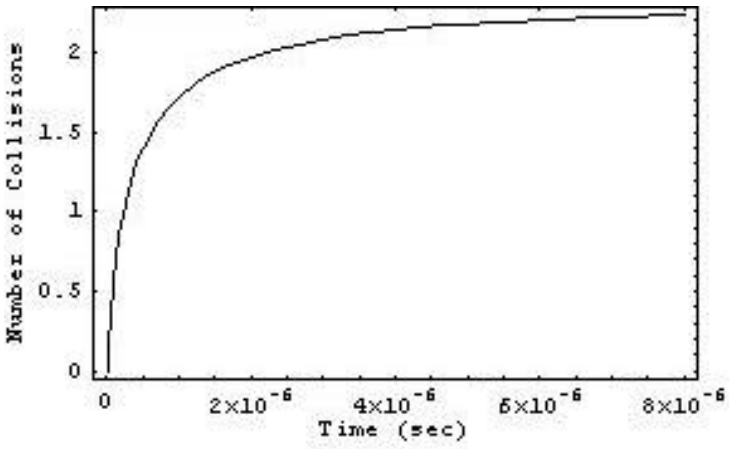

Figure 9-2 The figure illustrates the total number of collisions N_{coll} as a function of time for 0.1 ML desorbing material. The parameters for the calculation are given in the Table 9.1

10. REFERENCES

1. R. Srinivasan and B. Braren, *Chem. Rev.*, **89**, 1303 (1989), and references cited therein
2. Laser Ablation, Principles and Applications, edited by J. C. Miller *Springer Ser. Matter. Sci.* Vol. 28, edited by J. C. Miller (Springer, Berlin, 1994)
3. Photochemical Processing of Electronic Materials, edited by I. A. Boyd (Academic, London, 1992)
4. D. D. Dlott and M. D. Fayer, *J. Chem. Phys.* **92** 3798 (1990) and references therein
5. S. Georgiou, V.Zafiropulos, D. Anglos, C. Balas, V. Tornari, and C. Fotakis, *Appl. Surf. Sci.*, **127/129,** 738 (1998).
6. Pique, A.; McGill, R. A.; Chrisey, D. B.; Leonhardt, D.; Mslna, T. E.; Spargo, B. J.; Callahan, J. H.; Vachet, R. W.; Chung, R.; Bucaro, M. A.; *Thin Solid Films*, **355-356**, 536 (1999).
7. Tanaka K., Ido Y., Akita S., Yoshida Y., Yoshida T., 1987. In Proc. 2nd Japan-China Joint Symp. Mass Spectrom., p. 185. Osaka
8. M. Karas, F. Hillenkamp, *Anal. Chem.* **60,** 1193 (1988)
9. A. Vertes, R. D. Levine, *Chem. Phys. Lett.*, **171** 284 (1990)
10. A. Vertes, Gijbels R. R. D. Levine, *Rapid Commun. Mass Spectrom.* **4** 228 (1990)
11. J. W. Gibbs, *Scientific Papers*, Vol. **1**, Thermodynamics, Dover, New York.
12. L. D. Landau and E. M. Lifshitz:Statistical Physics, 3rd ed., Part I, Pergamon Press Oxford (1980)
13. E. N. Economou Exersises in Statistical Physics and Thermodynamics, 1st ed., University of Crete Press (1995)
14. Martynyuk M.M. *Sov. Phys. Tech. Phys.*, **19**, 793 (1974).
15. Martynyuk M.M. *Sov. Phys. Tech. Phys.*, **21**, 430 (1976).

16. Miotello A. and Kelly R. *Appl. Phys. Lett*., **67**, 3535 (1995).

17. J. H. Yoo, S. H. Jeong, R. Greif, R. E. Russo, *J. Appl. Phys.*, **88**, 1638 (2000)

18. Zhigilei L.V. and Garrison B.J., Appl. Phys. Lett. **74** 1341 (1999)

19. Zhigilei L.V. and Garrison B.J., *J. Appl. Phys.*, **88**, 1281 (2000).

20. Zhigilei L.V.; Kodali P.B.S.; Garrison B.J. *J. Phys. Chem B.*, **102**, 2845 (1998).

21. Kelly R. and Miotello A. *Appl. Surf. Sci.*, **96-98**, 205 (1996).

22. R. Kelly and A. Miotello, *Phys. Rev. E.*, **60**, 2616 (1999).

23. A. Miotello, R. Kelly, *Appl. Phys. A.*, **69**, S67 (1999).

24. B. Fain and S. H. Lin, *J. Chem. Phys.*, **91**, 2726 (1989).

25. £. Dutkiewicz, R. E. Johnson, A. Vertes and R. Pê drys, *J. Phys. Chem. A.*, **103**, 2925 (1999).

26. D. Kim and C. P. Grigoropoulos, *Appl. Surf. Sci.* **127-129**, 53 (1998)

27. D.E. Hare, J. Franken and D. D. Dlott, *J. Appl. Phys.* **77** 5950 (1995)

28. A. A. Oraevsky, R. Esenaliev, S. L. Jacques and F. K. Tittel, *Proc. SPIE* **2391** 300 (1995)

29. R. Cramer, R. F. Haglund, Jr. and F. Hillenkamp, *Int. J. Mass. Spectrom. Ion Processes* **169/170**, 51 (1997)

30. S. L. Jacques *Appl. Opt.* **32** 2447 (1993)

31. Yingling Y.G., Zhigilei L.V., Garrison B.J., *Nucl. Instr. Meth B.*, **180**, 171 (2001)

32. Y. Tsuboi, K. Hatanaka, H. Fukumura and H. Masuhara, *J. Phys. Chem.* **98,** 11237 (1994).

33. Yasuyuki Tsuboi, Hiroshi Fukumura, and Hiroshi Masuhara, *J. Phys. Chem.*, **99**, 10305 (1995)

34. Yasuyuki Tsuboi, Koji Hatanaka,, Hiroshi Fukumura, and Hiroshi Masuhara, *J. Phys. Chem. A.*, **102**, 1661 (1998) ; Koji Hatanaka, Nitsushi Kawao, Yasuyuki Tsuboi, Hiroshi Fukumura, and Hiroshi Masuhara, *J. Appl. Phys.* **82**, 5799 (1997)

35. Koji Hatanaka, Tamitake Itoh, Tsuyoshi Asahi, Nobuyuki Ichinose, Shunichi Kawanishi, Tsuneo Sasuga, Hiroshi Fukumura and Hiroshi Masuhara, Appl. Phys. Lett., **73**, 3498 (1998)

36. J. Levis, Annu. Rev. Phys. Chem. **45**, 4830 (1994).

37. Nishi, N. Shinohara, H. Okuyama, T., *J. Chem. Phys*., **80**, 3898 (1984).

38. Domen, K. Chuang, T.J., *Phys. Rev. Lett*., **59**, 1484 (1987).

39. K. Domen and T.J. Chuang, *J. Chem. Phys.* **90**, 3318 (1989) ; **90**, 3332 (1989).

40. W. C. Natzle, D. Padowitz and S.J. Sibener, *J. Chem. Phys.* **88**, 7975 (1988).

41. Cousins, L.M.; Leone, S.R.; *J. Mater. Res.*, **1988**, *3*, 1158.

42. L. M. Cousins, R.J. Levis and S.R. Leone, *J. Chem. Phys.* **91**, 5731 (1989).

43. L. M. Cousins, R.J. Levis and S.R. Leone, *J. Phys. Chem.* **93**, 5325 (1989).

44. Levis, R.J.; Waltman, C.J.; Cousins, L.M.; Copeland, R.G.; Leone, S.R.; *J. Vac. Sci. Technol.*, **A8**, 3118 (1990).

45. Campos, F.X.; Weaver, G.C.; Waltman, C.J.; Leone, S.R.; *J. Vac. Sci. Technol.*, **B10**, 2217 (1992).

46. F. X. Campos, C. J. Waltman and S. R Leone, *Chem. Phys. Lett.* **201,** 399 (1993).

47. Weaver, G.C.; Leone, S.R.; *Surf. Sci*., **1995**, *328*, 197.

48. G.C. Weaver and S.R. Leone, *J. Phys. Chem.* **100**, 4188 (1996).

49. R. Braun and P. Hess, *J. Chem. Phys.* **99**, 8330 (1993).

50. H. Niino, T. Sato and A. Yabe, *Appl. Phys. A* 69 (1999) S145

51. Niino, H.; Yabe, A.; *Appl. Surf. Sci.*, **1996**, *96-98*, 572.

52. P. K. Wu et al. J. Appl. Phys. **90** 3623 (2001)

53. Balzers Operating Instructions QMA 2nd Edition:5. 1989

54. R. Braun, P. Hess, Int. J. Mass. Spectrom. and Ion Processes 125 229 (1993)

55. C. -Cho, B. A. Collins, R.E. Hammer, J. C. Polanyi, C. D. Stanners, J. H. Wang, and G.-Q. Xu, J. Phys. Chem. **93**, 7761 (1989).

56. G. Herzberg, Electronic spectra of Polyatomic Molecules, (Van Nostrand Rainhold Company, 1966) pp. 548

57. CRC Handbook of Chemistry and Physics, 75th ed., CRC Press, Boca Raton, FL, 1995.

58. E. L. Cussler, Diffusion, Cambridge University Press, Cambridge, 1984

59. R. D. Goodwin, J. Phys. Chem. Ref. Data 18 (1989) 1565

60. D. W. Scott, G. B. Guthrie, J. F. Messerly, S. S. Todd, W. T. Berg, I. A. Hossenlopp, and J. P. McCullough, J. Phys. Chem. 66, 911 (1962)

61. R. C. Reid, J. M. Prausnitz, T. K. Sherwood, The Properties of Gases and Liquids, (McGRAW-Hill Book Company 3rd Edition)

62. NIST Chemistry WebBook, NIST Standard Reference Database National Institute of Standards and Technology, Gaithersburg MD, 20899 (http://webbook.nist.gov)

63. J. Kutzner, G. Lindeke, K.H. Welge and D. Feldman, J. Chem. Phys. **90**, 548 (1989).

64. S. M. Haskin and P. John, J. Phys. Chem. B., 103, 4566 (1999)

65. B. Meyer. *Low-Temperature Spectroscopy*, (American Elsevier Co., New York, 1971) and references therein.

66. Statistical Physics Landau and Lifshitz page 533 Pergamon Press

67. S. B. Kiselev Physica A 269, 252 (1999)

68. C. T. Avedisian, J. Phys. Chem. Ref. Data, 14 No(3), 695 (1985)

69. S. D. Lubetkin *Chem Soc. Rev.* 243 (1995)

70. M. Blander and J. L. Katz, *AlChE Journal* 21, 833 (1975)

71. M. Blander, D. Hengstenberg and J. L. Katz, *J. Phys. Chem.* 75 3613 (1971)

72. Debenedetti P. *Metastable Liquids: Concepts and Principles*; Princeton University Press: Princeton, NJ 1996.

73. Skripov V.P.; Pavlov P.A. Superheating and explosive boiling of liquids. *Sov. Tech. Rev. B. Therm. Phys.* **1989**, *2*, 171-207.

74. Skripov V.P. Thermodynamic stabilities of superheated and supercooled liquids. *Fluid Mechanics Research* **1992,** *21*, 43-50.

75. O. Yavas, P.Leiderer, H.K Park, C.P Grigoropoulos, C.C Poon W.P Leung, N.Do, A.C. Tam *Phys. Rev. Lett*. 70, 1830 (1993)

76. S. M. Haskin and P. John, *J. Phys. Chem. B* **103**, 4566 (1999)

77. R. Srinivasan and A. P. Ghosh, *Chem. Phys. Lett*. **143**, 546 (1988)

78. Dongsik Kim, Hee K. Park and Costas P. Grigoropoulos, *International Journal of Heat and Mass Transfer*, 44, 3843 (2001)

79. J. W. Elam and D. H. Levy, *J. Chem. Phys.* 106 368 (1997)

80. I. Noorbatcha, R.R. Lucchese and Y. Zeiri, *J. Chem. Phys*. **86**, 5816 (1987); *ibid* **89**, 5251 (1988).

81. R.Kelly and R.W. Dreyfus, *Surf. Sci.* **198**, 263 (1988).

82. R.Kelly, R.W Dreyfus *Nucl. Instr. Meth.* B 32 (1988) 341

83. R.Kelly, *J. Chem. Phys*. **92** 5047 (1990) and references therein.

84. R. W. Dreyfus, R. Kelly and R. E. Walkup, *Appl. Phys. Lett*. **49**, 1478 (1986)

85. H.M. Urbassek and D. Sibold, *Phys. Rev. Let*. **70**, 1886 (1993).

86. H. M. Urbassek and D. Sibold, *Phys. Rev. A* **43**, 6722 (1991).

87. I. NoorBatcha and R. R. Lucchese, Phys. Rev. B **36** 4978 (1987)

88. Hess W. P., A. G. Joly, K. M. Beck, R. M. Williams, J. T. Dickinson Appl. Phys. A 69 S389 (1999)

89. Herrmann, R. F. W., J. Gerlach, E. E. B. Cambell Appl. Phys. A 66 35 (1998)

90. Noack J., D. X. Hammer, G. D. Noojin, B. A. Rockwell, A. Vogel J. Appl. Phys. 83 7488 (1998)

91. Arnolds, H., Rehbein, C., Roberts, G., Levis, R. J., King D. A., Chem. Phys. Lett. **314** 389 (1999)

92. T. Ichimura, and Y. Mori, J. Chem. Phys. **58**, 288 (1973).

93. T. Ichimura, Y. Mori, H. Shinohara, N. Nishi, J. Chem. Phys. **189,** 117 (1994).

94. M. Preidel and R. Zellner, Ber. Bunsenges Phys. Chem. **93**, 1417 (1989).

95. J. Grimshaw and A. P. Silva, Chem. Soc. Rev. **10**, 181 (1981) and references therein.

96. A. MacLachlan and R. L. McCarthy, J. Am. Chem. Soc. **84,** 2519 (1962)

97. I. Franck and E. Rabinowitch, Trans. Faraday Soc. **30**, 120 (1934)

98. "Radical Formation and Trapping in the Solid Phase" by G. C. Pimentel, *Formation and Trapping of Free Radicals*, ed. A. Bass and H. Broida (Academic Press, Inc., New York, N.Y. 1960).

99. J. Shi and M. J. Bernhard, Int. J. Chem. Kinet. **29**, 349 (1997).

100. J. C. Scaiano and L. C. Stewart, J. Amer. Chem. Soc. **105**, 3609 (1983).

101. R. G. Kryger, J. P. Lorand, N. R. Stevens, N.R. Herron, J. Am. Chem. Soc. **99**, 7589 (1977).

102. C. -Cho, B. A. Collins, R.E. Hammer, J. C. Polanyi, C. D. Stanners, J. H. Wang, and G.-Q. Xu, J. Phys. Chem. **93**, 7761 (1989).

103. R. S. Davidson, J. W. Goodin and G. Kemp, *Adv. Phys. Organic Chem.*, 1984, **20,** 191 and references therein.

104. W. Dorrepaal and R. Louw, *Int. J. Chem. Kinetics*, 1978, **10**, 249.

105. D. Logan, C. A. Wight and V. A. Apkarian, *Chem. Phys.*, 1997, **217,** 99.

106. Y. Tsuboi, K. Hatanak, H. Fukumura, H. Masuhara, J. Phys. Chem. A 98 (1994) 11237.

107. A. Koubenakis, J. Labrakis and S. Georgiou, J. Chem.Soc., Faraday Trans. 94 (1998) 3427.

108. K. B. Carpenter, Determination of Organic Reactions Mechanisms John Willey (1984).

109. G. J. Szulczewski and J. M. White, J. Vac. Sci. Technol. A 15 (1997) 1526.

110. E. T. Jensen and J. C. Polanyi, J. Phys. Chem. 97 (1993) 2257.

111. S. H. Kim, P. C. Stair and E. Weitz, J. Chem. Phys. 108 (1998) 5080.

112. S. J. Garret, V. P. Holbert, P.C. Stair, and E. Weitz, J. Chem. Phys. 100 (1994) 4626.

113. A. Fahr, A. K. Nayak, M. J. Kurylo, Chem. Phys. 197 (1995) 195.

114. N. Astoin, J. Granier, M. Convier, J. Phys. Radium 19 (1958) 507.

115. S. Georgiou, A. Koubenakis, M. Lassithiotaki and J. Labrakis, J. Chem. Phys. 109 (1998) 8591.

116. A. Koubenakis, J. Labrakis, S. Georgiou, to be submitted.

117. G. Jancso and W. A. Van Hook, Chem. Rev. 74 (1974) 689.

118. D. A. Dows, J. Chem. Phys. 29 (1958) 484.

119. S. R Coon, K. B. Myli, and V. H. Grassian, J. Phys. Chem. 99 (1995) 16416.

120. R. Kopelman, J. Chem. Phys. 44 (1966) 3547.

121. E. Gelles and K. S. Pitzer, J. Amer. Chem. Soc. 75 (1953) 5259.

122. P. C. Samartzis, B. L. G. Bakker, D. H. Parker, and T. N. Kitsopoulos, J. Phys. Chem. A 103 (1999) 6106 and references therein.

123. R. E. Rebbert and P. Ausloos, J. Chem. Phys. 48 (1968) 306.

124. L. C. T. Shoute and P. Neta, J. Phys. Chem. 95 (1991) 4411.

125. L. E. Brus and V. E. Bondybey, *J. Chem. Phys*. **65** 71 (1976).

126. D. M. Lubman, C. T. Rettner and R. N. Zare, *J. Phys. Chem*., **86**, 1129 (1982)

127. R. Atkinson, S. M. Aschmann, Int. J. Chem. Kinet. **17** 33 (1985)

128. D. Raftery, M. Iannone, C. M. Phillips, R. M. Hochstrasser, Chem. Phys. Lett., **201** 513 (1993)

129. H. K. Park Ph. D. Thesis University of Berkeley (1994)

130. Zhigilei, L. V. Garrison, B. J. *Appl. Phys. Lett.* **71** 551 (1997)

PARTICIPATION IN CONFERENCES

A. Koubenakis , M. Lassithiotaki, and S. Georgiou
"Photodesorption Processes from Molecular van der Waals Films",
TMR Summer School Trends in Molecular Physics,
Nijmegen, Netherlands, July 1998. (Oral presentation)

A. Koubenakis, J. Labrakis, S. Georgiou, Y. G. Yingling, L. Zhigilei, B. J. Garrison, "Mechanisms of Material Ejection in the UV Irradiation of Model Molecular Solids: Implications for Matrix Assisted Laser Desorption" **Gordon Conference "Laser Material Interactions"**, USA, June 2000 (***Award to A. Koubenakis for Best Graduate Student Presentation***)

PUBLICATIONS

Publications in Journals

1. S. Georgiou, A. Koubenakis, H. Niino, A. Jabe, "Mechanisms in the UV irradiation of model molecular solids and liquids", Chem. Rev., issue on Laser Ablation of molecular substrates, Eds: S. Georgiou, F. Hillenkamp Febr. 2003

2. Koubenakis, J. Labrakis and S. Georgiou, "Pulse Dependence of Ejection Efficiencies in the UV Ablation of Bi-component van der Waals Solids", **Chem. Phys. Lett.,** 346, 54-60 (2001)

3. Y. G. Yingling, L. V. Zhigilei, B. J. Garrison, A. Koubenakis, J. Labrakis and S. Georgiou, "Influence of Analyte Volatility on Molecular Ejection Processes in Laser Ablation", **Appl. Phys. Lett.,** 78**,** 1631-1633 (2001)

4. S. Georgiou, C. Kosmidis, A. Koubenakis, W. Jia, and K.W. D. Ledinhgam, "Translational Characteristics in the Ablation of Chlorobenzene van der Waals Solids", **Phys. Chem. Chem. Phys.,** 1, 5339-5344 (1999)

5. S. Georgiou, A. Koubenakis, M. Lassithiotaki, and J. Labrakis, "Formation and Desoprtion Dynamics of Photoproducts in the UV Ablation of van der Waals Chlorobenzene Films at 248 nm", **J. Chem. Phys.,** 109, 8591-8600 (1998)

6. A. Koubenakis, J. Labrakis, and S. Georgiou "Reactivity Characteristics in the UV Ablation of Molecular van der Waals Solids", **J. Chem. Soc.: Faraday Trans.,** 94, 3427-3432 (1998)

7. S. Georgiou, A. Koubenakis, M. Syrrou and P. Kontoleta "The Importance of the Plume Ejection Time for the Fragmentation Yields Observed in the UV Ablation of Molecular van der Waals Films. Ablation of Chlorobenzene Films at 248nm", **Chem. Phys. Lett.**, 270, 491- 499 (1997)

8. S. Georgiou, A. Koubenakis, P. Kontoleta and M. Syrrou, "A Comparative Study of the UV Laser Ablation of van der Waals Films of Benzene Derivatives" **Laser Chem.,** 17, 73- 83 (1997)

9. S. Georgiou, A. Koubenakis, P. Kontoleta and M. Syrrou, "Induction and Memory Effects in the Ablation of Weakly Absorbing van der Waals films" **Chem. Phys. Lett.,** 260, 166-172 (1996)

Publications in Referred Proceedings

A. Koubenakis, J. Venturini and S. Georgiou, "Examination for "deuterium effect" in UV Ablation of molecular solids: a comparative examination of CH_3I and CD_3I", **Appl. Surf. Sci. ,** accepted for publication (2001)

A. Koubenakis, T. Elimioti, S. Georgiou, "A Comparative Study of the Desorption Efficiencies in the UV Irradiation of Molecular van der Waals Films Above and Below the Ablation Threshold", **Appl. Phys. A,** 86, S637-S641 (1999)

S. Georgiou, A. Koubenakis, J. Labrakis and M. Lassithiotaki "Photoproduct Desorption Dynamics in the UV Ablation of Model Molecular Solids. Ablation of Chlorobenzene Films at 248 nm", **Appl. Surf. Sci.**, 127/129 , 122 - 127 (1998)

No. of citations (2001)**: » 25**

ARTICLES IN BOOKS

M. Lassithiotaki, A. Koubenakis, J. Labrakis and S. Georgiou,

"*Desorption Dynamics Below and Above the Ablation Threshold of van der Waals Films*", in J. C. Vickerman, I. Lyon, N. P. Lockyer and J. E. Parks (Ed.), "Resonance Ionization Spectroscopy", Amer. Inst. of Physics, Washington (1998) pp. 347 - 352.